AN X-RAY INVESTIGATION

of the

THERMAL DECOMPOSITION OF

UNIRRADIATED AND IRRADIATED

SILVER PERMANGANATE.

by

G. S. WOODS, B.Sc. (Hons.), (Rhodes).

A thesis submitted in fulfilment of the requirements for the Degree of Master of Science of Rhodes University.

Department of Chemistry,
Rhodes University,
Grahamstown.

December, 1962.

A C K N O W L E D G E M E N T S .

The author wishes to thank Professor E.G. Prout, M.Sc., Ph.D., (S.A.), of Rhodes University, for his interest and encouragement throughout the period in which this work was carried out.

The author is also indebted to Messrs. F. van de Water and G. Ranftelshofer for their assistance in the technical aspects of the research, and to the South African Council for Scientific and Industrial Research for a grant held during part (1961) of the duration of this work.

C O N T E N T S

I N T R O D U C T I O N.

1. The first step in the study of the thermal decompositions of solids is an examination of the kinetics, since this casts much light on the mechanism of the reaction. It must be borne in mind, however, that a theoretical expression, derived on the basis of a particular mechanism, even if it fits the observed experimental results, is not conclusive proof of the validity of the mechanism when applied to the decomposition under examination.

Many decompositions are of the type

$$A(s) \longrightarrow B(s) + C(g) \qquad \ldots\ldots \qquad 1.01$$

and the kinetics are best studied by plotting the variation of p, the pressure of gas released, against time, t. The curves thus obtained are generally sigmoid in character, and may be divided into induction, acceleratory, and decay periods. The nature of these divisions varies from substance to substance, and may be changed in some instances; for example, grinding prior to decomposition[1], or in the case of hydrates, scratching of the crystal surface[2], tend to accelerate the decomposition. In addition, pre-irradiation with high or low energy radiations may alter the characteristics of a decomposition. This point will be enlarged upon later.

Very often, the first-formed fragments of B may retain the molecular volume of the parent phase A and be accommodated within the lattice of A; larger fragments of B will however generally have a different specific volume, and local deformation of the lattice will

occur. The energy associated with this deformation is called "strain energy". Thermodynamic considerations[3] show that, as a result of this strain energy, very small fragments of B will tend to revert back to A, while larger fragments, above a critical size, are stable with respect to the reaction A $\longrightarrow$ B + C. Consequently, further reaction tends to take place at the boundary between the two solid phases A and B, rather than lead to a large number of submicroscopic fragments of B.

Thus if the free energy of activation of the interface reaction is less than that for nucleation, growth of existing nuclei takes precedence over the formation of new ones, and the product phase assumes the form of compact nuclei distributed in a matrix of A. This has been shown in work on nucleation and growth of nuclei in barium azide[4], and in investigations on certain salt hydrates[5,6].

If, however, the activation free energy for nucleus formation is not very different from the free energy of activation for growth, a large number of very small nuclei are formed, and will not be observable; but the absence of visible nuclei does not mean, conversely, that these two activation energies are approximately equal, since growth of nuclei may be confined to one or two dimensions, and though large, they may not be observed. This point may be decided by consideration of the equation describing the p/t plot; for instance if instantaneous nucleation of the whole crystal surface occurs, then the remainder of the reaction is governed by the rate of progression of the interface into the crystal.

Nucleation occurs when local fluctuations in lattice energy provide the necessary activation energy, and usually takes place on the crystal surface, where imperfections, such as dislocations or even

macroscopic scratches are most often found. It may also occur at lattice imperfections or defects within the body of the crystal.

Suppose the decomposition of a single molecule leads to the formation of a nucleus. The probability for such a unimolecular decomposition is

$$k_1 = \nu \exp(-\Delta G_1/RT) \quad \ldots\ldots \quad 1.02$$

where ν is the frequency of lattice vibration and ΔG_1 is the activation free energy for nucleus formation. Now

$$\Delta G_1 = \Delta U - T\Delta S + P\Delta V$$
$$= \Delta U - T\Delta S \quad \text{for condensed phases.}$$

This is rewritten as $\Delta G_1 = E_1 - T\Delta S$ 1.03

Hence $$k_1 = s_1 \nu \exp(-E_1/RT) \quad \ldots\ldots \quad 1.04$$

where s_1 is the entropy factor $\exp(\Delta S/R)$. If there are N_o potential nucleus-forming sites then the rate of nucleus-formation is

$$dN/dt = k_1 (N_o - N) \quad \ldots\ldots \quad 1.05$$

where N is the number of nuclei at time t. Integrating, and neglecting possible loss of nucleus forming sites by their ingestion by growing nuclei :

$$N = N_o [1 - \exp(-k_1 t)] \quad \ldots\ldots \quad 1.06$$

Substitution into 1.05 leads to

$$dN/dt = k_1 N_o \exp(-k_1 t) \quad \ldots\ldots \quad 1.07$$

This is known as the Exponential Law for nucleus-formation.
In the beginning of the reaction, especially if k_1 is small, expansion of the exponential term in 1.06 is permissible, and retention of only the first two terms leads to

$$N \approx k_1 N_o t$$

i.e. $dN/dt = k_1 N_o$ 1.08

Such a linear relationship between the number of nuclei formed and time has been found for the dehydration of copper sulphate pentahydrate[5] and for chrome alum[6], although in the later stages of reaction N increases more rapidly than required by equation 1.07.

It has been found in the dehydration of nickel sulphate heptahydrate that the number of nuclei increase as the square of the time, and in the decomposition of barium azide, as the cube of the time. This may be accounted for by assuming that several successive decompositions are necessary to form a stable nucleus. It has been shown[8] that if β successive events, each of probability k_1, are necessary, then

$$N = \frac{N_o (k_1 t)^\beta}{\beta!} = Dt^\beta \quad ..... \quad 1.09$$

Alternatively, a stable nucleus may result from a polymolecular process involving the combination of two or more active intermediaries, each being formed at a constant rate. If $\beta - 1$ intermediaries are involved, then once again the equation 1.09 results. Thus, in the decomposition of barium azide, there might occur three successive decompositions of the unimolecular type, or one process involving two active intermediaries. On energetic grounds, Thomas and Tompkins[9] reject the former idea, and suggest that instead a stable nucleus is formed by the combination of two F-centres, each formed by the decomposition of a trapped positive hole and adjacent excited azide ion.

Before considering the growth rates of nuclei, it must be mentioned that the above equations dealing with rates of formation of nuclei neglect the effect of ingestion of potential sites by growing nuclei.

This question will be considered later.

Suppose that r is a size parameter of the nucleus, being length in the case of one-dimensional growth, the radius of a circular nucleus or the side of a square nucleus in two dimensions, and the mean radius of any three-dimensional polyhedral nucleus. The expression for the fraction of material decomposed, α, at time t, is derived in the following manner:

Let the growth rate be described by a function G, not generally a constant; then the size of a nucleus at time t, which commenced growth at a time $t = y$ is determined by the parameter

$$r(t,y) = \int_y^t G(x)\, dx \qquad \ldots\ldots \qquad 1.10$$

The size of the nucleus is a funtion of this parameter, and is given exactly by:

$$v(t,y) = \sigma [r(t,y)]^{\lambda} \qquad \ldots\ldots \qquad 1.11$$

where $\lambda = 1$, 2 or 3 and σ is a shape factor. The total size of all nuclei is then:

$$V(t) = \int_o^t v(t,y) \left[\frac{dN}{dt}\right]_{t=y} dy \qquad \ldots\ldots \qquad 1.12$$

On substituting from 1.10 and 1.11 this becomes

$$V(t) = \int_o^t \sigma \left[\int_y^t G(x)\, dx\right]^{\lambda} \left[\frac{dN}{dt}\right]_{t=y} dy \qquad \ldots \qquad 1.13$$

If the forms of the functions G and dN/dt are known, then V(t) and hence α, may be calculated.

When nucleation proceeds according to a power law

$$dN/dt = D\beta t^{\beta-1} \qquad \ldots\ldots \qquad 1.14$$

- and growth -

and growth is normal, the effect of overlap between growing nuclei being ignored, then, if a constant growth rate $G(t) = k_2$ is assumed, it may be shown that

$$\alpha = C't^n \quad \ldots\ldots \quad 1.15$$

where C' is a constant and $n = \beta + \lambda$. Since $\alpha = p/p_f$, where p_f is the final pressure developed in a closed system,

$$p = Ct^n \quad \ldots\ldots \quad 1.16$$

The Power Law, as this expression is called, holds well for calcium azide[10], silver oxide[11], and aged mercury fulminate[12], where n = 3, and for barium styphnate monohydrate[10], dehydrated lead styphnate[10] and aged silver oxalate[13]. In the case of barium azide, a better fit is obtained by allowing for an initial slow growth[9], and 1.15 is modified to

$$\alpha = C'(t - t')^n \quad \ldots\ldots \quad 1.17$$

The Power Law does not hold for fresh preparations of silver oxalate[13] or mercury fulminate[4]. The large value of n obtained with this latter substance (11.2 - 22.8) led Garner and Hailes[14] to introduce the concept of nuclei as being linear branching chains. Assuming a constant rate of formation of new nuclei, and a constant branching coefficient, k_3, the net rate of nucleus production becomes

$$dN/dt = k_1N_o + k_3N \quad \ldots\ldots \quad 1.18$$

From this it may be shown that

$$p = C'' \exp(k_3t) \quad \ldots\ldots \quad 1.19$$

The Exponential Law, equation 1.19, holds up to $\alpha = 0.5$ for large crystals of lead styphnate[15], and for fresh preparations of silver oxalate[13] and mercury fulminate[12], up to $\alpha = 0.3$.

If the number of nucleus-forming sites is limited, linear nucleation must be replaced by exponential nucleation (equation 1.07); once again, however, equation 1.19 results, with a different constant C''. Again, if the nucleus-forming sites are rapidly exhausted, then 1.18 is replaced by

$$dN/dt = k_3 N \quad \ldots\ldots \quad 1.20$$

and again the Exponential Law results, with yet a different constant C''.

To-day, it is thought that the concept of branching linear chain needs some modification, since this mechanism would tend to separate the crystal into mosaic blocks which would decompose very slowly. Hence, branching plate-like nuclei, not subject to the same objection, have been postulated. This does not, however, affect the form of equation 1.19.

A serious objection to the chain theory proposed above is the neglect of possible interference between branching nuclei. Prout and Tompkins[16] overcame this objection in the mechanism which they proposed for the potassium permanganate decomposition. The resemblance of the p/t plots to the hyperbolic tanh function suggested the function

$$(p - p_i)/p_2 = \tanh [k/2(t - t_{max})] \quad \ldots\ldots \quad 1.21$$

to Prout and Tompkins. The point of inflexion has co-ordinates (p_i, t_{max}); p is the oxygen pressure at time t, and $p_2 = p_f - p_i$ where p_f is the final pressure in the closed system. Since t_{max} corresponds to the time of 50% decomposition, therefore

$$\exp k(t - t_{max}) = p/p_f - p \quad \text{or}$$

$$\log [p/p_f - p] = kt + C \quad \ldots\ldots \quad 1.22$$

where C = -

where $C = -kt_{max}$. Hence a plot of log p/p_f-p against t should be a straight line of slope k. Prout and Tompkins found this to be so for potassium permanganate; in general, however, two constants k were needed owing to the asymmetry of the p/t plot.

A theoretical discussion involving a branching plane mechanism leads to the same equation as to that proposed empirically for the reaction. There are assumed to be n_o nuclei present originally in the crystal. These nuclei are considered to be molecules of $KMnO_4$ whose decomposition is highly favoured i.e. whose decomposition is attended by a lower activation energy than that associated with the majority of reactant molecules, by virtue of their situation at lattice imperfections. The nuclei are considered to be mainly on the crystal surface, but may also be present in the body of the crystal. Decomposition of these nuclei and the strain associated with the interface between product and reactant leads to the formation of cracks perpendicular to the crystal surface; at the mouths of these cracks decomposition will be favoured, and the reaction in this way penetrates into the crystal. The coating of product on the surfaces of these cracks leads to the formation of crevices "perpendicular" to them, and in this way a branching-plane mechanism is responsible for the spread of reaction.

We thus imagine the electronic deformation produced on a permanganate molecule by an adjacent molecule to increase the likelihood of decomposition. If there are n such molecules at a time t, then the rate of increase of potentially reactant permanganate molecules is

$$dn/dt = n_o + \alpha n/\delta t \quad \ldots\ldots \quad 1.23$$

where δt is the average time interval between production and

decomposition of such molecules, and α is the probability of branching. Initially, branching is unhindered, but since there are many centres from which branching can originate, interference results as the reaction proceeds, leading to the termination of branching. If β represents the probability of interruption then 1.23 becomes

$$dn/dt = n_o + (\alpha - \beta)n/\delta t \quad \ldots\ldots \quad 1.24$$

In the simplest case $\alpha\phi = \beta$, and the solution of 1.24 depends on ϕ. Certain boundary conditions of ϕ are known; at $t = 0$ it is zero, and it is unity at the point of inflexion since after this the value of $(\alpha - \beta)$ must change its sign. This is satisfied by the quotient x/x_i, where x_i is the extent of decomposition at the inflexion point.

Since n_o may be considered small, and because the velocity of reaction $dx/dt = n/\delta t$, hence 1.24 becomes:

$$dn/dt = \alpha\left(1 - \frac{x}{x_i}\right) n/\delta t = dn/dx \cdot dx/dt \quad \ldots \quad 1.25$$

i.e. $$dn/dx = \alpha\left(1 - \frac{x}{x_i}\right)$$

or $$n = \alpha\left(x - x^2/2x_i\right) \quad \ldots\ldots \quad 1.26$$

Now $2p_i = p_f$, and because the pressure of oxygen is proportional to the extent of decomposition

$$dp/dt = kp\left(1 - p/p_f\right) \quad \ldots\ldots \quad 1.27$$

where $k = \alpha/\delta t$ and is a constant if α and δt are constant during this period. Equation 1.27 may be integrated between limits; thus if t_{max} is the time when $p = p_i = \frac{1}{2}p_f$ then:

$$k\left(t - t_{max}\right) = \int_o^{p_f/2} p_f \cdot dp/[p(p_f - p)] \text{ or}$$

$$p/p_f - p = \exp k(t - t_{max}) \quad \ldots\ldots \quad 1.28$$

- This is the -

This is the relation found experimentally.

This mechanism is considered to break down after the maximum velocity. After this, the rate-controlling factor becomes the number of unreacted permanganate molecules remaining, and this is proportional to $(p_f - p)$. Not all of these molecules are favourably situated for decomposition, and hence

$$dp/dt = k'(p_f - p)\gamma \quad \ldots\ldots \quad 1.29$$

where γ denotes the probability of a favoured situation. Prout and Tompkins assumed that γ is determined by the ratio of the number of product molecules to the total number of molecules present, i.e. by p/p_f. This has the desired property of approaching unity as $p \longrightarrow p_f$. Hence, during the decay period, i.e. after the inflexion point,

$$dp/dt = k'(p_f - p).p./p_f \quad \ldots\ldots \quad 1.30$$

which on integration between limits reduces to 1.28 except that k is replaced by k'.

In the case of silver permanganate[17], the Prout-Tompkins equation, equation 1.28, was found to hold only up to a value $x = 0.1$, and the decay period was fitted by the unimolecular decay law:

$$\log (p_f - p) = kt + C \quad \ldots\ldots \quad 1.31$$

Thus, the mechanism operating over the decay period is slightly different to that for the decay period of $KMnO_4$. The Prout-Tompkins equation holds for the latter, and in its derivation it is assumed that certain undecomposed molecules of $KMnO_4$ have a greater probability of decomposing (by virtue of their situation next to, and consequent

electronic deformation by, adjacent product molecules) than others. The unimolecular decay equation, on the other hand, is derived on the assumption that all molecules, in blocks of unreacted permanganate embedded in a matrix of the product, have an equal probability for decomposition.

Alternatively, it was found that a modified form of the Prout-Tompkins equation

$$\log [p/p_f - p] = k \log t + C \quad \ldots\ldots \quad 1.32$$

fitted the complete decomposition. This equation is derived on the assumption that the branching coefficient, α, is not a constant, but varies inversely with time.

In a recent paper, Tompkins[18] has elaborated on the mechanism involved in the decomposition of permanganates. The thermal process is thought to be dependent upon the critical stretching frequency required to break the covalent Mn - O bond, and not an electron-transfer process since neither U.V. irradiation nor electron bombardment accelerate the decomposition. This critical frequency is most easily attained at the crystal surface, and the reaction spreads two-dimensionally over the surface at a more rapid rate than it penetrates the crystal. The surface layer quickly becomes a region of high disorder, consisting of product and intermediate molecules, and this layer obstructs emerging dislocations, causing them to pile up. With this process is associated a build-up of stress, which, when it exceeds the cohesive strength of the crystal, causes cracks to develop. Although stresses may relax, and the fissures close up, it is thought that the gas formed by decomposition prohibits this. Propagation of the crack into the crystal takes place at the end of the

crack, since large stress magnification occurs here, and dislocations formed at the tip will tend to extend the fissure.

The Prout-Tompkins equation has been found to be applicable to many substances. It has been found to fit the decomposition of small crystals of mercury fulminate, although not with the same success as for $KMnO_4$. It also fits the decompositions of nickel formate[19], especially if it is spread, and the decomposition of lead oxalate[20]. Amongst the permanganate decompositions studied, it holds for rubidium permanganate[21,23] the acceleratory periods of barium[22] and lithium[24] permanganates, and the complete decomposition of sodium permanganate[24] (not including the induction period). Lastly, Simpson[25] et al, have found for small, rapidly grown crystals of ammonium dichromate that the modified Prout-Tompkins equation (1.32) gives a good fit over the autocatalytic acceleratory stage, while for carefully grown and selected crystals the original Prout-Tompkins equation

$$\log p/p_f - p = kt + C$$

gives the best fit. They attribute this to the fact that in well-formed crystals fewer reaction chains develop, and the constant branching rate would be expected, whereas in very imperfect crystals, a branching coefficient varying inversely with time would be much more likely.

Various other formulae[26] for fractions of material decomposed have been derived assuming different nucleation formulae followed by different modes of progression of reaction into the crystal. These include that class of decomposition in which a "contracting interface" mechanism is involved. In all these derivations, however, ingestion of potential nucleus-forming sites by growing nuclei is neglected. This

difficulty is overcome in the following manner. Those potential nucleus-forming sites which are incorporated by already growing nuclei are considered as "phantom" nuclei. Suppose N_o to be the total number of potential nucleus forming sites at time $t = o$; then the actual number of such sites, $N'(t)$, decreases with time both because $N(t)$ of them become active and develop as growth nuclei, and $N''(t)$ of them (the "phantom" nuclei) are ingested by the growth of the $N(t)$ nuclei. Hence the decrease in the number of sites in time dt is

$$-dN' = dN + dN'' \quad \ldots\ldots \quad 1.33$$

where $$dN = k_1 N' dt \quad \ldots\ldots \quad 1.34$$

and $$dN'' = N'(1 - \alpha)^{-1} d\alpha \quad \ldots\ldots \quad 1.35$$

Combination of these equations gives:

$$\frac{dN'}{dt} + kN' + \frac{N'}{1 - \alpha} \cdot \frac{d\alpha}{dt} = 0 \quad \ldots\ldots \quad 1.36$$

Integration yields

$$N' = N_o (1 - \alpha) \exp(-k_1 t) \quad \ldots\ldots \quad 1.37$$

and hence $$\frac{dN}{dt} = k_1 N_o (1 - \alpha) \exp(-k_1 t) \quad \ldots \quad 1.38$$

by equation 1.34. Integration of 1.38 then yields:

$$N(t) = k_1 N_o \int_o^t \exp(-k_1 y) \cdot [1 - \alpha(y)] dy \quad \ldots\ldots \quad 1.39$$

and, if the nuclei grow three-dimensionally:

$$\alpha = \frac{\sigma k_1 N_o k_2^3}{Vo} \int_o^t \exp(-k_1 y) (t - y)^3 [1 - \alpha(y)] dy \quad \ldots \quad 1.40$$

since the volume $v(t,y)$ at time t of a nucleus formed at $t = y$ is:

$$v(t,y) = \sigma [k_2 (t - y)]^3$$

In 1.40, V is the final volume of product obtained from complete

decomposition.

Equation 1.40 may be solved for the important case of random nucleation followed by the overlapping of nuclei. As the nuclei grow larger, they must eventually impinge on one another, resulting in cessation of growth at the point of contact. The problem of accounting for the fact that, when nuclei overlap the fraction decomposed is less than that calculated from 1.40, which neglects impingement, is overcome by introducing the concept of the "extended" fractional decomposition, α_{ex}. This represents the total fraction of the reactant which would have decomposed in time t, neglecting overlap between growing nuclei and including the contribution of phantom nuclei. The rate of formation of all nuclei, including phantoms, is -dN'/dt, obtained from

$$N' = N_o \exp(-k_1 t) \qquad \ldots\ldots \qquad 1.41$$

which equation is itself obtained from integration of 1.33 if the term dN'' is negligible. The extended fractional decomposition is now obtained by calculating the total extended volume of all nuclei (including phantoms) with the assumption that cessation of growth due to impingement does not occur. Hence:

$$\alpha_{ex} = \frac{1}{V_o}\int_o^t v(t,y)\left[\frac{dN'}{dt}\right]_{t=y} dy$$

$$= \frac{\sigma k_2^{\,3} k_1 N_o}{V_o}\int_o^t \exp(-k_1 y)\,.\,(t-y)^3 dy = \frac{V_{ex}}{V_o} \qquad \ldots \qquad 1.42$$

Avrami[27] has shown that in the case of completely random nucleation

$$\frac{d\alpha}{d\alpha_{ex}} = 1 - \alpha \qquad \ldots\ldots \qquad 1.43$$

Thus from equations 1.42 and 1.43:

$$\alpha_{ex} = \int_o^{\alpha} \frac{d\alpha}{1-\alpha} = \frac{\sigma k_2^{\,3} k_1 N_o}{V_o}\int_o^t (t-y)^3 \exp(-k_1 y) dy \qquad 1.44$$

- or -

$$\text{or} \quad -\log(1-\alpha) = \frac{6\sigma N_o k_2^3}{V_o k_1^3}\left\{\exp(-k_1 t) - 1 + k_1 t - \frac{(k_1 t)^2}{2!} + \frac{(k_1 t)^3}{3!}\right\} \quad \ldots\ldots \quad 1.45$$

In the decay period, when t is large, 1.45 reduces to

$$-\log(1-\alpha) = \frac{\sigma N_o k_2^3}{V_o} t^3$$

$$\text{or} \qquad \alpha = 1 - \exp\left[-\frac{\sigma N_o k_2^3}{V_o} \cdot t^3\right] \quad \ldots\ldots \quad 1.46$$

$$\text{i.e.} \qquad \alpha = 1 - \exp(-kt^3) \quad \ldots\ldots \quad 1.47$$

This last equation, derived independently by Erofeyev[28], has become known as the Avrami-Erofeyev equation.

The equations mentioned and derived in this section constitute the most important descriptions of thermal decompositions. In view of the fact that pre-irradiation, as mentioned earlier, very often affects the decomposition of solids, it is instructive to examine the effect of interaction of both electromagnetic and particulate radiations with solids, and the damage to the structure which may be caused. Such a study may lead to a clearer understanding of nucleus formation and growth in the decomposition of solids.

IRRADIATION EFFECTS IN SOLIDS.

The effects of irradiation with ultra-violet light, low-energy electrons and X-rays will be considered more or less collectively, as the energies associated with these radiations preclude any direct displacements, the processes involved during irradiation being mainly of the electronic type.

A great deal of the knowledge of the nature of damage to ionic solids arises from the voluminous research on the colour centres produced in alkali halides[29, 30] by the above radiations. Alkali halides on irradiation exhibit photoconductivity and on prolonged irradiation become coloured. Investigation of this phenomenon, and the subsequent annealing of the colour centres on thermal or photo treatment, has established that during irradiation, excitons, and more important, free electrons, and their accompanying positive holes, are produced. Absorption of light in the F-band of irradiated halides is now attributed to F-centres, whose nature has now been unequivocally established as being the combination of an anion vacancy plus trapped electron. In addition, various other plausible configurations of defects have been postulated to account for the F'-, F_2-, R-, V- and M- bands found in these crystals. Mechanisms for the migration of vacancies, and also F- centres[31], have been advanced, and estimations of activation energies of migration, and jump frequencies, have been made.

The azides constitute the most extensively studied group of compounds on which investigations have been made on the effect of ultra-violet and electron radiation on decomposition. Garner and Maggs[32] irradiated barium and strontium azides with ultra-violet light, and microphotographs taken show that more nuclei are produced in the irradiated than in the unirradiated salt on equal periods of heating after irradiation Short exposures of U.V. produce no metallic nuclei, and it is suggested that "a latent image is produced, which is made developable by heat treatment." Longer illumination produces metallic nuclei, and prolonged exposures ultimately cause decomposition to take place at room temperature.

Gurney and Mott[33] proposed a mechanism for the photochemical reduction of silver halides (in particular, AgBr, which exhibits photoconductivity) in photographic emulsions, and Mott[34] proposed a similar mechanism for the formation and growth of nuclei in barium azide. In the case of AgBr, an electron is raised, by absorption of a photon, from the bound state in a bromide ion to a conduction band of the salt, leaving behind a positive hole (neutral bromine atom). The potential barrier for this electron to move from one metal ion to another is small, and the electron travels through the crystal to be trapped eventually at an already present silver speck. The negatively charged silver now attracts interstitial Ag^+ ions, and in this way the specks grow. A similar electrolytic process was visualised for barium azide.

Later experiments[35] showed that barium azide exhibits no photoconductivity; on these grounds, free electrons and positive holes cannot be produced, and Thomas and Tompkins put forward the now generally accepted theory that excitons[9], rather than free electrons, were produced on irradiation. The bimolecular combination of excitons (excited azide ions) trapped at cation vacancies was proposed to account for the dependance of the rate of photolysis on the square of the intensity of irradiation.

The most recent reports[36, 37], where decompositions were carried out on barium azide for periods as long as seventeen hours, show that the theory of bimolecular exciton combination is too simple to account for the photolysis. In these experiments, radiation from both high-pressure (continuous wavelengths, with the principal mercury lines superimposed) and low pressure (short wavelengths, predominantly the 2537 Å line of mercury) arcs were used to photolyse the salt. It was found

that for both lamps, the rate of decomposition at first fell slowly, then reached a minimum, and finally accelerated and then attained a constant value. If the high pressure lamp was filtered so as to pass wavelengths between 2400 and 4200 Å, it behaved like the low pressure lamp; the rate of photolysis varied in the same way with time, and varied with the second power of the intersity, I. If however, radiation below 3500 Å was totally excluded, then the rate of photolysis of fresh salt was much lower initially, and the rate of photolysis of salt pre-irradiated with the full arc into the constant rate period, varied as the first power of I.

The acceleratory process is attributed to a second mechanism coming into operation once substantial photolysis, and hence production of barium metal, has occurred. The following mechanisms are proposed to account for the complete photolysis. Light of wavelength 2537 Å (approximately) is absorbed in the tail of the first absorption band (previously thought to be an exciton band, but now considered to be rather an internal transition[38] of the azide ion). The excited azide ion, if adjacent to a special site, or "trap", may combine with an adjacent excited azide ion yielding nitrogen and two electrons, which are taken up by a Ba^{++} ion in the vicinity of the reaction, thus forming barium metal. The deceleratory process observed initially is due to the gradual consumption of such traps (considered to be either impurity atoms, or anion vacancies, or jogs in dislocations). Since the reaction involves two activated species, the rate will be proportional to the square of the intensity.

The acceleratory process involves firstly, the ionisation of a

barium atom, giving an electron into the conduction band of the crystal. Simultaneously, an electron is transferred from an adjacent azide ion giving a positive hole. Excited azide ions produced simultaneously by irradiation then react with the positive holes giving nitrogen and two electrons, which latter again combine with a barium atom. This reaction will proceed in a self-propagatory manner until such time as the barium can no longer be regarded as atomic i.e. the small groups of barium atoms formed at some stage reach a size large enough for recrystallisation to occur, and the metal specks formed have energy levels which are the same as for the bulk metal.

With light of longer wavelength (> 3500 Å), the bimolecular decomposition of two excited azide ions occurs with only a low efficiency, explaining the relatively low initial rate of photolysis. However, if the salt is first decomposed into the constant rate period, so that more barium pre-nuclei are present, then positive holes are produced faster than excited ions, because the photo-ionisation of Ba is more efficient than excitation of the internal transition, at longer wavelengths. The rate of supply of excited azide ions then becomes the limiting factor, and the energy for this excitation comes from the thermal energy of the lattice. Moreover, the rate depends on the first power of the intensity, since only the concentration of positive holes is proportional to the intensity.

The photolysis of potassium azide[35] is analogous to that of barium azide. It seems likely, therefore that the mechanism of decomposition is the same for both azides. It was noted that ultra-violet irradiation did not affect the subsequent thermal decomposition of KN_3, but the crystal did become coloured. It was thus concluded that after irradiation, potassium

azide contained anion vacancies, F-centres, and positive holes.

Maggs[39] subjected strontium azide to radium emission before decomposition. There was a three-fold increase in the acceleration coefficient and a reduction in the length of the induction period. Garner and Moon[40] found that nuclei formed on barium azide were similar in normal and radium-accelerated thermal decompositions, but that nuclei formed on the crystal face nearest the radium source were larger than on other faces. Garner et al[41] suggested that nuclei do not spread uniformly through the solid but that progress is hindered at grain boundaries. The reaction may however spread from grain to grain by way of suitable bridges, and the effect of radium emission is to remove hindrance of passage from grain to grain. McDonald[42] irradiated silver oxalate with ultra-violet light and in this compound finds no evidence of a spread from one particle to another. The decomposition, as shown by a gradual darkening in colour, starts simultaneously in all particles.

Prout and Tompkins[43] found a surface effect in mercuric oxalate pre-illuminated with ultra-violet light. The illumination alters only the initial part of the decomposition. Cathode rays accelerated through 10 - 30 kV had the same effect; a beam of 50 mA accelerated through 50 v caused no acceleration in the subsequent decomposition, but during bombardment a loss of mass and a large evolution of gas was found. They suggest that on irradiation, an electron is freed from the surface and trapped at a mercury "ion" in the second layer. This electron transference, followed by an intramolecular change, results in the formation of mercurous oxalate, which salt is more rapidly decomposed on thermal

treatment than is the mercuric salt. With the high electron beam of 50 mA, groups of molecules at the surface are detonated, explaining the loss of mass and evolution of gas.

Silver oxalate has been examined by Benton and Cunningham[44] and by Tompkins[45]. The photolysis has been explained by the absorption of quanta forming free electrons and positive holes; if some electrons are trapped on silver atoms adjacent to the corresponding positive holes for a short period, the concentration of such sites will be proportional to the intensity. Most of the free electrons recombine with positive holes so that the concentration of free electrons is proportional to the square root of the intensity. Decomposition occurs when a free electron is trapped at a site giving (COO^-) Ag (COO) Ag, which breaks down by electron transference to give silver atoms and an oxalate radical. This process would result in a rate proportional to the 1.5 power of the intensity; the fact that the actual power observed is 1.67 is explained by the additional trapping of electrons by silver atoms.

Decomposition has been observed by electrons in the case of potassium chlorate[46] (22 volt electrons), oxalic acid[47] (6 eV electrons) and sodium azide[48]. Groocock and Tompkins[49] studied the effects of electron bombardment on solid azides. In the case of barium azide, they concluded that bombardment involved electron ejection into the conduction band, or photoelectric emission to form positive holes, which latter capture electrons from the primary beam or from surrounding F-centres.

Bowden and Singh[50] irradiated explosives with both X-rays and high energy electrons, as well as with neutrons and fission fragments

from U^{235}. They found that X-rays produced metallic nuclei in lead and silver azides, and that the decomposition of lithium azide, at a temperature low enough to prevent explosion, had its induction period shortened by pre-irradiation. Sodium azide[51] decomposed under X-ray bombardment with a rate proportional to the intensity, indicating single trapped excitons. Potassium perchlorate[52], under X-ray irradiation, turned golden-brown, and after prolonged irradiation, decrepitated violently. Oxygen gas was liberated on solution; the mechanism proposed was that excitons were produced and trapped at imperfections. Bimolecular conbination of two excitons yielded oxygen and two chlorate ions.

Having examined the effects of low energy radiation on solids, the effects of high energy radiations will now be reviewed. These comprise neutrons, protons, relativistic electrons, and gamma-rays, this latter category including the very shortest X-rays. In this energy range, actual displacement of atoms or ions from lattice sites into interstitial positions is possible; Seitz and Koehler[53] have estimated that the minimum energy necessary for displacement of atoms into interstitial positions is of the order of 25 eV for most materials. The energy of neutrons varies from about 2 MeV for fast neutrons to 0.025 eV for "thermal" neutrons. Fast neutrons produce damage mainly by collision processes, when target atoms are knocked out of place. Neutron capture by atomic nuclei is almost negligible for neutrons with energies greater than 0.1 MeV, so that this process is limited mainly to thermal neutrons, and occurs when materials of suitable capture cross-section are irradiated with such netrons, as, for example, the (n, α) reactions of boron and lithium. If the transmutation product is stable, then this process is

- tantamount -

tantamount to the introduction of impurity atoms; if however, it is unstable, then gamma-rays of capture and decay are emitted. The atom involved in such a process may be given sufficient recoil energy to displace it into an interstitial position.

When a fast neutron "collides" with a nucleus it transfers energy to that nucleus. If the energy imparted is above a certain threshold value, then a primary knock-on is formed, which ploughs a track through the material. Kinchin and Pease[54] have analysed the interaction of such a charged knock-on, the analysis being based on the following assumptions: (i) That the knock-on loses energy entirely by ionisation until its kinetic energy falls below the limiting energy for ionisation, E(i), given by

$$E(i) = 1/8\ (M/m)\ I \qquad \ldots\ldots \qquad 1.48$$

where M = mass of the moving knock-on, m = electronic mass, and I = lowest electronic excitation energy. (ii) That all knock-ons with kinetic energy less than E(i) lose energy by elastic collisions, in which they behave like billiard balls, with lattice atoms; and (iii) that an atom will be displaced from its lattice site by collision only if it receives kinetic energy greater than some threshold energy. The outcome of this theory is that a cascade of displaced atoms is produced, and that the damage is most dense at the end of the ion track.

Alternative models for the displacement of atoms are offered in the displacement-[55] and thermal-[56] spike theories of Brinkman and Seitz respectively.

Flanagan has investigated the effect of γ-ray[57] and neutron[58] bombardment on the thermal decomposition of lead styphnate. Gamma-rays

(1.8×10^8 r) had no apparent effect, but neutrons shorten the induction period, and greatly enhance the acceleratory processes of the thermal decomposition. The total neutron flux is the important quantity, not that flux associated only with fast or with slow neutrons. On the basis of irradiation and decomposition experiments with both the monohydrate and with the dehydrated salt, he concludes that radiation damage is the alteration of styphnate units rather than displaced ions and vacancies. Damage due to the reaction $N^{14}(n,p)\ C^{14}$ and to fast neutrons apparently have the same efficiency.

The effect of reactor irradiation on the thermal decomposition of silver oxalate[59] has been investigated recently. An effect was obtained after annealing for an hour at 80°C; the irradiation increased the rate of the acceleratory period, but did not affect the decay period. No explicit mechanism was proposed, but it was suggested that γ-rays created electron traps, while fast neutrons created "germ" nuclei.

As mentioned before, electrons of sufficient energy to produce displacement are in the relativistic range. Since, for electron energies in excess of the threshold value necessary for displacement, displacement cross-sections are very small, and since electron/target-atom collisions are heavily biased toward small energy transfer, knock-ons produced will seldom have sufficient energy to produce secondaries. Thus the damage due to high energy electrons consists mainly of isolated pairs of vacancies and interstitials.

Gamma-rays traversing matter may impart kinetic energy to target nuclei, but most will transfer energy to the individual electrons of the target. It has been shown[60] that some of the Compton and photoelectrons

produced by γ-rays may exceed the threshold value for displacement, and the disordering by γ-rays of Cu_3Au and germanium[61] has been observed. Damage in the form of isolated vacancies and interstitials, will be distributed evenly throughout the solid, as the absorption of γ-rays is small enough to ensure this.

Seitz[62] has proposed another mode of interaction of γ-rays with matter. Localised regions of electronic excitation (excitons) are produced, which travel through the solid until they encounter a lattice imperfection, such as a jog in a dislocation line, when they discharge their energy to the lattice as thermal energy. Heating at such jogs can induce the production and boiling off of vacancies. Also, free electrons and positive holes created by irradiation may recombine and release the associated energy.

The effect of X-ray and γ-ray bombardment on the thermal decomposition of ammonium perchlorate has been studied by Anderson, Freeman and Campisi[63]. The greater initial and maximum rates of reaction as a result of pre-irradiation were attributed to the presence of electronic defects in the form of positive holes. In comparison with the unirradiated perchlorate, which underwent a surface reaction followed by a contracting interface reaction, opaque nuclei formed in the body of the crystal during irradiation grew in size on subsequent thermal treatment.

Prout[64] studied the effect of pre-irradiation with γ-rays from a spent fuel facility and from a Co^{60} "hot-spot" on the thermal decomposition of potassium permanganate. He observed, with increasing irradiation doses, a progressive shortening of the induction period and an acceleration of the reaction. Violent physical fracturing was observed during

the early stage of the acceleratory process; moreover, the effects with pre-irradiated ground crystals were similar to those for whole crystals except that after a certain critical dose, the length of the induction period remained constant, i.e. a saturation effect was observed. A similar effect was obtained with silver permanganate.

The theory proposed to account for the damage is outlined below. Potassium (or silver) ions were considered to be displaced from their lattice sites into interstitial positions as a result of collisions with Compton electrons generated by γ-rays. Damage was envisaged as isolated vacancy/interstitial pairs, randomly distributed in the crystal, with vacancies separated from interstitials by about four or five interatomic distances. Subsequent thermal treatment caused the recombination of vacancies and interstitials, the accompanying release of Wigner energy creating a "decomposition spike". Kinchin[65] reports a release of 10 eV on recombination of an interstitial carbon atom and vacancy in graphite, so that the suggested release of energy in the permanganates is quite feasible. During the induction period annealing takes place, and the number and size of the centres of decomposition increase; the strain on the parent lattice accompanying this process leads to the fracture at the end of the induction period. The saturation effect found with ground crystals is due to the fact that grinding itself causes vacancies, so that a point will be reached in the γ-irradiation when instantaneous annealing of the displaced atoms will occur.

Activation energies for the process occurring during the induction period, namely 1.31 eV for $KMnO_4$, and 1.09 eV for $AgMnO_4$, indicate the migration of vacancies. This order of magnitude is comparable with

those obtained for vacancy migration in cold-worked copper[66] and molybdenum[60].

Subsequently, a study was made of the effect of γ-rays on the thermal decompositions of rubidium permanganate [21], and barium permanganate[22], and the permanganates of lithium, sodium and caesium[24]. All showed irradiation effects, but the magnitude of the effects on lithium and barium permangantes were relatively less than for the other permanganates examined. If a constant displacement energy is assumed, the density of displaced cations, and consequently the irradiation effect, should depend on the atomic weight of the cation. However, comparison of the effects on the permanganates of the alkali metals Na, K, Rb and Cs show that no such systematic variation with increasing atomic weight is evident; the effect with $NaMnO_4$, for example, is of comparable magnitude to that with $CsMnO_4$.

For reactor γ-rays, and γ-rays from cobalt and fission products, the Compton effect has the largest cross-section[67]. Also, it has been shown[68], that for γ-rays of 1 MeV or less the number of atoms displaced per cm^3 per second is a maximum for the very light elements, and declines very rapidly with increasing atomic number until it becomes zero for 1 MeV γ-rays and a displacement threshold of 25 eV, at atomic weight 125.

Thus, the original suggestion that the irradiation effect is primarily due to cations displaced by Compton electrons is invalidated. Prout has suggested, however, that the displacement mechanism proposed by Varley[69] would account very well for the irradiation effects in the permanganates. This mechanism applies to highly ionic compounds: during irradiation, some of the negative ions may be stripped of electrons and

become temporarily positively charged. These ions, now positive, may be ejected into interstitial positions by Coulombic repulsion of the surrounding cations, after which they may regain electrons and attain their original charge. For such a mechanism to operate in an ionic compound, it is necessary that the cross-section for multiple ionisation be large, and that the recombination time for the electrons must be long enough to allow the stripped ion to attain its interstitial position, and finally, that the interstitial go far enough to be stable against its immediate return on regaining electrons.

Alternatively, a cation may be ejected from its position adjacent to a multiple ionised anion. Durup and Platzman[70] have shown that multiple ionisation of a K^+ ion in KCl, if ionised by ejection of an L_1 electon, followed by an intramolecular Auger cascade, results in a mean final charge, in units of electronic charge, of 5.4. Even for less tightly bound electrons in the M-shell, the mean final charge is 2.

Prout considers that the multiple ionisation of permanganate ions is more probable than that of the cation, because of the larger number of atoms exposed to γ-rays. Examination of a model of several unit cells of $KMnO_4$, shows, however, that spatially, the cations have greater freedom of movement than the permanganate anions; this will be rendered even greater by the reduction in ionic radius accompanying multiple ionisation[71]. Consequently, Coulombic repulsion results in interstitial cations and cation vacancies. This mechanism offers an explanation which is far more consistent with the experimental results than the former.

The small effect in $Ba(MnO_4)_2$ is considered to arise from the ability of the product to accommodate itself in the parent lattice.

The absence of an effect in $LiMnO_4$ except after very heavy doses may emphasize the importance of simultaneous multiple ionisation of anion and cation in producing damage, as it has been shown by Durup and Platzman that Auger cascades in lithium ions in LiF are not possible, and it is very likely that the same applies to Li^+ ions in $LiMnO_4$.

Prout and Herley report that the decomposition of lead oxalate[72] is accelerated by γ-ray bombardment, and suggest a mechanism of damage similar to that proposed for the permangantes. Silver oxide[73], however, shows no effect on pre-irradiation with either thermal or fast neutrons or Co^{60} γ-rays, and Prout suggests that those substances likely to be affected in the same way as the permanganates will be those decomposing according to a branching-chain mechanism, and containing a simple metal cation. Also, decomposition spikes produced should create sufficient strain to fracture the crystal and create new reactive surfaces. Simpson et al[74] have irradiated ammonium dichromate with γ-rays, and found no substantial effect; this may either be in accordance with Prout's suggestion, in that the ammonium radical is complex and unwieldy and hence resists displacement, or it may be that the intensity of radiation used, stated to be small, was insufficient to have any pronounced effect. Only further work on ammonium dichromate would resolve this ambiguity.

THE APPLICATION OF X-RAY AND ELECTRON DIFFRACTION TO THE STUDY OF THERMAL DECOMPOSITIONS, AND THE DETECTION OF RADIATION DAMAGE IN SOLIDS.

There is not a great deal of literature on the use of diffraction methods to follow the course of thermal decompositions in solids. However, some of the more important research in this field will be described.

The decomposition of silver oxalate has been studied, using X-ray diffraction, by Griffith[75]. He finds that the silver formed is polycrystalline and exhibits preferred orientation, which he suggests may be due to the orientating influence of the undecomposed oxalate lattice.

Burgers et al[76] have studied the reduction of solid K_2PtCl_6, K_2PtCl_4 and $(NH_4)_2PtCl_6$ by hydrogen, using X-rays. Breakup into slightly disorientated bloaks is found in K_2PtCl_4 as the reduction proceeds, and in this salt and in K_2PtCl_4 the KCl and platinum formed are both polycrystalline and exhibit preferred orientation, as shown by the intense arcs formed on the Debye-Scherrer rings produced during decomposition. The ammonium salt yields NH_4Cl and platinum; in this case the chloride formed volatilises and the platinum is found to have only a weak texture. It is suggested that the chloride formed in the case of the potassium salts may have some orientating influence on the platinum.

Sawkill[77] has decomposed silver azide in the beam of an electron microscope and followed the decomposition in this manner. Electron micrographs taken show an increase in the density of the silver specks formed during decomposition, rather than an increase in their number, as the reaction proceeds. Two forms of silver are produced; some is randomly oriented as shown by diffraction rings, and the rest is highly oriented as shown by the intense arcs on the rings.

Similarly, Goodman[78] has decomposed magnesium hydroxide in an electron microscope beam. Decomposition occurs in a highly ordered manner; electron diffraction photographs show that the cubic MgO formed has its [111] direction and $[\bar{1}10]$ direction parallel to the [0001] and $[01\bar{1}0]$ directions of the hexagonal $Mg(OH)_2$, respectively. The accompanying

- figures show -

The accompanying figures show the structure of $Mg(OH)_2$ seen at right angles to [001], of the intermediate structure, and finally that of MgO, also at right angles to [111].

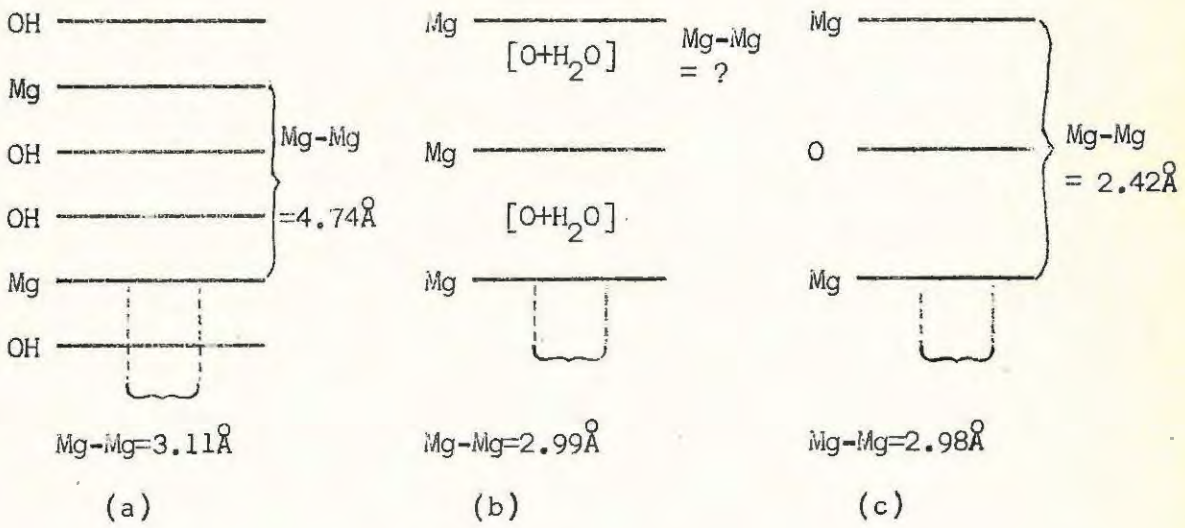

FIG 1.1.

The conversion requires that half of the hydroxyl groups between two adjacent magnesium sheets combine with the hydrogens of the other half to be expelled as water molecules. The Mg-Mg distance in the hexagonal sheets of magnesium atoms changes from 3.11Å to 2.98Å and the distance between these sheets from 4.74 to 2.42Å. The diffraction patterns show that this occurs in stages. During the first stage, the a spacing for a hexagonal system changes from 3.12Å to 2.99Å. This corresponds to a change in the Mg-Mg distance in the basal plane from 3.12Å to 2.99Å, exactly that required in the [1$\bar{1}$1] plane of MgO. The structure is then represented as in (b). Further decomposition results in a gradual decrease in intensity of the inner spots until they finally disappear, leaving only the reflections due to MgO. This is interpreted as a reshuffle of the (0001), or (111), planes until theyhave the order and

dimensions between them required for MgO.

Most inorganic nitrates decompose giving nitrite and oxygen on exposure either to γ-rays[79] or X-rays[80]. X-ray diffraction photographs taken by Cunningham and Heal[80] show that a nitrite ring is formed in the KNO_3 photograph only after 8 - 17 % decomposition by X-rays, and they conclude that nitrite is formed initially not at localised sites, in concentrations sufficient to give a diffraction pattern, but as single nitrite ions. This conclusion is borne out by infra-red absorption measurements made by these investigators.

The thermal decomposition of ammonium dichromate[74] has been studied with the aid of X-ray diffraction. During the early stage of the reaction the crystals become coloured a deep red; X-ray photographs show that this is not due to a polymorphic transformation. The final black solid obtained at 195.5°C is amorphous to X-rays; after treatment at 385°C, X-ray photographs show that chromium is present at Cr_2O_3.

X-ray diffraction, as a means of detecting radiation damage to solids, has been used far more extensively than in examining thermal decompositions. Changes in lattice parameters are a general feature in neutron-irradiated substances, and may be determined by precision X-ray measurements. Lattice expansions have been observed in diamond, silicon carbide, and magnesium oxide by Tucker and Senio[81]. They point out that defects produced by irradiation are most stable in crystals where tight binding is prominent, there being no effects, for example in germanium or silicon. This is because the activation energy for defect migration in metallic substances is low, and at room temperature they are not given any chance to accumulate, but anneal out immediately. Copper

crystals[82], for example, show X-ray effects only when irradiated and photographed at 12°K.

Crawford and Wittels[83] have found anisotropic changes in the lattice parameters of quartz, beryl, chrysoberyl and zircon. They conclude that bombardment effects in these substances are primarily dependent on crystal structure, the nature and distribution of "free space" in the structure influencing the distribution of defects. In silica-like structures the basis is of linked SiO_4 tetrahedra, and oxygen atoms need only be displaced 1Å to be trapped at interstitial "cages". The results with zircon are of particular interest; after an irradiation of 3×10^{20} neutrons, anisotropic expansion results, along with the breaking up of the crystal into mosaic blocks disorientated by greater than 3°. Laue transmission photographs show the formation of extra reflections probably due to the scattering by interstitials and vacancies residing at preferred positions. These effects are found to anneal out almost completely at 1600°C.

Neutron damage to graphite[84, 65], in view of its importance as a moderator, has been extensively studied. It is found that the lattice expands and shrinks in the c_o- and a_o- directions respectively, the distortion being due to the anisotropic displacement of carbon atoms by impinging fast neutrons. The pronounced effect in graphite is undoubtedly due to the highly anisoptropic nature of the layered carbon lattice. Broadening of X-ray peaks occurs, owing to the bending and slipping of crystal planes as the crystallites break up. These effects anneal out on subsequent heating, with an accompanying release of a large amount of stored energy.

- In diamond -

In diamond irradiated with 3.8×10^{20} fast neutrons, Levy and Kammerer[85] have found a very diffuse pattern resembling that of a liquid[86], and it has been shown[87] that this effect would result if about one half of the atoms had been displaced, thus causing extreme distortion of the structure. This state of affairs closely resembles that found in the metamict minerals[88], which have been rendered completely amorphous by radiation from radioactive minerals in close proximity over geological periods of time, yet have retained their external morphology.

Another effect which may be induced by irradiation is an allotropic phase charge. Black phosphorus[89], in addition to the change in c-parameter produced by interstitials, shows extra lines on the diffraction pattern after reactor irradiation due to the formation of the red allotrope. In white tin[90], irradiation exposures of 10^{18} nvt at liquid nitrogen temperature drastically accelerated the subsequent change to the grey modification on heating, yet X-ray pictures show that irradiation itself did not cause any transformation. It has been suggested that the strains set up around interstitials may act as embryos for nucleation, or that possibly thermal spikes associated with knock-ons may take minute volumes of material into a temperature region where nucleation may be initiated.

As a result of fast-neutron bombardment of about 10^{20} nvt at $100^{\circ}C$, monoclinic zirconia (ZrO_2) was transformed to the cubic phase[91], normally stable only above $1900^{\circ}C$. However, it appears that this change is complicated by the prescence of impurities, as high-purity specimens would not transform under irradiation.

- Another effect -

Another effect which may show up in X-ray diffraction patterns arises as follows: an interstitial atom in an otherwise perfect lattice gives extra scattering distributed in angle according to the atomic scattering factor, f. Vacancies on the other hand, are identical to normal scattering centres with negative scattering power. In low concentration, the diffraction effects of vacancies and interstitials (caused for example by irradiation) may be calculated. If there are n_i interstitials and n_v vacancies, the background scattering will be increased by an intensity

$$I \approx (n_i + n_v)f^2 \qquad \ldots\ldots \qquad 1.49$$

The intensities of the Bragg reflections are lowered by an equal amount[92].

Interstitials and vacancies also cause distortion of the lattice; in metals, vacancies act as centres of contraction, whereas interstitials give rise to a slight expansion. In ionic crystals both act as centres of expansion. This distortion of the lattice gives rise to diffraction effects over and above the abovementioned. To understand this, it is necessary to consider the effect of thermal vibrations of atoms on the intensities of X-ray beams.

Because the frequencies of vibration of atoms are very much less than X-ray frequencies, the rays, on entering a crystal, "see" the atoms displaced from their mean positions at any instant. This results in an increase in incoherent scattering and a corresponding diminution of the intensities of the Bragg reflections. In inorganic substances this effect is not pronounced except at high temperatures, but in organic crystals, where the amplitudes of vibration of the constituent atoms

are large even at ordinary temperatures, there is a severe cut-off in intensities from a Bragg angle of 50-60°. The ratio T, of the actual intensity, to that which would be observed were there no thermal motion is

$$T = \exp\left[-2B\,(\sin\theta/\lambda)^2\right] \quad \ldots\ldots \quad 1.50$$

where B is a constant for a given crystal depending on the mean square amplitude of vibration, θ the Bragg angle, and λ the X-ray wavelength[93]. Huang[94] has shown that in a monatomic lattice treated as an isotropic elastic continuum, departing from perfection only in containing a random distribution of point defects each acting as a distortion centre according to the equation of classical elasticity theory

$$u = c/r^2 \quad \ldots\ldots \quad \ldots\ldots \quad 1.51$$

then an artificial temperature factor of the form exp (- 2M) arises. (u is the displacement of an atom distant r from an imperfection characterised by the "strength" c.) This factor is of the same form as the temperature factor T discussed. In addition, Huang finds a slowly varying background intensity

$$I = Nf^2\,[1 - \exp(-2M)] \quad \ldots\ldots \quad 1.52$$

where N is the number of atoms, and M a constant. Finally, the theory predicts a diffuse scattering to arise in the neighbourhood of the Bragg directions. This "Huang" scattering is distributed around the reciprocal lattice[95] point in the form of a lemniscate whose axis is parallel to the line from the origin to the reciprocal lattice point and whose centre is the reciprocal lattice point.

The Huang analysis is equally valid whether the pressure centres are on lattice sites or not, and this renders it readily applicable to the radiation damage situation where the pressure centres are vacancies

and interstitials, in low concentration and randomly located. It must be noted, however, that the three Huang effects are superimposed on the lattice expansion generally found, and on the effects due to the vacancies and interstitials themselves, apart from the distortion they produce. Also, the Huang analysis breaks down in the case of damage of the very extreme type. It will be noticed that the theory predicts no broadening of the Bragg reflections; in very badly damaged graphite and lithium fluoride[96] this latter effect becomes apparent.

Tucker and Senio[97] have interpreted their results with neutron-irradiated boron carbide on Huang's model: Boron carbide has a hexagonal unit cell; the boron atoms form icosahedra and the carbon atoms lie in chains of three parallel to the c-axis. Each central carbon is attached only to the two end carbons, and these in turn are each bound to three boron atoms.

Single crystals of boron carbide were subjected to doses of 6.4×10^{18}, 1.4×10^{19} and 3×10^{20} neutrons/cm^2. These irradiations correspond to burnups of 0.4, 0.8 and 15% of all the atoms present (due to the reaction $B^{10}(n,\alpha)\ Li^7$) respectively. The most striking features produced are shown in Laue patterns of single crystals; there is a gradual decrease in intensity of the Laue spots, and an increase in that of the diffuse scattering surrounding the reciprocal lattice points with increasing dose. Examination of the zero-level Weissenberg pattern showed that the changes in Bragg intensities were of two types. Firstly, there was a strong, highly anisotropic (six times greater in the c-direction than in the a-direction) artificial temperature factor present. In addition, a few moderate or weak reflections, particularly the ($\bar{2}02$

reflection, had actually increased in intensity, showing that, in addition to the artificial temperature factor, there were actual changes in the parameters of the atoms, due to irradiation. Also, it was found that, for the heaviest irradiation, the c-axis contracted by 1.38%, while the a-axis expanded 0.89%.

Fourier profiles were drawn for the irradiated and unirradiated crystal, the sections being placed on an equal basis by setting the intensities of the (201) reflection, the strongest, equal, for the irradiated and the unirradiated specimen. Comparison of the areas under the peaks for the central carbon atom showed that 47% of the central carbon atoms had been removed by irradiation. Further, the two end carbons had been each displaced 0.12Å toward the central carbon atom, while the boron atoms attached to the end carbons were displaced 0.06Å in the same direction. The changes were interpreted as follows: owing to collisions, central carbon atoms occasionally were knocked out of equilibrium position into interstitial positions. On other occasions, the end carbons were similarly dislodged. However, when an end carbon is removed, the central carbon to which it is attached moves into approximately the position previously occupied by the end carbon, where it can bond with the surrounding borons rather than remain bonded to a single carbon. The considerable attraction between the end carbons causes them to be displaced 0.12Å toward each other and to pull the borons to which they are attached, with them.

The strong diffuse scattering after 3×10^{20} neutrons cm^{-2} is not due to a degradation of the lattice-vibration spectrum to lower frequencies, as they were unable to decrease the intensity of such scattering

by photographing at liquid nitrogen temperature. The diffuse scattering was thus attributed to static lattice defects. Annealing of these defects was found to occur in the range 700-900°C along with the accompanying disappearance of the X-ray effects.

These examples show the method of approach to the investigation of changes occurring in solids, either due to thermal decomposition or radiation damage.

2. PREVIOUS WORK ON SILVER PERMANGANATE.

The space group and unit cell size of $AgMnO_4$ were first determined by X-ray methods by Büssem and Herrmann[98]. These were checked subsequently when Sasvari carried out a "direct" crystal-structure analysis[99].

The unit cell is monoclinic, and the structure has been described as being similar to a deformed $BaSO_4$ structure. The unit cell contains four "molecules" of $AgMnO_4$, and its dimensions are: $a = 6.65$ Å, $b = 8.27$ Å, $c = 7.127$ Å, while the angle β between the a- and c-directions is 92° 29.5'. All atoms are in general positions of the space-group $P2_1/n$, namely (e) $\pm (x,y,z;\ x + \frac{1}{2}, \frac{1}{2} - y, z + \frac{1}{2})$, and the parameters of the atoms, as determined by direct methods, are as tabulated:

		x	y	z
Ag	(e)	.25	.31	.34
Mn	(e)	.25	-.03	-.31
O(1)	(e)	.25	-.103	.456
O(2)	(e)	.25	.175	.605
O(3)	(e)	.02	-.068	.750
O(4)	(e)	.48	-.068	.750

A Fourier analysis carried out later[100] by Sasvari enabled him to refine the parameters of the silver and manganese atoms as follows:

	x	y
Ag	.25	.323
Mn	.25	-.033

The Fourier synthesis does not, however, provide dependable results with respect to the positions of the oxygen atoms because the lighter atoms become blurred in projection, particularly if they are of larger diameter than the heavier atoms.

The resulting MnO_4 tetrahedra are distorted, and have Mn - O distances between 1.48 Å and 1.86 Å. Each silver atom has two oxygen neighbours at ca. 2.21 Å and four more at distances between 2.58 Å and 2.72 Å. The accompanying projection on (001) (Fig 1.2) is drawn from these specifications.

The thermal decomposition has been studied by Prout and Tompkins and the mechanism proposed for decomposition is similar to that for $KMnO_4$. The p/t plots are fitted by the modified Prout-Tompkins equation[17]

$$\log p/p_f - p = k \log t + c \quad \ldots\ldots \quad 1.32$$

or the original Prout-Tompkins equation[1]

$$\log[p/p_f - p] = kt + c \quad \ldots\ldots \quad 1.22$$

The equation

$$\log (p - p_f) = kt + c \quad \ldots\ldots \quad 1.31$$

however gives a better fit over the decay period[1].

Prout and Tompkins found that neither pre-irradiation with ultra-violet light nor pre-bombardment with 20 kV electrons affected the subsequent thermal decomposition. Prout and Sole[1] found that a spectacular effect is produced by neutrons or γ-rays; the induction

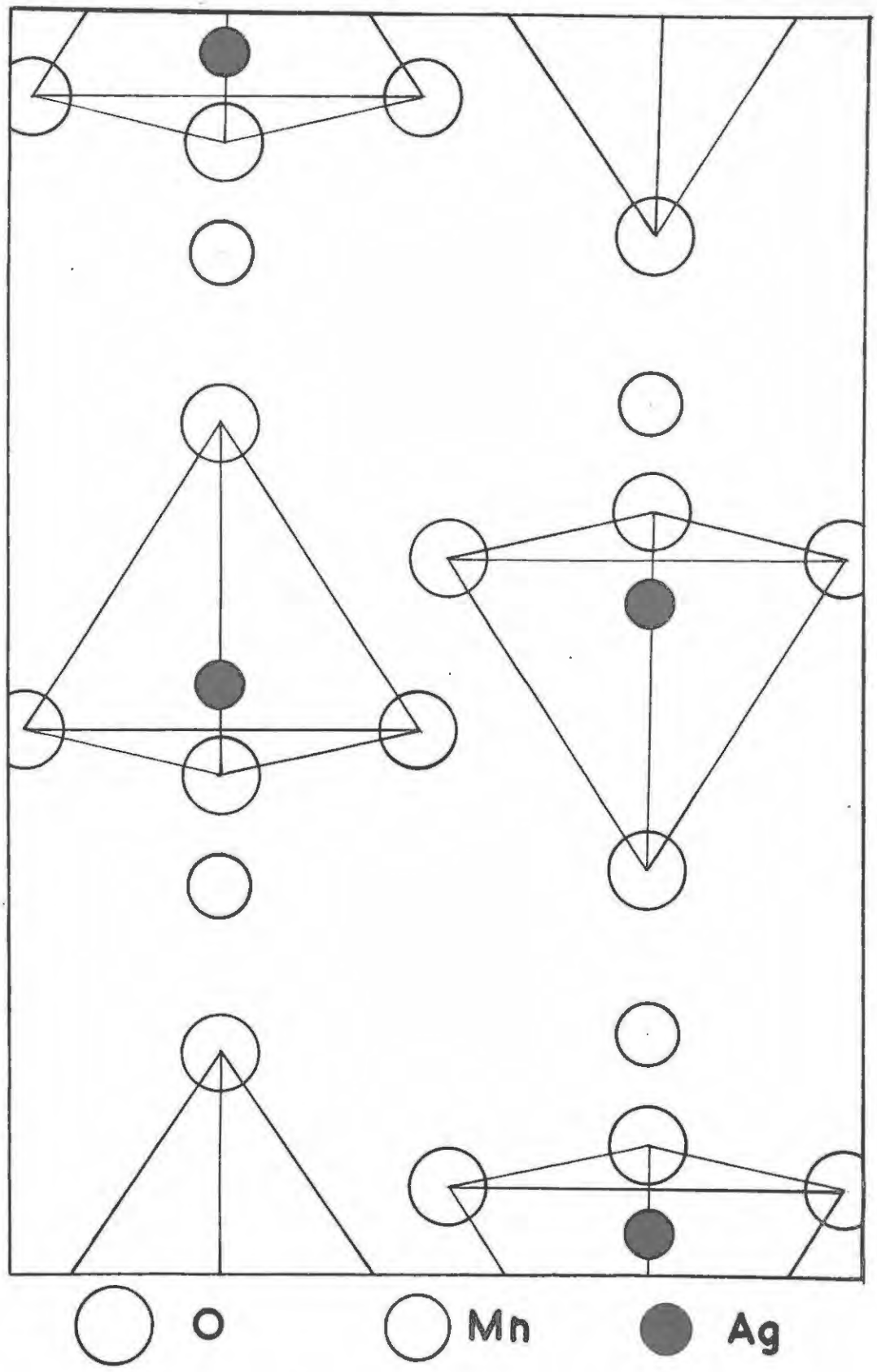

Fig. 1.2

period is shortened, and its variation, at constant temperature, with dosage is given by

$$\log t = kI + c \qquad \ldots\ldots \qquad 2.1$$

where t = time of irradiation

I = length of the induction period.

Physical fracture of the whole crystals occurs at the onset of the acceleratory period. Moreover, the onset of fracture of irradiated material always occurs at a pressure above that given by unirradiated $AgMnO_4$, supporting the idea that product molecules are formed in excess of those formed during "normal" decomposition. The processes involved in irradiation and subsequent thermal treatment are identical to those proposed for $KMnO_4$.

Recent work by Russian investigators[101] confirms the results of Prout and Tompkins with U.V., and of Prout and Sole with Co^{60} γ-rays. In addition they report that the decomposition is accelerated by 200 KeV electrons. Pretreatment with CO or H_2S, which cause partial reduction of the $AgMnO_4$, caused very strong acceleration at the initial moment of decomposition. The mechanism of damage by pre-irradiation, they suggest, almost certainly involves ionisation processes rather than direct displacement of ions by γ-rays.

A little work[1, 102], preliminary to a full investigation, has been done on the diffraction of X-rays by decomposed $AgMnO_4$. However, no account has been taken of the crystal structure in interpreting the results and no care was taken in preparation, selection and setting up of the crystals. X-ray photographs of irradiated and unirradiated crystals showed no detectable difference, but this is almost certainly due to the

grossness of the crystals used. Laue photographs of the irradiated crystals decomposed for 14 minutes at 115°C showed broken spots, and considerable asterism; further Laue photographs of completely decomposed irradiated and unirradiated specimens are identical. The asterism in the irradiated crystals shows up at the end of the induction period; immediately prior to the acceleration of the reaction.

3. OBJECTS OF THE RESEARCH.

Firstly, it was proposed to examine the thermal decompositions of unirradiated and irradiated silver permanganate crystals by means of X-ray diffraction methods in the hope that this would cast more light on the mechanisms involved in the decomposition of silver permanganate in particular, and the group of permanganates in general. Silver permanganate was chosen because it is the only permanganate which, when decomposed in the unirradiated state, undergoes no splintering or disintegration, but retains its external shape to the end of the decomposition and thus allows a single crystal X-ray study to be made.

Secondly, there are two conflicting views on the processes involved during irradiation with γ-rays. As mentioned before, Prout has proposed a process involving the multiple ionisation of ions followed by the ejection of cations into interstitial positions, while Russian investigators[101] propose a purely electronic process. It was reasoned that if there was any movement of ions, then this movement should show up in the electron density profiles of irradiated crystals. It was thus proposed to synthesise profiles passing through the silver and manganese ions before and after irradiation, as was done by Tucker and Senio with boron carbide, and to compare the areas under the curves. Tucker and Senio interpreted the drop in area under their curves as being due to the displacement of atoms; a similar drop in the area under the profile through, for example, silver ions, would mean the displacement of silver ions, thus

- bearing out -

bearing out the theory put forward by Prout.

Finally, the Russians[101] have reported that a new phase appears in the solid as a result of radiolysis. This should be detectable by employing the sensitive technique of X-ray diffraction.

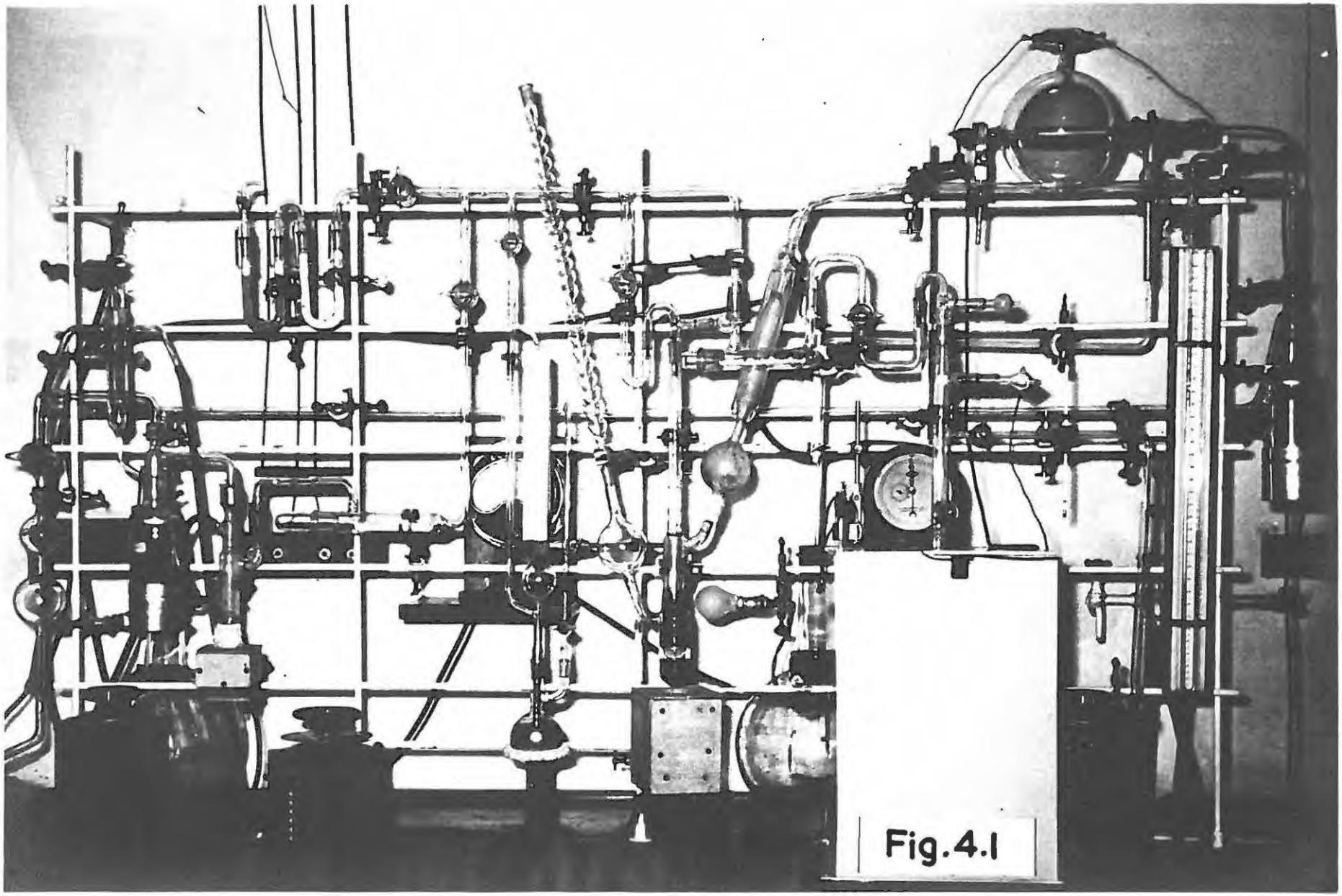

Fig.4.1

APPARATUS.

4.1 The Vacuum Line and Decomposition Chambers.

This is essentially the same apparatus as that used by Herley[103] in the study of the thermal decomposition of silver oxide, except that the device for producing cathode rays in the neck of the electrical furnace was dispensed with. The apparatus is shown in figures 4.1 and 4.2, and may be divided for convenience of description into

(a) The Pumping System.

This consists of a mercury diffusion pump, B , backed by a Speedivac rotary oil pump, A. These pumps are separated by a cold trap C, which, however, was not used owing to the unavailability of "dry ice", and an oil trap, D.

E is a safety device for controlling the flow rate of water through the condenser in the diffusion pump B. It consists of a tube of 2 inches diameter, clamped vertically, and having two 1/4 inch tubes entering horizontally, and diametrically opposite each other, at the top. These tubes are the inlet and overflow tubes for water; the 2 inch tube itself tapers at the bottom to an outlet tube carrying water to the condenser in B. The 2 inch tube contains a test-tube of one inch diameter, which in turn contains about 5 ml of mercury. One lead of the electric mains to the heater B1 is connected through the mercury when the flow rate of water is sufficiently high to buoy up the 1 inch tube; should the flow rate of water drop, then the inner tube also drops breaking the electrical circuit and switching

- off the -

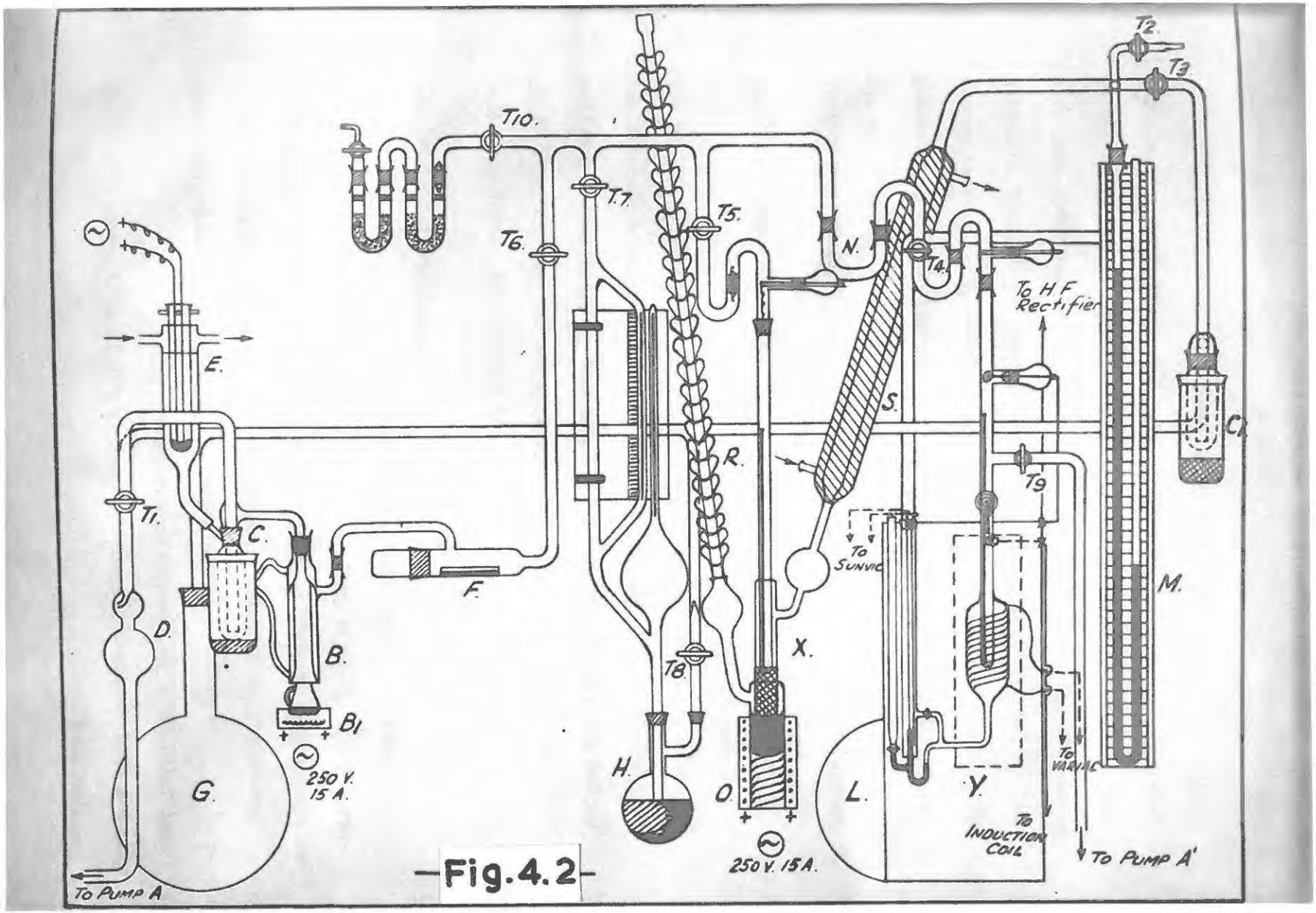
T10.
T7.
T6.
T5.
T2.
T3
N.
T4.
To H F Rectifier
E.
S.
C1
R.
T9
T1.
C.
To Sunvic
F.
M.
D.
B.
X.
T8.
B1
250 V. 15 A.
H.
O.
L.
Y.
To Vacuic
To Induction Coil
To Pump A'
To Pump A
250 V. 15 A.
G.

—Fig. 4.2—

off the heater B1.

B1 is an asbestos box with lid containing a 100 watt horizontal heating coil, connected to the mains through a vraiable resistance. Any mercury vapour escaping from the diffusion pump is trapped in C. The glass boat in trap F contains P_2O_5 which removes any water vapour. The vacuum reservoir G, used to lower the level of the mercury in the McLeod gauge H, is connected through the double oblique tap T1, and is isolated from the decomposition system X by the tap T3. Another trap C1 prevents any vapours from leaving the system X.

(b) The McLeod Pressure Gauge.

This is connected to F by way of tap T6. T10 connects the vacuum line to the atmosphere through a U-tube containing calcium chloride; T7 isolates the McLeod Gauge from the rest of the system, and T8, a two-way oblique tap connected both to G and to the atmosphere through a capillary, lowers or raises the mercury in H.

The volume of the McLeod as measured by Herley[103] was 108.36 cm^3; this volume is necessary for converting the McLeod readings to absolute units of pressure by means of the gas laws

(c) The Decomposition Chambers.

The pumps and pressure gauge are connected to the decomposition chambers X and Y through taps T4 and T5 respectively.

The chamber X consists of a pyrex tube of 19 mm internal diameter sealed into a double boiling system. The inner boiling

liquid was acetic acid (BP = 118°C), and the outer, amyl acetate (BP = 142°C). A thermometer attached to the side of X by means of wax allows of an immediate check on temperature at all times during a decomposition. The outer tube is heated by a furnace, O, connected to the mains through a Variac. Condensers R and S remove the organi vapours; S is connected to either the atmosphere or to the pumps by taps T2 and T3 respectively. Fine adjustment of the pressure over the inner liquid is effected by admitting air through T2, or withdrawing air through T3. The pressure above this liquid is measured by the manometer M. This method gives a temperature control of approximately 0.05°C.

On commencing a run, crystals are lowered into the decomposition chamber by a greased ground-glass winch, shown in the diagram.

It was felt that the same single crystal with a fixed setting on the X-ray goniometer head should be used throughout a decomposition and consequently a constant-temperature electric furnace, large enough to admit the whole goniometer head, was constructed according to the following specifications (see figure 4.3).

A wide bore Pyrex tube of diameter 34 mm i.e. large enough to admit the goniometer head, was sealed into an air-jacket of diameter 58 mm and length 24 cm, the outlet of which was joined to a 2 mm capillary tube bent as shown. The tap T1, sealed into the capillary, allows air to escape from the furnace, when opened, via tube D, which is open to the atmosphere through a slit in the rubber stopper S. Tap T2 controls the volume of mercury in the U-bend K. The levels

Fig. 4.3

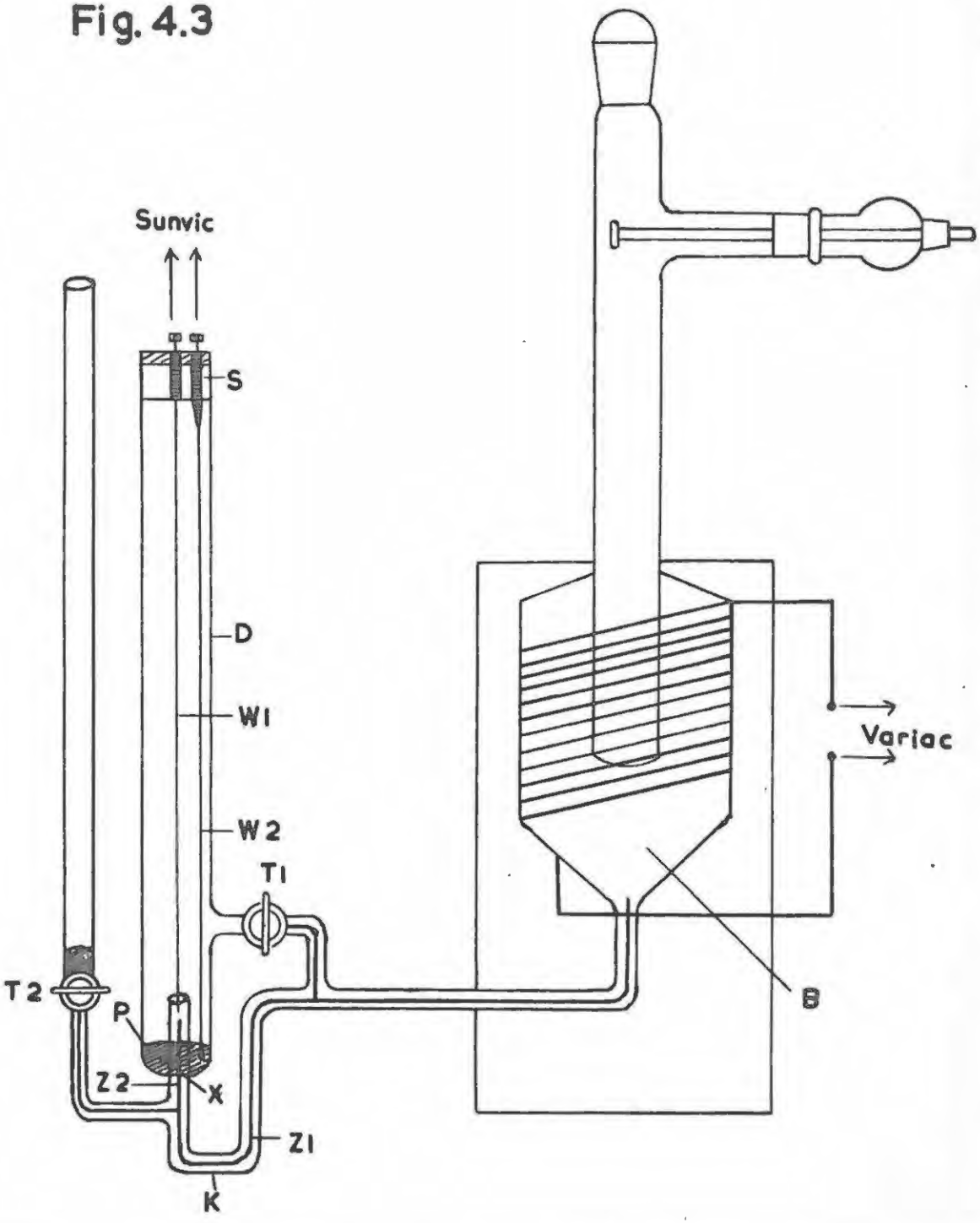

of mercury in the two arms of K, Z1 and Z2, rise or fall as the gas expands or contracts with T1 closed. The mercury pool P inside the temperature control is connected to the mercury in Z2 by means of a small piece of platinum wire X, sealed into Z2. The mercury inside the capillary tube is in contact with a platinum wire W1, while another platinum wire W2 dips into P.

An electric wire of resistance 150 ohms is wound round the air-jacket B. The windings are separated from the glass by asbestos paper, and a thick layer of plaster of Paris followed by a wrapping of asbestos cord over the wire, cuts down heat losses. The furnace is connected to the output of a Variac.

W1 and W2 are connected to the control terminals of a Sunvic hot-wire control which regulates the Variac. The whole furnace system, apart from the constant temperature device, is placed in an asbestos box packed with asbestos wool, and the complete system is housed in a large plywood box packed with vermiculite as heat insulator Herley found that a similar furnace built on a smaller scale gave a control of about 0.1° at $350^{\circ}C$, and since it was not proposed to exceed an operating temperature of $130^{\circ}C$ in this work, the temperature control from this furnace was expected to be adequate.

4.2 The X-Ray Generators and Accessories.

Two generators were used. The first, a Philips PW 1009, is of the sealed-tube type, and was operated at a voltage of 40 kV, and a tube-current of 20 mA, using a copper anticathode. The other generator, a Hilger and Watts Microfocus Generator, has a demountable anticathode,

- and the tube -

and the tube is evacuated continuously during operation by means of an oil diffusion pump backed by a rotary oil pump. Once again, a copper anticathode was used.

Both the Rotation and Weissenberg Goniometers used in this work were made by Unicam. The Rotation instrument has an optical collimator which greatly facilitates the accurate orientation of specimens. Because the goniometer heads on these instruments are interchangeable, crystals to be photographed in the Weissenberg goniometer could be orientated on the rotation goniometer and then transferred to the Weissenberg goniometer.

Two types of film were used throughout this work. Kodak "Kodirex" was normally used, because of its speed, except when it was required to determine intensities. In the latter instances Kodak Industrex D X-ray Film was used. The Kodirex was developed in Kodak D19b Developer for five minutes at 20°C and then fixed, after short immersion in a stop-bath of 3% acetic acid, in Kodak X-ray Fixer. The fixing time was five minutes with agitation followed by 10 minutes suspension in the fixer solution. Finally, the films were washed in running water for an hour, and then dried in a fume cupboard so as to minimise the sticking of dust to the film.

4.3 The Photometer.

The Steinheil Densitometer used by Brandt[104] for measuring the densities of spectral lines was modified in order to measure the intensities of diffraction spots on single crystal X-ray photographs. The following modifications were made to the instrument, shown in figure 4.4.

The light source used by Brandt was replaced by a Philips cold-lamp

Fig 4.4

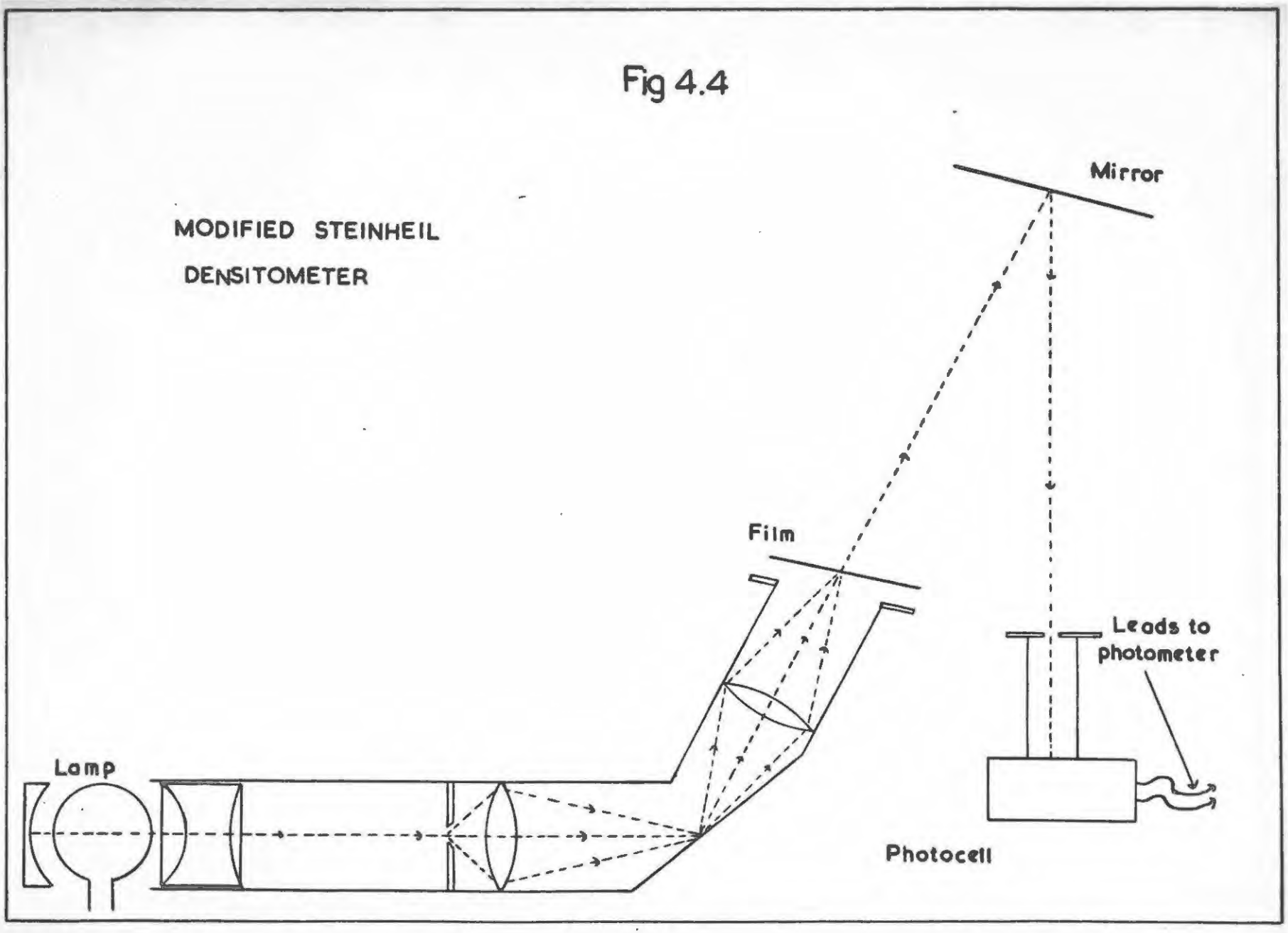
MODIFIED STEINHEIL
DENSITOMETER
Mirror
Film
Leads to
photometer
Lamp
Photocell

rated at 50 watts, since the original light source was not intense enough. Since the Philips lamp generates a considerable amount of heat during use it was cooled by means of a stream of compressed air. The lamp was run at 8 volts D.C., the voltage being supplied by a suitably tapped bus-battery which was charged during use from the mains by a battery-charger. A variable resistance connected in the circuit allowed a constant check to be made on the voltage across the filament during operation. This arrangement supplied an extremely stable voltage, and hence light output, during operation.

In addition, the barrier layer photocell and galvanometer used by Brandt were replaced by a photo-emissive search-head, and an electronic photometer both manufactured by the Photovolt Corporation of New York. The photo-cell itself was covered with a head with an adjustable aperture to allow measurement of spots of different sizes. The search-head, consisting of the photo-cell and lead-wires which connect it to the photometer were kept in a desiccator over silica gel when not in use, as deposition of atmospheric moisture on the apparatus caused the electrical insulation to break down.

The Photovolt Photometer has a meter with two scales, one of which gives direct readings of density, and the other, direct readings of light transmission. The mains current to the instrument was supplied from a constant voltage source.

The whole system was found to be extremely stable and gave reproducible results when used in conjunction with the Dawton positive-print technique for measurement of integrated intensities (see Section 5).

5. EXPERIMENTAL

5.1 Preparation and Description of the Silver Permanganate Crystals.

The crude crystals were prepared by running two solutions, one of 53.8 g silver nitrate in 1000 ml distilled water, and the other of 50 g potassium permanganate in 1000 ml water, into 700 ml of distilled water. Both reagents used were of A.R. quality. The resulting 2700 ml of solution on cooling down to $0^{\circ}C$ yielded 50 g of crude crystals of silver permanganate.

At first it was decided to recrystallise the $AgMnO_4$ by rapid cooling and the techniques described below were tried. Separate solutions saturated with $AgMnO_4$ at $45^{\circ}C$ were cooled to $20^{\circ}C$ (room temperature) and to $0^{\circ}C$ respectively over 12 hour periods. Both attempts resulted in prismatic crystals of hopper development, from 3-6 mm in length and 0.5 mm thick. Slow cooling of saturated solutions from $45^{\circ}C$ to $30^{\circ}C$ and from $45^{\circ}C$ to $20^{\circ}C$ in an oven over a period of three days resulted in large chunky crystals plus a fine sludge.

Solutions saturated at $65^{\circ}C$ were cooled in thermos flasks over 24 hour periods. Once again large (1.0 - 1.5 cm in length) prismotic crystals with irregular faces were produced. Suspension of a glass spike in the cooling solution produced poorly formed crystals on the spike.

Evaporation methods were then resorted to; solutions saturated at $40^{\circ}C$ and at room temperature were placed in an air thermostat at $41^{\circ}C$. Examination of the deposits after periods of two to three days revealed

chunky crystals of pin-head size.

As a result of observations made during the above attempts the method finally adopted was as follows. Solutions of $AgMnO_4$ saturated at 40°C were poured onto flat porcelain tiles at room temperature (23°C). The initial fast cooling produced nuclei, which then grew to crystals of 1 mm length and 0.5 mm thickness. This technique was refined by using a large perspex sheet in place of the tiles, and crops of crystals of the above size were grown.

The crystals were stored in a desiccator over silica gel, as prolonged exposure to the atmosphere eventually caused surface decomposition, thus destroying the excellent light reflections obtained from the crystal faces.

An optical goniometric analysis by Dr. H. Eales of the Geology department showed the crystals to be rhombic in cross-section. perpendicular to the needle-axis, identified as the c-axis. The unique axis (b-axis) bisects the obtuse angle (106° 48') of the rhombus. In general only four well developed faces were present in the zone of the c-axis, but on some crystals subsidiary faces did develop.

Optimum Crystal Size.

The optimum size[105] of crystals to be used in X-ray investigations is given by

$$t = 2/\mu \quad \ldots\ldots \quad 5.1$$

where t is the thickness in centimetres, and μ the linear absorption coefficient of the crystal. This latter quantity may be calculated from the mass absorption coefficients, μ_m [106], of the constituent elements

- using -

using

$$\mu = \rho \Sigma p \mu_m \quad \ldots\ldots \quad 5.2$$

where the summation is over all the constituent elements, ρ is the density of the compound, and p the proportion of each element in the compound. For silver permanganate used in conjunction with CuKα radiation of wavelength 1.54 $\mathring{A}$,

ρ = 4.27 g cm^{-3}

μm (Ag) = 223 cm^2 g^{-1}

μm (Mn) = 284 cm^2 g^{-1}

μm (O) = 12.7 cm^2 g^{-1}

This gives

μ = 762.1 cm^{-1},

and t = 0.0026 cm.

Since handling of crystals of these dimensions is impracticable, crystals of length 0.5 mm and 0.05 cm were selected from the recrystallised crops under a microscope.

5.2 The X-Ray Investigation of Unirradiated and Irradiated Silver Permanganate.

Prout has postulated that during the irradiation of permanganates, interstitial cations and vacancies are produced when cations are ejected from their lattice positions following the multiple ionisation of permanganate ions and/or cations themselves. Thus it was decided to synthesise electron density profiles through the silver and manganese ions before and after irradiation in order to determine whether in fact expulsion of cations from lattice sites does occur.

5.2 (a) Examination of the Structure Factors.

Sasvari has elucidated the $AgMnO_4$ structure and the parameters found by him are listed on page 40. Evidence set out below shows however that these parameters cannot be absolutely correct, and it was thought that a Fourier analysis of the unirradiated material might make refinement of these values possible. It was also reasoned that for comparative purposes a Fourier analysis of the unirradiated $AgMnO_4$ would be of value.

Sasvari reports zero intensities (and hence structure factors) for the reflections 130 and 150, yet unambiguous indexing shows these reflections both to be present albeit relatively weak. He reports, however, that background scatter on the oscillation photographs which he used might have prevented the emergence of some of the weaker reflections. This is evidently so.

Also, estimated intensities are recorded for the reflections 210, 230 and 250, yet structure factors calculated on the basis of his parameters are recorded as zero. This is the more serious error, and must be ascribed to the fact that the x co-ordinates of the Ag and Mn ions are given as exactly 0.25, and the oxygen atoms are placed symetrically about the line x = 0.25. That this cannot be so is shown below.

The general formula for the structure factor F(hkl) of the reflection hkl is given by:

$$F(hkl) = \sum_{n=1}^{N} f_n \exp 2\pi i(hx_n + ky_n + lz_n) \quad \ldots\ldots\ldots \quad 5.01$$

- where -

where N = number of atoms in the unit cell

f_n = scattering powers of the ions (atoms) for the scattering angle θ for the reflection (hkl)

x,y,z = atomic (ionic) co-ordinates of the atoms (ions) expressed as fractions of the cell edges, a, b and c.

Thus, for a reflection of the type (hko):

$$F(hko) = \sum_{n=1}^{N} f_n \exp 2\pi i(hx_n + ky_n) \quad \ldots\ldots\ldots \quad 5.02$$

Now, since for every atom (ion) at the point (xyz) in the space-group $P2_1/n$, to which $AgMnO_4$ belongs, there are three more generated by symmetry at $(\bar{x},\bar{y},\bar{z})$ $(\frac{1}{2} + x, \frac{1}{2} - y, \frac{1}{2} + z)$ and $(\frac{1}{2} - x, \frac{1}{2} + y, \frac{1}{2} - z)$ insertion of these values into 5.02 yields.

$$\left.\begin{aligned} F(hko) &= 4\sum_{n=1}^{N/4} f_n \cos 2\pi hx \cos 2\pi ky \text{ for } (h+k) \text{ even} \\ F(hkO) &= -4\sum_{n=1}^{N/4} f_n \sin 2\pi hx \sin 2\pi ky \text{ for } (h+k) \text{ odd} \quad \ldots\ldots \end{aligned}\right\} \quad 5.03$$

(Values of $\cos 2\pi hx$ are obtained from International Tables for X-Ray Crystallography: Volume II). Thus all structure factors are real, and have positive or negative values according as their phases are 0 or

For the 210 reflection, the sine equation 5.03 holds. By virtue of their x parameters being 0.25, none of Ag, Mn, O(1) or O(2) can contribute to F(210). For O(3)

$\sin 2\pi hx \sin 2\pi ky = -.239$ and for O(4),

$\sin 2\pi hx \sin 2\pi ky = +.239$ and hence these contributions to F(210) cancel one another, making F(210) = 0.

- The same -

The same result is obtained for F(230) and F(250), and hence we conclude that the parameters are incorrect.

5.2 (b) Theory of the Fourier Analysis.

It may be shown that the electron density at any point in a crystal may be represented by the formula:

$$\rho(xyz) = \frac{1}{V} \sum_{h=-\infty}^{\infty} \sum_{k=-\infty}^{\infty} \sum_{l=-\infty}^{\infty} F(hkl)\exp\{-2\pi i(hx + ky + lz)\} \quad \ldots\ldots \quad 5.04$$

is the electron density at the point (xyz) and V is the volume of the unit cell. From this it may be shown that the electron density projected on a point (xy) in the 001 face of the unit cell is:

$$\rho(xy) = \frac{1}{Ac} \sum_{h=-\infty}^{\infty} \sum_{k=-\infty}^{\infty} F(hko)\exp[-2\pi i(hx+ky)] \quad \ldots\ldots\ldots \quad 5.05$$

where Ac is the area of projection of the unit cell. If the structure factor F(hko) be expressed as:

$$F = A + iB$$

$$\text{where } A(hkO) = \sum f_n \cos 2\pi(hx_n + ky_n)$$

$$B(hkO) = \sum f_n \sin 2\pi(hx_n + ky_n) \quad \ldots\ldots\ldots \quad 5.06$$

then, since

$A(hkO) = A(\bar{h}\bar{k}O)$ and $B(hkO) = -B(\bar{h}\bar{k}O)$, 5.05 may be rid of complex quantities and expressed as:

$$\rho(xy) = \left(\frac{1}{Ac}\left[F(000)+2\sum\sum\{A(hkO)\cos 2\pi(hx+ky)+B(hkO)\sin 2\pi(hx+ky)\}\right]\right.$$

$\ldots\ldots\ldots$ 5.07

The summation is taken over only half of the reciprocal lattice since the terms have now been taken in groups of two; this does not apply to the term F(000) however. F(000) is equal to the total number of electrons in the unit cell, and for $AgMnO_4$ has the value 416.

- Equation -

Equation 5.07 may be further simplified. Since the space-group $P2_1/n$ is centro-symmetrical all B values are zero and hence, since $A(hk0) = F(hk0)$

$$\rho(xy) = \frac{1}{Ac}\left[F(000) + 2\sum\sum F(hko)\cos 2\pi(hx + ky)\right] \quad \ldots\ldots\ldots \quad 5.08$$

This contains terms such as $F(hk0)\cos 2\pi(hx + ky)$ which may be expanded as follows:

$$F(hk0)\cos 2\pi hx \cos 2\pi ky - F(hk0)\sin 2\pi hx \sin 2\pi ky \quad \ldots\ldots\ldots \quad 5.09$$

This expression was obtained in simplifying from 5.05 by combining the terms $(hk0)$ and $(\bar{h}\bar{k}0)$. The corresponding expression for the terms $(\bar{h}k0)$ and $(h\bar{k}0)$ is

$$F(\bar{h}k0)\cos 2\pi hx \cos 2\pi ky + F(\bar{h}k0)\sin 2\pi hx \sin 2\pi ky \quad \ldots\ldots\ldots \quad 5.10$$

Combination of 5.09 and 5.10 yields terms like

$$[F(hk0) + F(\bar{h}k0)]\cos 2\pi hx \cos 2\pi ky - [F(hk0) - F(\bar{h}k0)]\sin 2\pi hx \sin 2\pi ky \quad \ldots\ldots\ldots \quad 5.11$$

Now if we let

$$A_1 = F(hk0) + F(\bar{h}k0)$$

$$A_2 = F(hk0) - F(\bar{h}k0)$$

then the expression 5.11 may be written as

$$A_1 \cos 2\pi hx \cos 2\pi ky - A_2 \sin 2\pi hx \sin 2\pi ky \quad \ldots\ldots \quad 5.12$$

The total summation may then be expressed as

$$\sum_h\left[\sum_k \cos 2\pi ky\right]\cos 2\pi hx - \sum_h\left[\sum_k \sin 2\pi ky\right]\sin 2\pi hx \quad \ldots\ldots\ldots \quad 5.13$$

- It must be -

It must be noted that since the terms have now been taken together in groups of four, the summation must be made over the positive indices only. Moreover, the terms F(h00) and F(0k0) do not occur in groups of four, and this must also be taken into account on summation. Hence the complete expression for the electron density is

$$\rho(xy) = \frac{1}{Ac}\left[F(000) + 2\sum_{h=1}^{\infty} F(h00)\cos 2\pi hx + 2\pi\sum_{k=1}^{\infty} F(0k0)\cos 2\pi ky + 2\sum_{k=1}^{\infty}\left\{\sum_{h=1}^{\infty} A_1 \cos 2\pi hx\right\}\cos 2\pi ky - 2\sum_{k=1}^{\infty}\left\{\sum_{h=1}^{\infty} A_2 \sin 2\pi hx\right\} \sin 2\pi ky\right] \quad \ldots\ldots\ 5.14$$

In practice the expressions in square brackets in the expression 5.13 may be evaluated in preliminary tables (see tables 5.4a and 5.4b, will give the coefficients to be used in the final summations. In other words, the expressions in square brackets are evaluated for groups of reflections with a given value of h, the result being a series of ordinates at particular values of y. Suppose these quantities be called C(h,y); then the quantities obtained from the sine terms are S(h,y). The final summation is then

$$\sum_h [C(h,y)\cos 2\pi hx - S(h,y)\sin 2\pi hx] \quad \ldots\ldots\ (5.15)$$

There is, of course, no reason why 5.13 cannot be written

$$\sum_k\left[\sum_h \cos 2\pi hx\right]\cos 2\pi ky - \sum_k\left[\sum_h \sin 2\pi hx\right]\sin 2\pi ky \quad \ldots\ldots\ 5.16$$

In this case, the quantities C(k,x) and S(k,x) arise in the course of computation, and the final summation would then be

$$\Sigma [C(k,x)\cos 2\pi ky - S(k,x)\sin 2\pi ky] \quad \ldots\ldots\ 5.17$$

5.2 (c) The Determination of Integrated Intensities.

Both the phases and amplitudes of the structure factors must be known before a Fourier synthesis can be performed. The phases for silver permanganate are all either 0 or π, making the structure factors either positive or negative, and these phases are known from Sasvari's work. The amplitudes may be obtained from the measured intensities of the reflections since $|F| \propto I^{\frac{1}{2}}$. The following technique was developed for obtaining the integrated intensities of reflections.

The Dawton Positive-Print Technique.

The method developed by Dawton[107] for determining integrated intensities has, as Buerger[108] points out, the same basis as that of making a perfect picture of an object by photography. If the entire photographic procedure is properly controlled, the photograph obtained should reflect, point for point, the same amount of light as the original object.

In the corresponding case of X-ray photography, this involves taking the original X-ray on a specific film, developing it in a certain way, printing this negative on a suitable film, which becomes a "positive", and developing the positive in a controlled way. If the negative and positive processes are appropriately matched, the resulting positive print consists of a series of transparent spots on a dense black background, the total transmission of each spot being directly proportional to the integrated intensity reaching the spot on the original X-ray film.

It may be shown[109] that a necessary requirement for the making

of perfect prints is that the photographic density D of the positive be a linear function of the logarithm of the relative exposure of the negative (log E). This is equivalent to saying that the transmission T of the positive be a linear function of the relative exposure E of the negative. Since it has been established that the reciprocity law is obeyed by films exposed to X-rays i.e. that the exposure is equal to the product of beam intensity and time, hence, if as in the case of the spots on an X-ray film, the time factor is constant, the exposure is proportional to the intensity, and in turn, the transmission of the positive will be a linear function of the intensity on the negative (up to some limiting value of the density).

Arising from this, also, is the requirement that

$$\gamma_P \gamma_N = 1 \quad \ldots\ldots \quad \ldots\ldots \quad 5.18$$

where P and N refer to positive and negative, and γ is the slope of the straight portion of the wave of D vs. log E. It may be noted that the "γ" of a film is a measure of its contrast; a large value of γ denotes high contrast, and vice-versa.

In deciding on the correct materials and procedures to adopt to give suitable positive prints, it is necessary to consider (i) the choice of X-ray film to be used as negative, and the determination of its γ-curve, (ii) the correct developing conditions to use so as to develope the negative to a suitable γ-value, (iii) the choice of a positive film, and finally (iv) experimenting with printing times for the positive so as to obtain a linear relationship between the transmission of the positive and the exposure (and hence intensity) of the negative. Each of these factors will be

reported in turn.

(i) It was decided to investigate the properties of Industrex D X-ray film for use as the negative rather than Kodirex. The relative speeds of these films are 27 and 55 respectively, and since Industrex D is the slower film and therefore has the finer grain, it is much less prone to background fogging caused by incoherently scattered radiation.

(ii) It is recommended that Industrex D be developed for 5 minutes at 20°C in Kodak D 19 b developer. Under these conditions, however, the resulting γ is approximately 3, and the corresponding positive film would thus have to be developed to a γ of 0.3. A review of available films which could possibly be used for positive prints had indicated that Kodak Commercial Ortho Sheet-film might be suitable, however, and it was decided that this should be developed to a γ of at least 0.5. Hence it was decided to try to lower the γ for Industrex D to a value of 2 by some method, so that the condition 5.18 would be satisfied.

At first, shorter developing times in D 19 b were tried but to no avail. Following Buerger[110], Kodak D 76 developer, to which 2 cc 1% KI and 20 cc 2.5% KBr had been added per 4 litres of developer, was tried, and this had the desired effect. Experiment showed that pre-soaking of the film in water for 2 minutes, followed by 3 minuts developing in this solution with constant agitation at 20°C lowered the γ to a value near 2. The film was then dipped into a stop-bath of 3% CH_3COOH and fixed for 10 minutes in Kodak X-ray Fixer solution, and finally washed for 30 minutes in running water.

- The γ was -

The γ was measured from the slope of the D vs log E curve, which was obtained as follows: A small circular hole was cut in a lead sheet which fitted into the flat plate camera in front of the film. The camera was clamped 230 cm from the X-ray window so that the beam fell exactly on the hole. (The beam was located using a Geiger-Muller counter). With the generator running at 27 kV and 1.6 mA and with the camera in the position mentioned, the exposures tabulated in table 5.1 gave a suitable range of densities. The final D vs log E curve is drawn from these data (figure 5.1). Densities were measured on the instrument described on page 26.

(iii) Kodak Commercial Ortho Sheet-film had the desired characteristics for use as the positive. Development, with constant swabbing with cotton wool affixed to a hoe-shaped glass rod for 8 1/4 minutes at 20°C in Kodak D 76 developer, after presoaking the film for 2 minutes in water resulted in a γ of 0.5. Fixing was accomplished using constant agitation for 10 minutes in Kodak Acid Fixing Salt with Hardener, and the film was then washed for 30 minutes.

The D 76 developer was found to deteriorate very rapidly. In order to prevent this, the developer was made up in two parts. The one solution, containing borax only, was made up separately from the other, which contains "Metol", sodium sulphite and hydroquinone, and these components were mixed just prior to use. Furthermore, all solutions were allowed to equilibrate

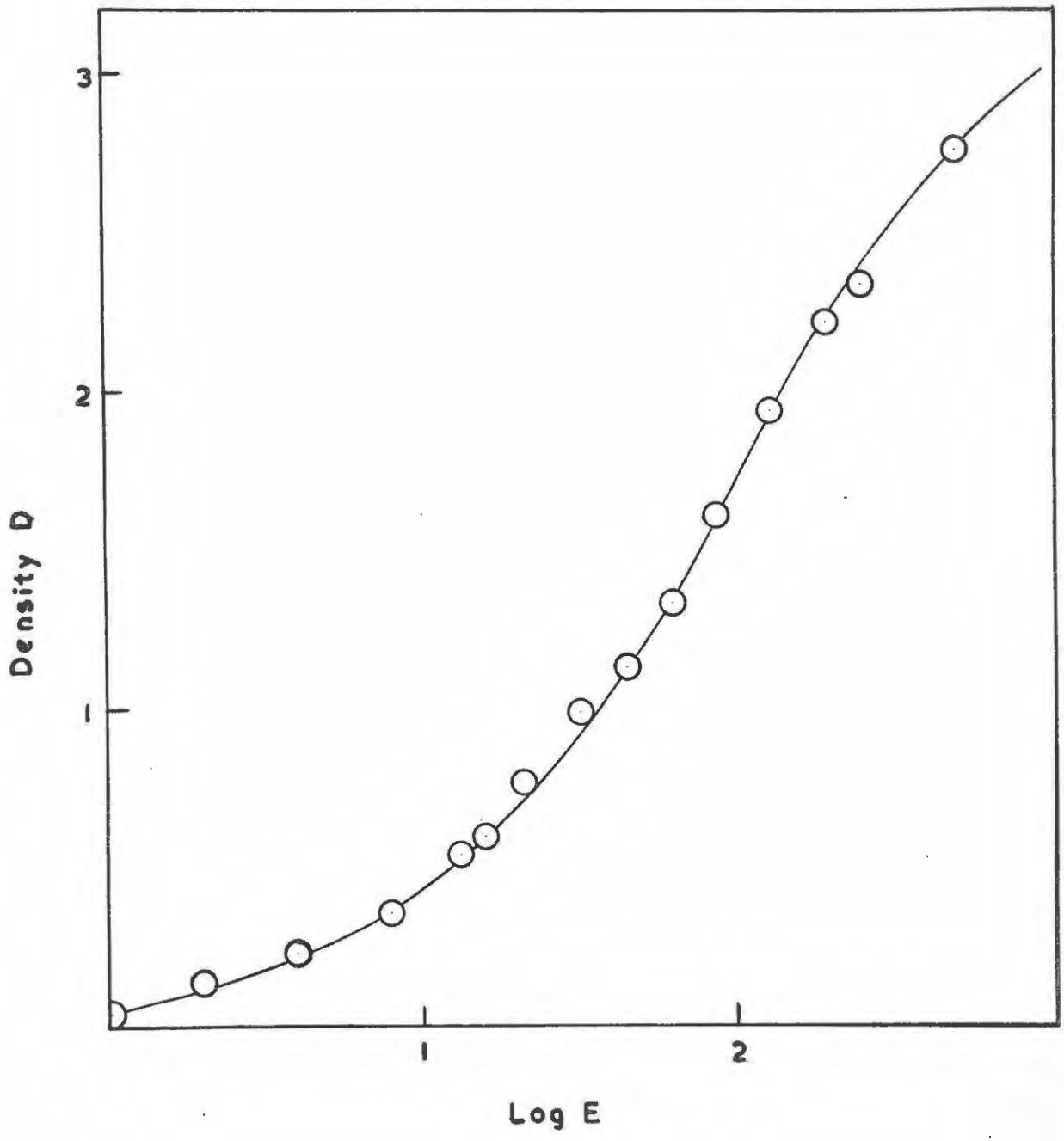

Fig 5.1

Exposure Time of Negative.	Relative Exposure (E)	Log E	D
23 secs.	1.022	0.01	0.050
45 "	2	0.30	0.145
1.5 min.	4	0.60	0.240
3 "	8	0.90	0.360
5 "	13.3	1.13	0.545
6 "	16	1.20	0.595
8 "	21.3	1.33	0.770
12 "	32	1.51	0.985
17 "	45.3	1.66	1.125
24 "	64	1.81	1.325
33 "	88	1.95	1.595
48 "	128	2.11	1.930
75 "	200	2.30	2.205
96 "	256	2.41	2.330
192 "	512	2.71	2.750

TABLE 5.1.

Exposure Time of Negative.	Trans. of Pos. for 22 Sec. Printing.	Trans. of Pos. for 24 Sec. Printing.	Trans. of Pos. for 25 Sec. Printing.
23 secs.	0	0	0
45 "	2.25	1.75	2.0
1.5 min.	5.25	5.0	3.75
3 "	8.25	8.75	5.25
5 "	17.25	15.5	15.0
6 "	17.75	18.0	16.5
8 "	26.75	24.5	23.5
12 "	42.25	44.0	41.5
17 "	54.25	59.0	53.5
24 "	66.25	71.0	66.5
33 "	98.75	103.5	104.0
48 "	131.25	148.5	141.5
75 "	133.25	156.0	171.5
96 "	155.25	161.0	171.5
192 "	167.25	181.0	176.5

TABLE 5.2.

in a thermostat for at least 2 hours before use, and the developing itself was carried out in the thermostat.

(iv) In order to ensure accurate exposures in printing the positives a printing box was specially constructed. The box is about 7 feet long and made to accommodate a printing frame about 5 inches by 7 inches. This printing frame has a piece of opal glass (which transmits 21% of the light falling on it) which diffuses the printing light so as to prevent direct shadows of dust particles from appearing on the print; moreover it is spring-loaded to ensure perfect contact between negative and print. Matters were arranged so that the light source was 6 feet from the film.

The light source was a small 5 c.p. bulb which was fed by a constant voltage stabilizer to ensure uniform light output. The voltage across the filament was 5 volts. With this set-up it was found that an exposure of 24 seconds gave a good linear relationship between the exposure of the negative and transmission of the positive up to a density of 2 on the negative (see figure 5.2). The data for this graph are found in table 5.2, along with the transmissions for printing times of 23 and 25 seconds. Although linearity was also obtained for these printing times, the point of departure from linearity was at a density less than 2. Obviously, the choice of printing time must be for 24 seconds, as this value gives the widest range of linearity between transmission of the positive and exposure (and hence intensity) of the negative.

- Thus -

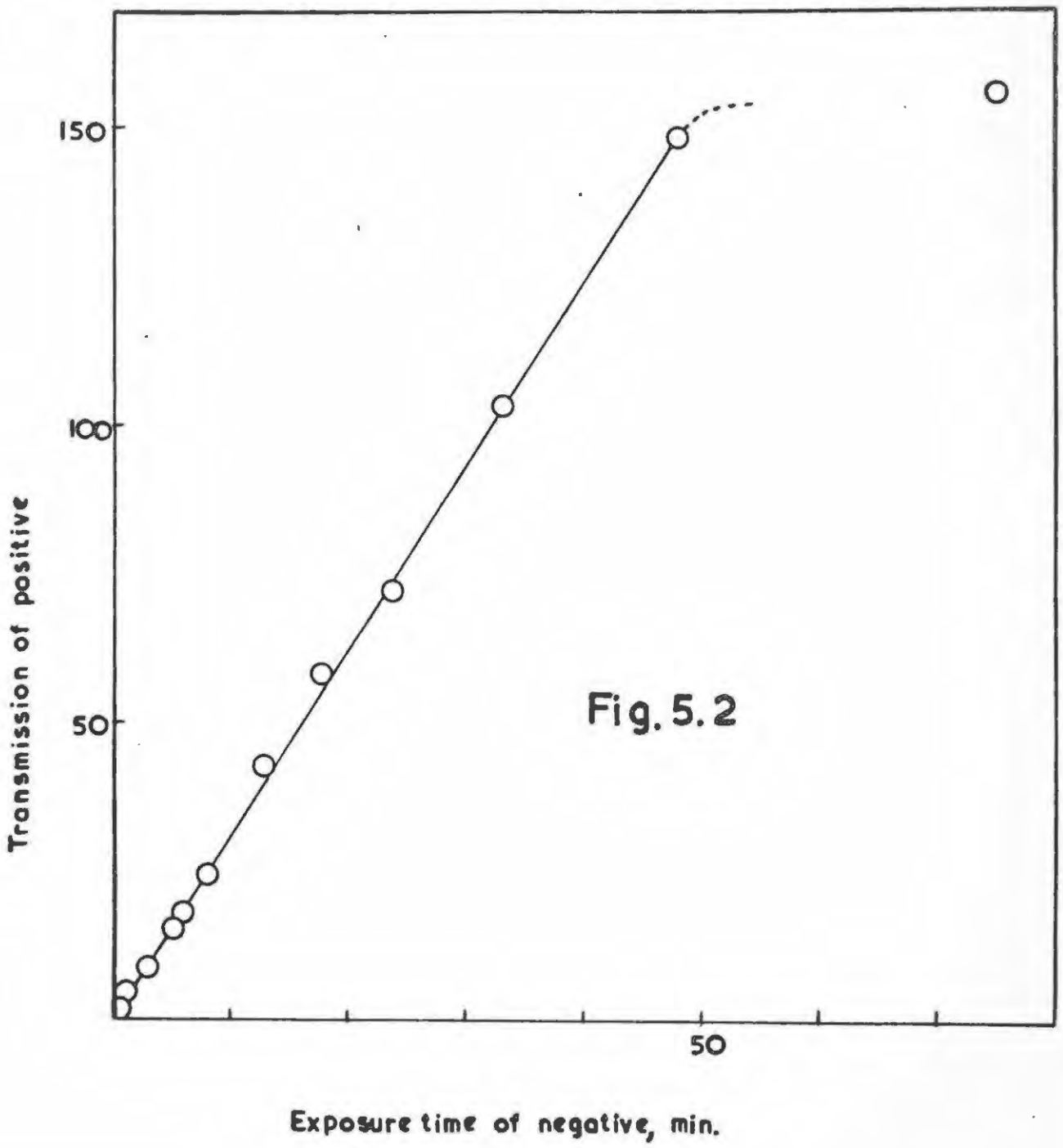
150
100
50
50
Transmission of positive
Exposure time of negative, min.

Fig. 5.2

Thus by following the procedure described above, it was possible to measure the integrated intensities of all those spots on the X-ray negative whose densities lay below 2, and if the exposure time of the negative was suitably chosen so that the darkest spots had densities of 2 or less, this would include all the spots on the photograph. On the other hand, the exposure had to be chosen so that the faintest spots did emerge on the photograph.

5.2 (d) The Measurement of Intensities.

Densities for the plotting of the γ-wave curve for Industrex D film were measured by adjusting the photometer so as to read densities directly. The aperture covering the photoemissive cell in the search head was opened so that its size was less than that of the spot to be measured, and the spot adjusted until its image fell on the aperture.

The transmissions of the spots on the positive print were measured as follows: Firstly, the instrument was adjusted with the aperture closed so as to give zero deflection. The aperture was then opened so that all the light from the spot in question fell on the photocell. Keeping the aperture exactly the same size, the transmission of the background immediately next to the spot was then measured, and the transmission of the spot obtained by substracting the background reading from that of the spot.

For low θ angles, the $K\alpha_1$ and $K\alpha_2$ diffraction spots were superimposed and no difficulty was experienced in measuring their intensities. At high θ angles, however, these two spots were resolved. The intensities of such spots were thus measured by measuring the

separate transmissions of the two components and then adding them.

5.2 (e) The Fourier Analysis of Irradiated and Unirradiated Silver Permanganate.

For a projection of the electron density on the 001 face of the unit cell it is necessary to know the values of the structure factors of the F(hk0) type. Hence a normal beam Weissenberg photograph was made on Industrex D film with the crystal rotating about its c-axis. With the Hilger Generator running at 50 kV and 3 mA and an exposure of 20 hours, the resulting photograph recorded the densest spots as having a density <2, while even the very faintest reflections appeared. Hence the intensities of the whole range of spots could be measured on a single positive point.

The crystal was oscillated through 220° on the Weissenberg goniometer during exposure, and in this way all spots were recorded on the film at least four times, thus enabling an average value of the intensities to be taken.

This procedure was followed both for an unirradiated crystal and for an irradiated (300 Mrad) crystal both exactly of the same dimensions.

The spots on the negatives were numbered in Indian ink to facilitate identification when measuring intensities, and positive prints were made. The intensities were measured as described in Section 5.2(c), and the spots were indexed by means of a Weissenberg chart supplied by the makers of the Weissenberg goniometer.

It may be shown that the amount of energy E(hkl) diffracted in the spectrum hkl as the crystal rotates uniformly about an axis

- normal

normal to the X-ray beam is

$$E(hkl) = K' L(hkl)\, p(hkl) |F(hkl)|^2 \quad \ldots\ldots \quad 5.19$$

The quantity E may be identified with the measured value of the integrated intensity I(hkl): since

$$I(hkl) = K' L(hkl)\, p(hkl) |F(hkl)|^2 \quad \ldots\ldots \quad 5.20$$

K′ is a constant for the experiment concerned, but L, the Lorentz factor, and p, the polarisation factor vary from reflection to reflection. The polarisation factor allows for the fact that the X-ray beam is weakened by polarisation of the diffracted beam to a varying extent depending on the angle of diffraction; it is dependent only on this angle and not on experimental conditions and its value is

$$p(hkl) = (\tfrac{1}{2} + \tfrac{1}{2} \cos^2 2\theta) \quad \ldots\ldots \quad 5.21$$

The Lorentz factor depends however, on the experimental arrangement i.e. on the method of recording the diffracted beams on the photographic plate. This factor allows for the fact that each reciprocal lattice point spends a finite time in passing through the surface of the sphere of reflection, and that this time varies with the distance of the point from the origin of the reciprocal lattice. For the zero level of the reciprocal lattice i.e. for reflections hk0, in this case, with the X-ray beam normal to the rotation axis of the crystal this value is

$$L(hkl) = 1/\sin 2\theta \quad \ldots\ldots \quad 5.22$$

Substitution of the values for L and p into 5.20 gives

$$I(hkl) = K(1 + \cos^2 2\theta/\sin 2\theta) |F(hkl)|^2 \quad \ldots\ldots \quad 5.23$$

The new constant K incorporates the 2 found in the denominator of 5.21. Tables of the function $(1 + \cos^2 2\theta/\sin 2\theta)$ as a function

of sin Θ may be found in Internation Tables, Vol. II. It is then necessary to multiply each experimental intensity I by $(Lp)^{-1} = (\sin 2\theta/1 + \cos^2 2\theta)$ to obtain the true intensity. The value of O(hkl) for the reflection hkl is obtainable from the expression

$$\theta(hkl) = \sin^{-1}[\frac{\lambda}{2} (h^2/a^2 \sin^2\beta + k^2/b^2)^{\frac{1}{2}}] \ldots\ldots \quad 5.24$$

There is no need to take into account any multiplicity in the formula for the integrated intensity, since for reflectionsof the type hkO it is in every case 4 in the monoclinic system, and this factor may be throught of as included in the constant K.

Strictly speaking, account should be taken of corrections for both primary and secondary extinction, absorption, and the effect of the thermal vibrations of the atoms on the intensities of the diffracted beams. Corrections for extinction are extremely difficult to make, so this was not attempted. Since the most accurate procedure in a comparative study is to use crystals of exactly the same size and shape, and this was in fact done for irradiated and unirradiated crystals, thus the absorption correction, which depends on the shape and size, was considered unimportant being the same for both crystals. Correction for thermal vibrations of the atoms depends on a previous knowledge of the crystal structure and is anyway an approximation in most cases. Moreover, Bradley[111] points out that in moderately or highly absorbing crystals the thermal effect and absorption effects may cancel one another to some extent. In any event, no correction was made for the thermal effect.

- Table 5.3 -

Table 5.3 shows a list of the reflections recorded. The intensities are in arbitrary units; the structure factors for unirradiated $AgMnO_4$ have however, been normalised so that F(600) = 138, following Sasvari. The signs of the structure factors were obtained from Sasvari's paper, except those of 540, 560, 640, 720 and 1.10.0; which reflections are not recorded by him. In these cases the signs were inferred by calculation of structure factors using his parameters. Furthermore, since the signs of F(130) and F(150) could not be inferred by this method, these structure factors were omitted from the synthesis.

Also shown in the table are values of $\sin\theta$, $\sin\theta/\lambda \times 10^8$ and $(Lp)^{-1}$ for each reflection. The quantity $\sqrt{I(Lp)^{-1}}$ is the unnormalised structure amplitude and F the normalised structure factor for the unirradiated specimen. The quantities I_{Irr} are intensities of the irradiated specimen, normalised so that the strongest reflection, 200, has the same intensity as the unirradiated specimen, and F_{Irr} is the structure factor for the irradiated specimen.

Tables 5.4a and b give values of $2A_1$ and $2A_2$ for unirradiated $AgMnO_4$ (see equations 5.12 and 5.14), and are drawn up using the fact that, for the space-group $P2_1/n$,

$$\left.\begin{aligned} F(hk0) &= F(\bar{h}k0) \text{ for } (h+k) \text{ even} \\ F(hk0) &= -F(\bar{h}k0) \text{ for } (h+k) \text{ odd} \end{aligned}\right\} \quad \ldots\ldots\ldots \quad 5.25$$

Allowance has been made here for the fact that F(000) occurs only once, and terms like F(h00) and F(0k0) appear only twice, whereas terms like F(hk0) appear four times in the summation.

Table 5.5 gives calculated values of the preliminary

TABLE 5.3

Index hko	Sin θ	Sin θ/λ x 10^{-3}	$(Lp)^{-1}$	Intensity I (hko) for Unirrd.	$\sqrt{I(Lp)^{-1}}$ for Unirrd.	$F_{Unirrd.}$	I (hko) for Irrad.	$F_{Irrad.}$
020	.1862	.121	.392	798	17.7	132	475	102
120	.2305	.1500	.499	2246	33.5	250	1460	202
200	.2716	.177	.606	4254	50.2	$\overline{375}$	4254	$\overline{375}$
210	.2871	.186	.648	189	11.1	$\overline{83}$	121	$\overline{66}$
130	.3106	.202	.716	6	2.1	15	-	-
220	.3294	.214	.769	1098	9.2	217	583	158
040	.3725	.242	.909	302	15.0	112	167	92
230	.3895	.254	.966	12	3.4	26	-	-
140	.3964	.257	.990	156	12.5	$\overline{93}$	121	$\overline{82}$
320	.4479	.291	1.179	423	22.3	$\overline{167}$	279	$\overline{135}$
240	.4610	.300	1.230	250	17.6	$\overline{131}$	246	$\overline{130}$
150	.4850	.315	1.326	10	3.7	27	-	-
250	.5391	.350	1.546	14	4.7	$\overline{35}$	-	-
400	.5434	.354	1.565	894	37.4	279	521	213
060	.5595	.363	1.629	74	11.0	82	86	88
420	.5742	.374	1.684	75	11.2	$\overline{83}$	70	$\overline{81}$
160	.5749	.374	1.686	482	28.5	213	480	212
260	.6212	.404	1.852	106	14.0	$\overline{104}$	103	$\overline{103}$
440	.6586	.427	1.949	165	17.9	134	172	136
360	.6913	.449	1.992	373	27.3	$\overline{203}$	393	$\overline{208}$
520	.7041	.458	2.000	92	13.6	101	90	100

- continued -

TABLE 5.3 continued.

Index hko	Sin θ	$\frac{\text{Sin } \theta}{\lambda} \times 10^{-3}$	$(Lp)^{-1}$	Intensity I (hko) for Unirrd.	$\sqrt{I(Lp)^{-1}}$ for Unirrd.	$F_{Unirrd.}$	I (hko) for Irrad.	$F_{Irrad.}$
520	.7041	.458	2.000	92	13.6	101	90	100
340	.7422	.482	1.970	12	4.7	35	-	-
080	.7449	.484	1.965	25	7.0	$\overline{52}$	-	-
180	.7580	.493	1.934	90	13.2	98	97	102
460	.7793	.507	1.869	42	8.8	66	46	69
540	.7791	.507	1.869	8	3.9	$\overline{29}$	-	-
280	.7929	.516	1.812	48	9.3	70	70	84
600	.8149	.529	1.704	200	18.5	$\overline{138}$	145	$\overline{117}$
620	.8362	.542	1.585	52	9.1	48	42	60
380	.8498	.551	1.495	136	14.3	$\overline{106}$	149	$\overline{111}$
560	.8792	.571	1.292	237	17.5	130	273	140
640	.8960	.582	1.164	46	7.4	$\overline{55}$	35	$\overline{48}$
480	.9217	.600	.959	84	9.0	$\overline{67}$	88	$\overline{68}$
1.10.0	.9423	.612	.790	24	4.1	$\overline{30}$	-	-
720	.9690	.630	.541	212	10.7	$\overline{80}$	198	$\overline{77}$

TABLE 5.4a

k/h	0	2	4	6
0	416	$\overline{750}$	558	$\overline{276}$
2	$\overline{264}$	276	$\overline{332}$	192
4	224	$\overline{524}$	536	$\overline{220}$
6	164	$\overline{416}$	264	
8	$\overline{104}$	280	$\overline{268}$	

$$2A_1 = 2[F(hko) + F(\bar{h}ko)]$$

TABLE 5.4b

k/h	1	2	3	5	7
1		$\overline{332}$			
2	1000		$\overline{668}$	404	$\overline{320}$
3		104			
4	$\overline{372}$		140	$\overline{116}$	
5		$\overline{140}$			
6	852		$\overline{812}$	520	
8	392		$\overline{424}$		
10	$\overline{120}$				

$$2A_2 = 2]F(hko) - F(\bar{h}ko)]$$

coefficients C(k,x) and S(k,x) while table 5.6 gives the corresponding coefficients C(h,y) and S(h,y) both for unirradiated $AgMnO_4$. These were evaluated with the aid of Beevers-Lipson strips, which are in fact tables of the functions $(2A_1 \cos 2\pi hx)$ and $(2A_2 \sin 2\pi hx)$ for values of the amplitudes, $2A_1$ and $2A_2$, ranging from -900 to -100 and 100 to 900 in intervals of 100, and from -100 through zero to 100 in intervals of units. There exist strips for values of the function, for fixed $2A_1$ and h values, for all values of x in $1/120^{ths}$ from 0 to $30/120^{ths}$.

Values of these functions from $x = 30/120^{ths}$ to $x = 60/120^{ths}$ may be obtained if it is remembered that the function $\cos 2\pi hx$ is symmetrical about the point $x = 1/4$ if h is even, antisymmetrical if h is odd, while $\sin 2\pi hx$ is symmetrical about this point if h is odd, and antisymmetrical if h is even. (Note that table 5.5 shows the values calculated for all values of x between $0/120^{ths}$ and $30/120^{ths}$, but only values for values of y of $2n/120^{ths}$ are shown in table 5.6, to save space; the odd values were also calculated, but are not shown.

If equation 5.13 is used as the starting point, thus involving the quantities C(h,y) and S(h,y), the final synthesis is in the y-direction for a chosen value of x. Similarly, starting with 5.16 leads to a synthesis in the x-direction for a chosen y. Since it was intended to check the x- and y- parameters of the atoms, which would involve syntheses in both directions, both the (k,x) and (h,y) preliminary coefficients were evaluated.

The final summations for unirradiated $AgMnO_4$ are shown in

- table 5.7 -

TABLE 5.5

PRELIMINARY SUMMATIONS: Values of $\Sigma\ 2A_1 \cos 2\pi hx\ [= C(h,x)]$ and $\Sigma\ 2A_2 \sin 2\pi hx\ [= S(k,x)]$ FOR ALL VALUES OF k.

x(120ths)	0	2	4	6	8	10	12	14	16	18	20	22	24	26	28	30
C(0,x)	$\overline{468}$	$\overline{447}$	$\overline{396}$	$\overline{348}$	$\overline{336}$	$\overline{378}$	$\overline{460}$	$\overline{539}$	$\overline{553}$	$\overline{444}$	$\overline{180}$	220	694	1144	1467	1584
C(2,x)	136	122	89	61	64	112	199	294	354	339	220	4	$\overline{267}$	$\overline{533}$	$\overline{728}$	$\overline{800}$
C(4,x)	$\overline{208}$	$\overline{200}$	$\overline{188}$	$\overline{190}$	$\overline{229}$	$\overline{310}$	$\overline{418}$	$\overline{511}$	$\overline{537}$	$\overline{450}$	$\overline{226}$	117	522	906	1180	1280
C(6,x)	$\overline{152}$	$\overline{166}$	$\overline{203}$	$\overline{255}$	$\overline{307}$	$\overline{340}$	$\overline{343}$	$\overline{303}$	$\overline{215}$	$\overline{85}$	76	251	419	557	648	680
C(8,x)	12	29	77	144	216	274	304	292	234	130	$\overline{6}$	$\overline{160}$	$\overline{310}$	$\overline{435}$	$\overline{519}$	$\overline{548}$
S(1,x)	0	$\overline{68}$	$\overline{135}$	$\overline{195}$	$\overline{247}$	$\overline{288}$	$\overline{315}$	$\overline{330}$	$\overline{330}$	$\overline{315}$	$\overline{288}$	$\overline{247}$	$\overline{195}$	$\overline{135}$	$\overline{69}$	0
S(2,x)	0	$\overline{114}$	$\overline{154}$	$\overline{86}$	54	194	256	219	131	100	240	604	1156	1753	2217	2392
S(3,x)	0	22	43	61	77	90	99	103	103	99	90	77	61	43	22	0
S(4,x)	0	$\overline{54}$	$\overline{95}$	$\overline{118}$	$\overline{119}$	$\overline{104}$	$\overline{85}$	$\overline{78}$	$\overline{93}$	$\overline{142}$	$\overline{221}$	$\overline{325}$	$\overline{436}$	$\overline{534}$	$\overline{604}$	$\overline{628}$
S(5,x)	0	$\overline{29}$	$\overline{57}$	$\overline{83}$	$\overline{104}$	$\overline{122}$	$\overline{133}$	$\overline{139}$	$\overline{139}$	$\overline{133}$	$\overline{122}$	$\overline{104}$	$\overline{83}$	$\overline{57}$	$\overline{29}$	0
S(6,x)	0	98	150	126	24	$\overline{126}$	$\overline{271}$	$\overline{347}$	$\overline{293}$	$\overline{82}$	288	770	1287	1751	2070	2184
S(8,x)	0	$\overline{90}$	$\overline{168}$	$\overline{222}$	$\overline{244}$	$\overline{228}$	$\overline{173}$	$\overline{80}$	42	186	340	489	622	726	792	816
S(10,x)	0	$\overline{12}$	$\overline{25}$	$\overline{37}$	$\overline{49}$	$\overline{60}$	$\overline{71}$	$\overline{80}$	$\overline{89}$	$\overline{97}$	$\overline{104}$	$\overline{109}$	$\overline{114}$	$\overline{118}$	$\overline{119}$	$\overline{120}$

- continued -

TABLE 5.5 continued.

x(120^{ths})	1	3	5	7	9	11	13	15	17	19	21	23	25	27	29
C(0,x)	$\overline{462}$	$\overline{425}$	$\overline{370}$	$\overline{336}$	$\overline{351}$	$\overline{417}$	$\overline{503}$	$\overline{558}$	$\overline{517}$	$\overline{331}$	5	452	928	1329	1554
C(2,x)	134	106	73	58	83	151	248	332	358	293	123	$\overline{126}$	$\overline{405}$	$\overline{644}$	$\overline{782}$
C(4,x)	$\overline{188}$	$\overline{195}$	$\overline{186}$	$\overline{204}$	$\overline{265}$	$\overline{363}$	$\overline{469}$	$\overline{536}$	$\overline{511}$	$\overline{355}$	$\overline{67}$	316	722	1063	1254
C(6,x)	$\overline{155}$	$\overline{181}$	$\overline{228}$	$\overline{281}$	$\overline{326}$	$\overline{347}$	$\overline{327}$	$\overline{264}$	$\overline{155}$	$\overline{7}$	162	337	492	609	673
C(8,x)	16	49	108	180	248	293	304	268	186	65	$\overline{82}$	$\overline{236}$	$\overline{376}$	$\overline{483}$	$\overline{542}$
S(1,x)	$\overline{34}$	$\overline{103}$	$\overline{166}$	$\overline{222}$	$\overline{269}$	$\overline{303}$	$\overline{324}$	$\overline{332}$	$\overline{324}$	$\overline{303}$	$\overline{269}$	$\overline{222}$	$\overline{166}$	$\overline{103}$	$\overline{34}$
S(2,x)	$\overline{63}$	$\overline{145}$	$\overline{132}$	$\overline{21}$	130	238	248	175	101	142	394	862	1460	2015	2348
S(3,x)	10	32	52	70	84	95	102	104	102	95	84	70	52	32	10
S(4,x)	$\overline{28}$	$\overline{77}$	$\overline{110}$	$\overline{121}$	$\overline{112}$	$\overline{93}$	$\overline{79}$	$\overline{82}$	$\overline{114}$	$\overline{178}$	$\overline{271}$	$\overline{380}$	$\overline{489}$	$\overline{574}$	$\overline{623}$
S(5,x)	$\overline{14}$	$\overline{43}$	$\overline{70}$	$\overline{94}$	$\overline{113}$	$\overline{128}$	$\overline{137}$	$\overline{140}$	$\overline{137}$	$\overline{128}$	$\overline{113}$	$\overline{94}$	$\overline{70}$	$\overline{43}$	$\overline{14}$
S(6,x)	52	133	148	84	$\overline{47}$	$\overline{204}$	$\overline{322}$	$\overline{339}$	$\overline{208}$	86	518	1030	1531	1933	2155
S(8,x)	$\overline{46}$	$\overline{132}$	$\overline{198}$	$\overline{236}$	$\overline{241}$	$\overline{206}$	$\overline{130}$	$\overline{23}$	111	262	416	559	679	764	811
S(10,x)	$\overline{6}$	$\overline{19}$	$\overline{31}$	$\overline{43}$	$\overline{54}$	$\overline{65}$	$\overline{76}$	$\overline{85}$	$\overline{94}$	$\overline{101}$	$\overline{107}$	$\overline{112}$	$\overline{116}$	$\overline{119}$	$\overline{120}$

TABLE 5.6

PRELIMINARY SUMMATIONS: Values of $\Sigma 2A_1 \cos 2\pi ky$ and $\Sigma 2A_2 \sin 2\pi ky$ FOR ALL VALUES OF h.

y(120ths	0	2	4	6	8	10	12	14	16	18	20	22	24	26	28	30
C(0,y)	20	9	$\overline{30}$	$\overline{112}$	$\overline{232}$	$\overline{356}$	$\overline{428}$	$\overline{393}$	$\overline{235}$	2	236	388	418	350	261	220
C(2,y)	$\overline{384}$	$\overline{358}$	$\overline{257}$	$\overline{37}$	303	676	933	926	610	89	$\overline{432}$	$\overline{741}$	$\overline{741}$	$\overline{503}$	$\overline{224}$	$\overline{104}$
C(4,y)	200	201	166	32	$\overline{229}$	$\overline{564}$	$\overline{834}$	$\overline{885}$	$\overline{653}$	$\overline{200}$	296	643	734	608	421	336
C(6,y)	28	13	28	87	152	206	237	236	196	119	14	$\overline{106}$	$\overline{223}$	$\overline{322}$	$\overline{389}$	$\overline{412}$
S(1,y)	0	745	1225	1275	897	308	$\overline{141}$	$\overline{156}$	316	1041	1632	1799	1521	1001	465	0
S(2,y)	0	72	130	159	158	$\overline{132}$	$\overline{96}$	$\overline{68}$	$\overline{64}$	$\overline{97}$	$\overline{166}$	$\overline{265}$	$\overline{376}$	$\overline{478}$	$\overline{551}$	$\overline{576}$
S(3,y)	0	$\overline{874}$	$\overline{1362}$	$\overline{1281}$	$\overline{747}$	$\overline{90}$	327	309	$\overline{95}$	$\overline{645}$	$\overline{1068}$	$\overline{1201}$	$\overline{1049}$	$\overline{726}$	$\overline{358}$	0
S(5,y)	0	342	574	622	491	248	10	$\overline{117}$	$\overline{69}$	146	450	721	842	746	438	0
S(7,y)	0	$\overline{66}$	$\overline{130}$	$\overline{188}$	$\overline{238}$	$\overline{277}$	$\overline{304}$	$\overline{318}$	$\overline{318}$	$\overline{304}$	$\overline{277}$	$\overline{238}$	$\overline{188}$	$\overline{130}$	$\overline{66}$	0

table 5.7. The values of the electron densities along the line x = 30/120^{ths} for values of y from 0/120^{ths} to 60/120^{ths} are shown in the last two rows of this table. To obtain the values of the electron density at the points between y = 0/120^{ths} and y = 30/120^{ths}, the second last row must be read from left to right; reading the last row from right to left gives density values at the points between y = 30/120^{ths} and y = 60/120^{ths}.

In performing the final summations it is advisable to keep the sums of the odd and even sines and cosines apart, because of their different symmetries about the point y = 1/4. In the example shown in table 5.7, the second last row was obtained by subtracting the sum of the even and odd sines from the cosine terms, while the last row was obtained by adding the difference between the even and odd sines, in that order, to the cosine terms. This procedure is followed for all syntheses along the lines x = 30/120^{ths} down to x = 0/120^{ths}. In the syntheses along the lines x = 31/120ths to x = 60/120ths the symmetry properties of the trigonometric functions demand that to obtain density values from y = 0/120^{ths} to y = 30/120^{ths}, the difference between the even and odd sines, in that order, be subtracted from the cosines, while values between y = 30/120^{ths} and 60/120^{ths} are arrived at by adding the sum of the even and odd sine terms to the cosine terms.

Figure 5.3 shows a plot of the electron density along the line x = 30/120^{ths} from y = 0 to y = 60/120^{ths} for unirradiated $AgMnO_4$. The full curve is that obtained from the experimental structure factors while the dotted curve is that obtained from Sasvari's figures by carrying out another synthesis analogous to that described above, but using his structure factors.

- Figure 5.4 -

TABLE 5.7

FINAL SUMMATIONS FOR $x = 30/120^{ths}$.

$y(120^{ths})$ at $x = 30/120$

	0	1	2	3	4	5	6	7	8	9	10	11	12	13	14	15
F(000)	416	416	416	416	416	416	416	416	416	416	416	416	416	416	416	416
$C(0,\frac{30}{120})$	1584	1584	1584	1584	1584	1584	1584	1584	1584	1584	1584	1584	1584	1584	1584	1584
	20	17	9	$\overline{5}$	$\overline{30}$	$\overline{64}$	$\overline{112}$	$\overline{168}$	$\overline{232}$	$\overline{297}$	$\overline{356}$	$\overline{403}$	$\overline{428}$	$\overline{427}$	$\overline{393}$	$\overline{328}$
$\overline{800}$ C2	$\overline{800}$	$\overline{796}$	$\overline{783}$	$\overline{761}$	$\overline{731}$	$\overline{693}$	$\overline{647}$	$\overline{595}$	$\overline{535}$	$\overline{470}$	$\overline{400}$	$\overline{325}$	$\overline{247}$	$\overline{166}$	$\overline{84}$	0
1280 C4	1280	1251	1169	1036	857	640	396	133	$\overline{133}$	$\overline{396}$	$\overline{640}$	$\overline{857}$	$\overline{1036}$	$\overline{1169}$	$\overline{1251}$	$\overline{1280}$
680 C6	680	647	550	400	210	0	$\overline{210}$	$\overline{400}$	$\overline{550}$	$\overline{647}$	$\overline{680}$	$\overline{647}$	$\overline{550}$	$\overline{400}$	$\overline{210}$	0
$\overline{548}$ C8	$\overline{548}$	$\overline{501}$	$\overline{367}$	$\overline{170}$	57	274	444	536	536	444	274	57	$\overline{170}$	$\overline{367}$	$\overline{501}$	$\overline{548}$
SUM COSINES	2632	2618	2578	2500	2363	2157	1871	1506	1086	634	198	$\overline{175}$	$\overline{431}$	$\overline{529}$	$\overline{439}$	$\overline{156}$
2392 S2	0	251	497	738	972	1196	1406	1600	1778	1934	2072	2185	2276	2340	2379	2392
$\overline{628}$ S4	0	$\overline{131}$	$\overline{255}$	$\overline{369}$	$\overline{467}$	$\overline{544}$	$\overline{598}$	$\overline{625}$	$\overline{625}$	$\overline{598}$	$\overline{544}$	$\overline{467}$	$\overline{369}$	$\overline{255}$	$\overline{131}$	0
2184 S6	0	675	1283	1767	2077	2184	2077	1767	1283	675	0	$\overline{675}$	$\overline{1283}$	$\overline{1767}$	$\overline{2077}$	$\overline{2184}$
816 S8	0	332	607	776	812	607	479	169	$\overline{169}$	$\overline{479}$	$\overline{707}$	$\overline{812}$	$\overline{776}$	$\overline{607}$	$\overline{332}$	0
$\overline{120}$ S10	0	$\overline{60}$	$\overline{104}$	$\overline{120}$	$\overline{104}$	$\overline{60}$	0	60	104	120	104	60	0	$\overline{60}$	$\overline{104}$	$\overline{120}$
SUM EVEN SINES	0	1067	2028	2792	3290	3483	3364	2971	2371	1652	925	297	$\overline{152}$	$\overline{349}$	$\overline{265}$	88
SUM ODD SINES	0	0	0	0	0	0	0	0	0	0	0	0	0	0	0	0
	2632	1551	550	$\overline{292}$	$\overline{927}$	$\overline{1326}$	$\overline{1493}$	$\overline{1465}$	$\overline{1285}$	$\overline{1018}$	$\overline{727}$	$\overline{472}$	$\overline{279}$	$\overline{180}$	$\overline{174}$	$\overline{244}$
	2632	3685	4606	5292	5653	5640	5235	4477	3457	2286	1123	122	$\overline{583}$	$\overline{878}$	$\overline{704}$	$\overline{68}$

- continued -

TABLE 5.7 continued.

$y(120^{ths})$ at $x = 30/120$

	16	17	18	19	20	21	22	23	24	25	26	27	28	29	30
F(000)	416	416	416	416	416	416	416	416	416	416	416	416	416	416	416
$C(0,\frac{30}{120})$	1584	1584	1584	1584	1584	1584	1584	1584	1584	1584	1584	1584	1584	1584	1584
	$\overline{235}$	$\overline{123}$	2	123	236	327	388	420	418	392	350	303	261	231	220
$\overline{800}$ C2	84	166	247	325	400	470	535	595	647	693	731	761	783	796	800
1280 C4	$\overline{1251}$	$\overline{1169}$	$\overline{1036}$	$\overline{857}$	$\overline{640}$	$\overline{396}$	$\overline{133}$	133	396	640	857	1036	1169	1251	1280
680 C6	210	400	550	647	680	647	550	400	210	0	$\overline{210}$	$\overline{400}$	$\overline{550}$	$\overline{647}$	$\overline{680}$
$\overline{548}$ C8	$\overline{501}$	$\overline{367}$	$\overline{170}$	57	274	444	536	536	444	274	57	$\overline{170}$	$\overline{367}$	$\overline{501}$	$\overline{548}$
SUM COSINES	307	907	1593	2295	2950	3492	3876	4084	4115	3999	3785	3430	3296	3130	3072
2392 S2	2379	2340	2276	2185	2072	1934	1778	1600	1406	1196	972	738	497	251	0
$\overline{628}$ S4	131	255	369	467	544	598	625	625	598	544	467	369	255	131	0
2184 S6	$\overline{2077}$	$\overline{1767}$	$\overline{1283}$	$\overline{675}$	0	675	1283	1767	2077	2184	2077	1767	1283	675	0
816 S8	332	607	776	812	707	479	169	$\overline{169}$	$\overline{479}$	$\overline{607}$	$\overline{812}$	$\overline{776}$	$\overline{607}$	$\overline{332}$	0
$\overline{120}$ S10	$\overline{104}$	$\overline{60}$	0	60	104	120	104	60	0	$\overline{60}$	$\overline{104}$	$\overline{120}$	$\overline{104}$	$\overline{60}$	0
SUM EVEN SINES	661	1375	2138	2849	3427	3806	3959	3883	3602	3157	2600	1978	1324	665	0
SUM ODD SINES	0	0	0	0	0	0	0	0	0	0	0	0	0	0	0
	$\overline{354}$	$\overline{468}$	$\overline{545}$	$\overline{554}$	$\overline{477}$	$\overline{314}$	$\overline{83}$	201	513	842	1185	1552	1972	2465	3072
	968	2282	3731	5144	6377	7298	7835	7967	7717	7156	6385	5508	4620	3795	3072

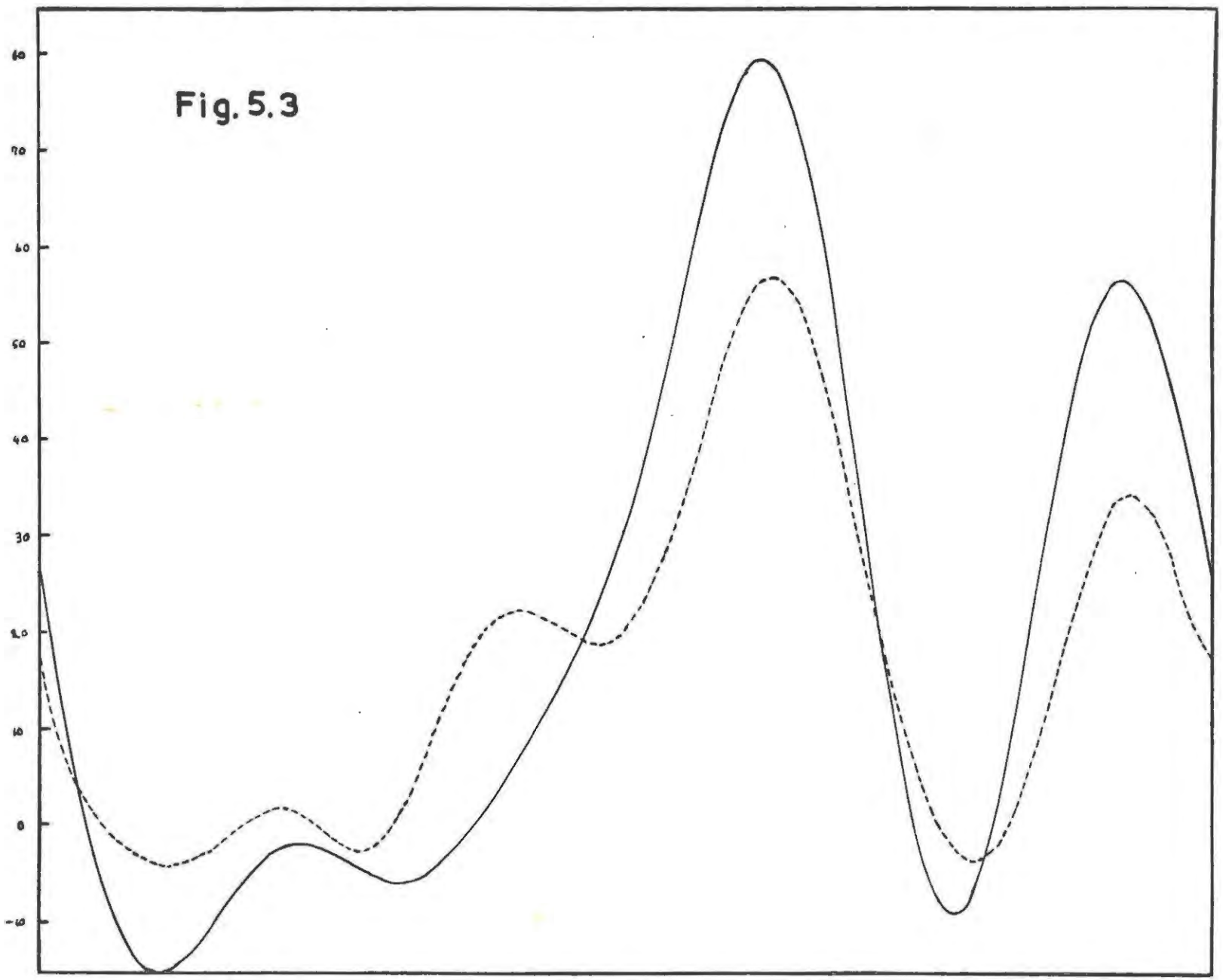
Fig. 5.3
80
70
60
50
40
30
20
10
0
-10

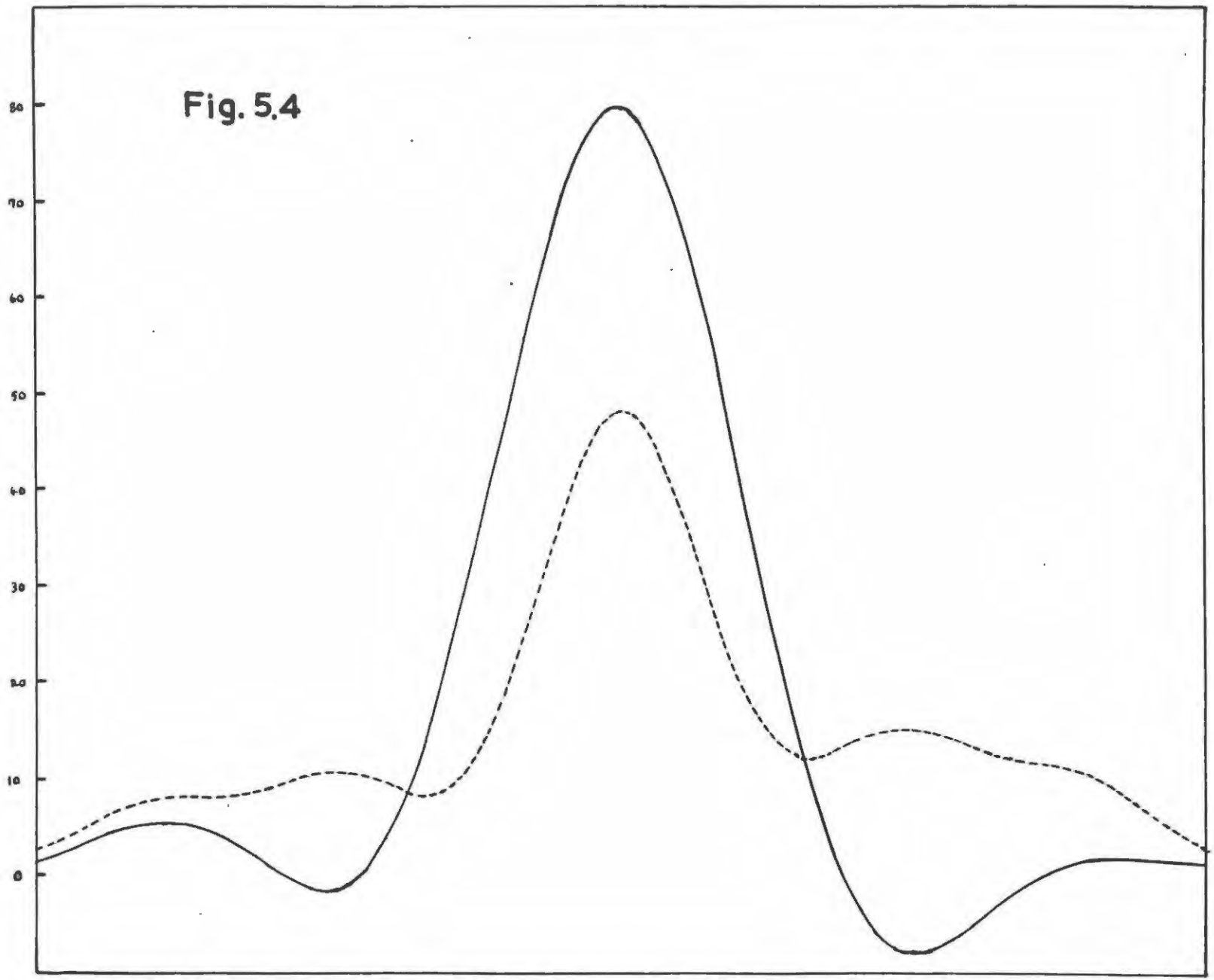
Fig. 5.4
80
70
60
50
40
30
20
10
0

Figure 5.4 shows a similar plot of the electron density for unirradiated $AgMnO_4$ at y = $37/120^{ths}$, for x = 0 to x = $60/120^{ths}$. This y value was chosen because it is the y coordinate of the silver atom and it was hoped to show that the corresponding x coordinate was not exactly 0.25, as reported by Sasvari. Once again the full line is the experimental result, and the dotted line Sasvari's result. Yet another plot at y = $56/120^{ths}$ through the manganese was drawn, but is not shown.

In addition to the syntheses shown, others for x values of 0, 2 ..... $28/120^{ths}$, and x = 32, 34 ..... $60/120^{ths}$ were made. The resulting profiles were then used to draw an electron density contour map (projection parallel to [001]), shown in figure 5.5. This map covers one quarter of the unit cell in projection, and is all that is necessary, since symmetry repeats this quadrant in the entire projection.

Exactly the same procedures were carried out for the irradiated (300 Mrad) $AgMnO_4$, using the structure factors listed in table 5.3. Figures 5.6, 5.7 and 5.8 show profiles (in full line) for irradiated $AgMnO_4$ at x = $30/120^{ths}$ for y = 0 to $60/120^{ths}$, and at y = $37/120^{ths}$ and y = $56/120^{ths}$ for x = 0 to $60/120^{ths}$. The dotted profiles are of the unirradiated $AgMnO_4$ and are drawn in for comparative purposes. These profiles are through the peaks of the silver and manganese atoms.

The profiles mentioned so far enable a check to be made of movement of ions only in the ab plane of the unit cell. In order to check for any movement in the c direction it was necessary to synthesise electron density profiles through the projection on the

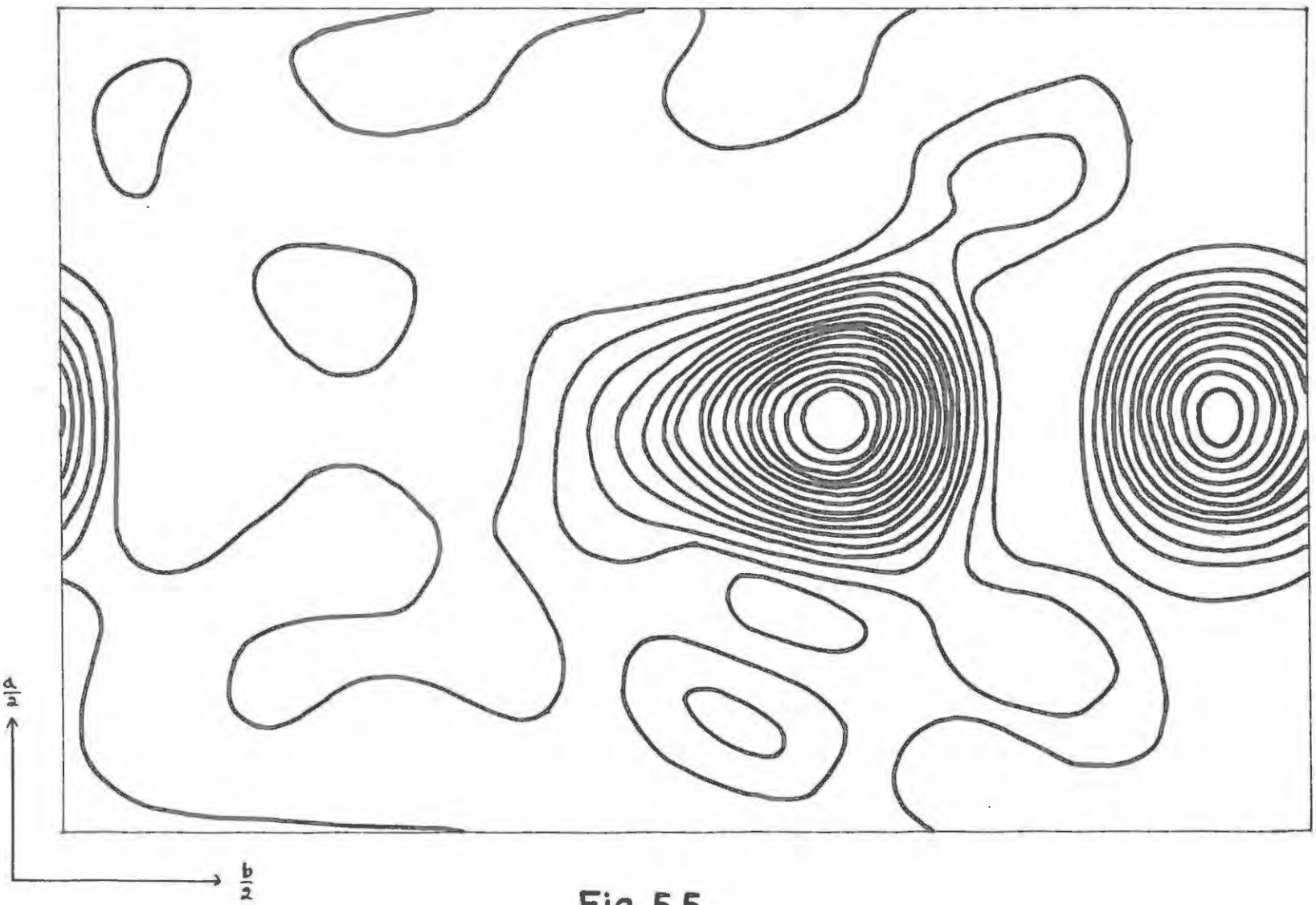

Fig. 5.5

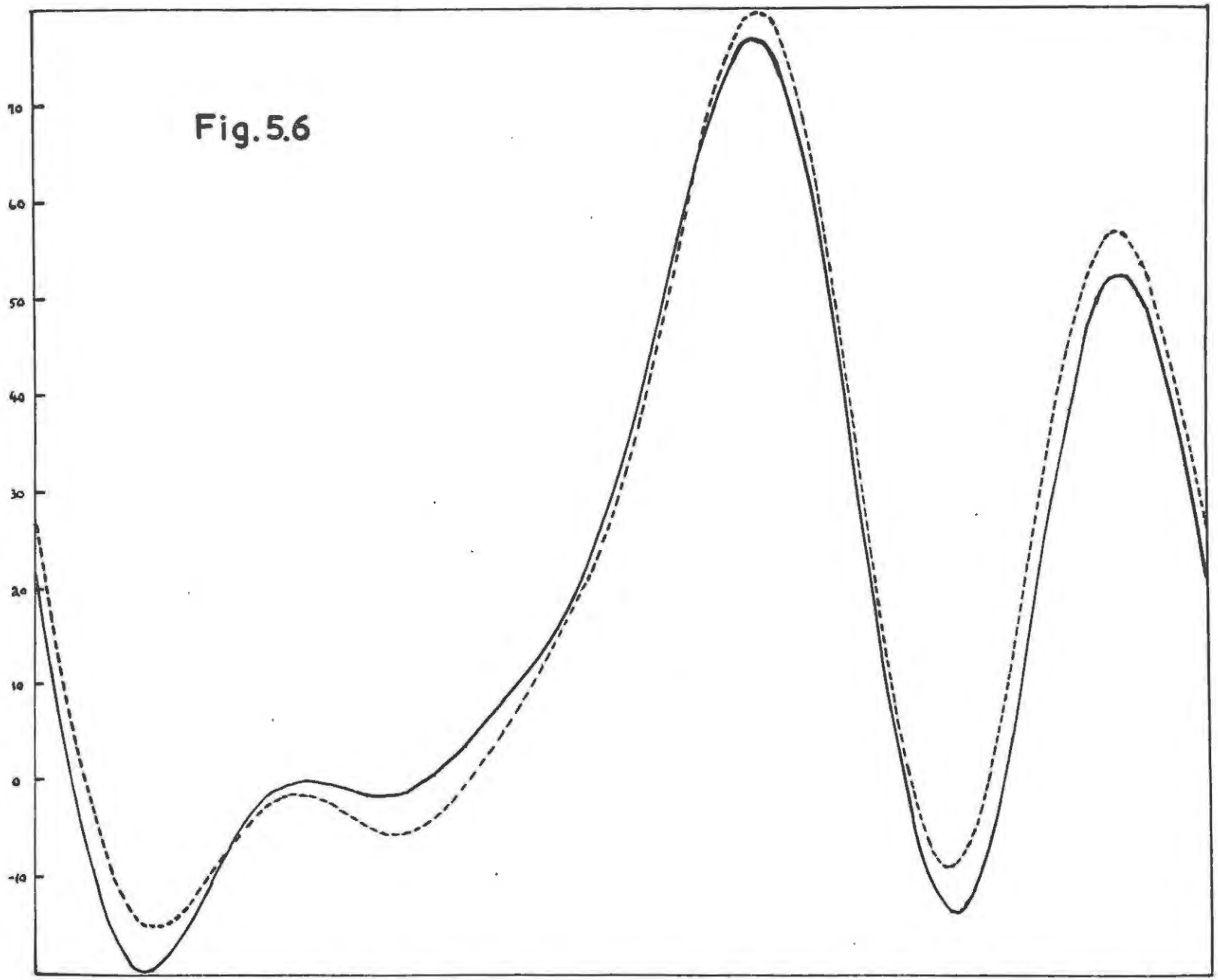
Fig. 5.6
70
60
50
40
30
20
10
0
-10

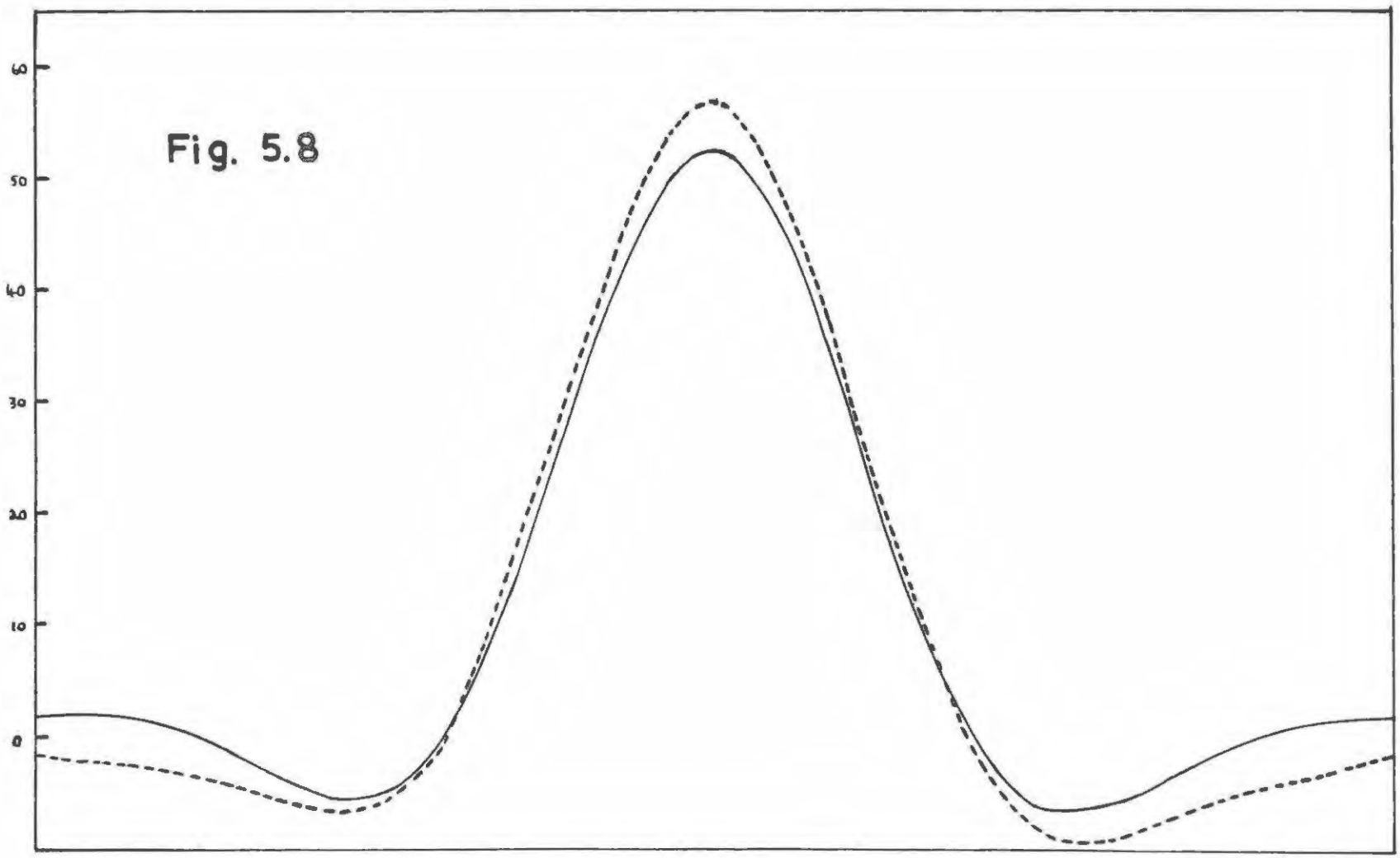
Fig. 5.8

TABLE 5.8

Index okl	Sin θ	$\frac{\text{Sin } \theta/\lambda}{\times 10^{-8}}$	$(Lp)^{-1}$	$I_{Unirrd.}$	$F_{Unirrd.}$	$I_{Irrd.}$ (Rel.)	$F_{Irrd.}$
011	.1427	.093	.294	903	$\overline{66}$	639	$\overline{55}$
020	.1862	.121	.392	1692	$\overline{103}$	1692	$\overline{103}$
021	.2152	.140	.460	1650	112	1371	100
002	.2162	.141	.463	186	$\overline{38}$	552	$\overline{64}$
031	.2993	.194	.682	1569	$\overline{133}$	1530	$\overline{129}$
013	.3373	.219	.795	42	23	90	34
032	.3530	.230	.845	9	$\overline{12}$	6	$\overline{9}$
040	.3725	.242	.909	573	93	615	30
023	.3739	.243	.913	27	20	33	22
041	.3876	.253	.960	195	$\overline{56}$	234	$\overline{19}$
033	.4279	.278	1.104	837	124	750	115
042	.4304	.279	1.112	39	$\overline{27}$	42	$\overline{27}$
004	.4323	.281	1.121	453	$\overline{92}$	519	$\overline{96}$
014	.4423	.287	1.157	603	$\overline{107}$	1014	$\overline{137}$
024	.4707	.306	1.267	69	38	51	32
051	.4776	.310	1.295	24	23	27	24
060	.5595	.363	1.629	414	106	327	98
053	.5670	.368	1.656	69	$\overline{43}$	78	$\overline{45}$
025	.5716	.372	1.672	108	$\overline{55}$	96	$\overline{51}$
062	.5987	.389	1.773	66	$\overline{44}$	66	$\overline{43}$
054	.6351	.412	1.890	138	$\overline{66}$	165	$\overline{71}$

- continued -

TABLE 5.8 continued.

Index okl	Sin θ	Sin θ/λ x 10^{-8}	$(Lp)^{-1}$	$I_{Unirrd.}$	$F_{Unirrd.}$	$I_{Irrd.}$ (Rel.)	$F_{Irrd.}$
006	.6485	.422	1.927	243	88	291	95
016	.6551	.426	1.938	108	$\overline{59}$	135	$\overline{65}$
045	.6561	.426	1.938	27	29	51	40
071	.6603	.429	1.949	12	$\overline{20}$	6	$\overline{14}$
026	.6747	.439	1.976	21	$\overline{26}$	30	$\overline{31}$
064	.7062	.458	2.000	30	$\overline{32}$	51	$\overline{40}$
073	.7276	.473	1.988	33	33	48	39
080	.7449	.484	1.965	12	$\overline{20}$	6	$\overline{14}$
046	.7478	.486	1.957	30	31	42	36
081	.7521	.489	1.949	15	$\overline{22}$	4	$\overline{19}$
017	.7623	.496	1.923	45	38	20	43
027	.7793	.507	1.869	591	135	158	119
0.74	.7818	.509	1.855	51	$\overline{40}$	23	$\overline{45}$
056	.7982	.519	1.789	39	34	20	41
037	.8067	.523	1.748	30	$\overline{29}$	11	$\overline{30}$
047	.8433	.549	1.538	210	$\overline{73}$	414	$\overline{101}$
091	.8445	.549	1.538	108	$\overline{52}$	168	$\overline{64}$
066	.8557	.557	1.456	36	29	141	57
008	.8648	.528	1.393	93	$\overline{46}$	105	$\overline{48}$
018	.8696	.565	1.361	276	79	351	87
057	.8882	.577	1.224	33	26	66	36
076	.9191	.597	.982	72	34	138	47

- continued -

the unirradiated and irradiated crystals used were of practically the same size and shape.

As before, the signs of the structure factors were taken from Sasvari's paper, and the signs of those structure factors not listed by him were inferred by calculations made using his parameters.

In the calculations of electron densities projected on the 100 face the factor F(000) = 416 was not included, since the measured structure factors are in arbitrary units. No attempt was made to place them on a comparatively absolute basis as was done in the case of the 001 projection.

Profiles were drawn through the silver ion ($y = \frac{37}{120}$, $z = 41/120$) for y (120^{ths}) at $z = 41/120$, and for y (120^{ths}) at $y=37/120$, and are shown in figures 5.9 and 5.10 respectively. The dotted line represents the unirradiated, and the full line the irradiated, profile. They were also drawn through the manganese ion ($y = \frac{4}{120}$, $y = 23/120$) for y (120^{ths}) at $z = 23/120$, and z (120^{ths}) at $y = 4/120$, and these are shown in figures 5.11 and 5.12. Once again the dotted line represents the unirradiated and the full line the irradiated, profile.

5.2 (f) Discussion of the Electron Density Profiles.

(i) It is of interest to compare the profiles drawn through the electron density projected parallel to [001] from the experimental data and from Sasvari's figures. Close scrutiny of figure 5.3 shows that the locations of the silver and manganese peaks drawn using experimental structure factors differ from those drawn from Sasvari's figures. According to the experimental

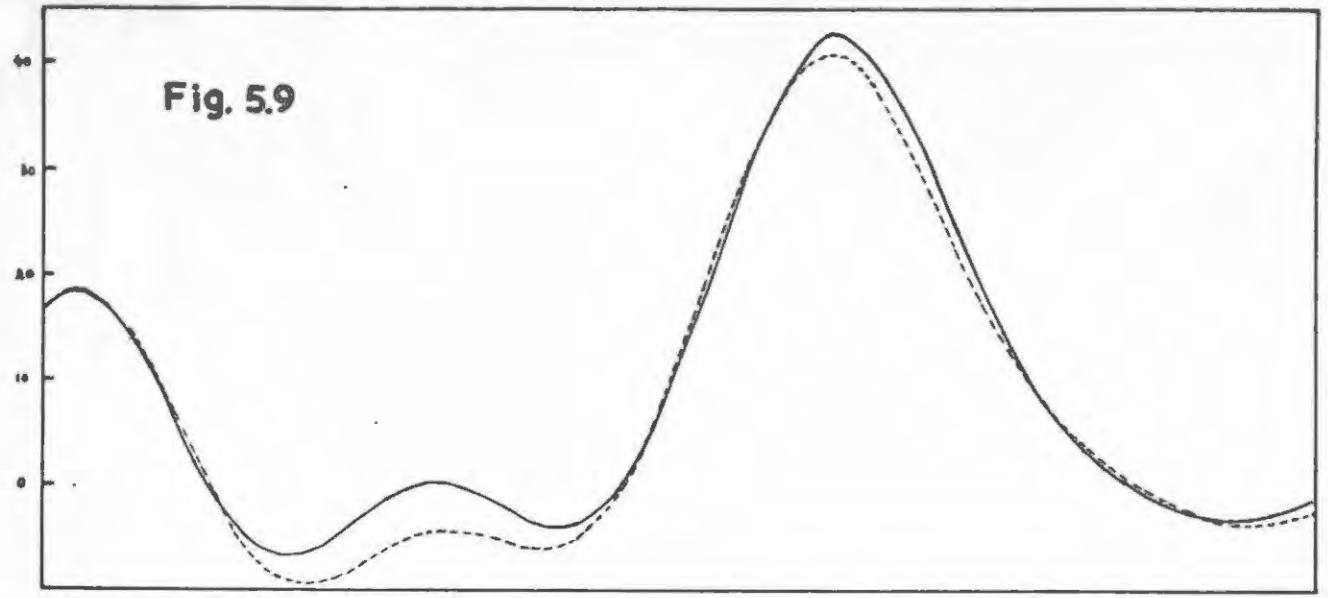

Fig. 5.9

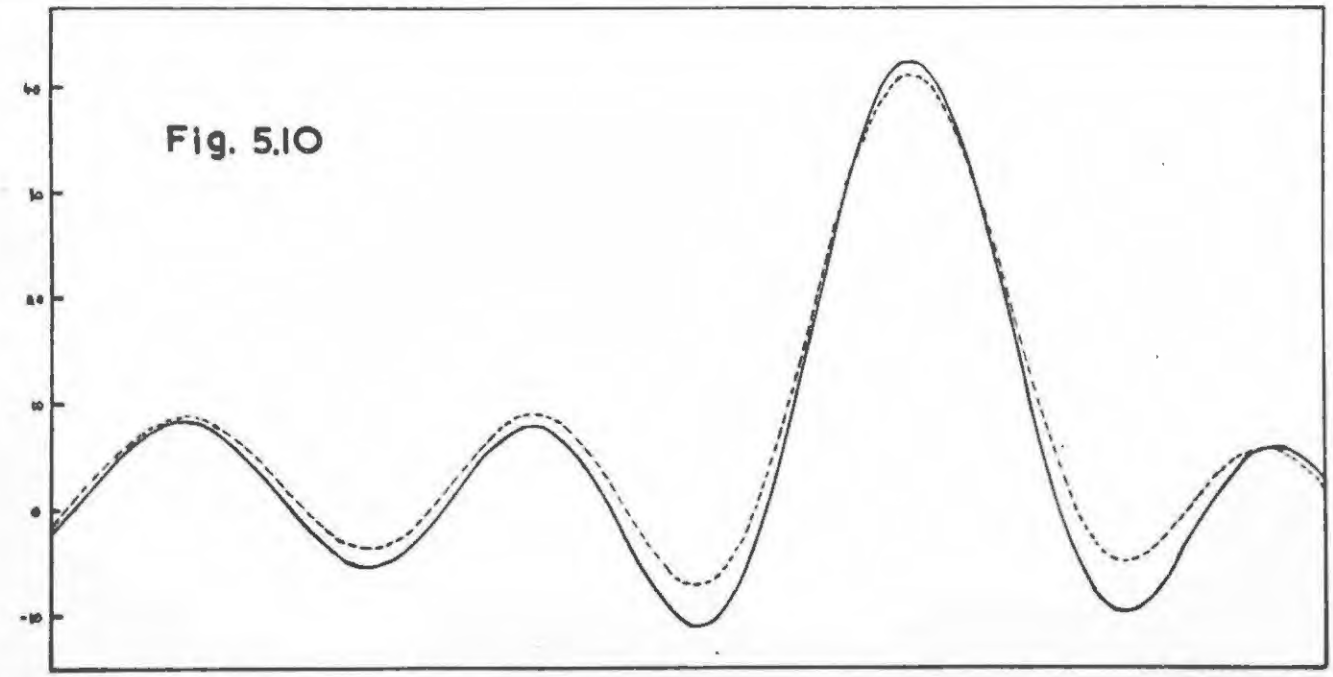

Fig. 5.10

results, the silver has y = 0.310 and the manganese y = -0.038, instead of the values y = 0.323 and y = -0.033, respectively, given by Sasvari. These small changes do not however, affect the calculated structure factors F(hk0) appreciably.

On the other hand, figure 5.4 shows that the x-parameter of silver is not exactly 0.25, as given by Sasvari, but is in fact 0.248. Similarly a profile drawn through the manganese shows that its x-parameter also differs from 0.25, and is in fact 0.249. These small changes although not affecting the majority of the structure factors F(hk0) appreciably, do cause the calculated $|F|$ for the reflections 130, 230, 150 and 250 to have small values, and not to be zero as recorded by Sasvari. These values do not agree very well with the measured $|F|$ values, but this is not to be expected, as no absorption correction was made to the measured intensities, as the main object in mind was not a structure analysis but a comparison of the profiles of irradiated and un-irradiated specimens. Nevertheless, it is felt that this is a small improvement on Sasvari's parameters.

(ii) Comparison of the profiles drawn through the electron densities projected on the 001 face of the unit cell (figures 5.6, 5.7 and 5.8) show that there is a small drop in the area under the silver and manganese peaks of the irradiated specimen. This drop, however, is almost definitely not due to an irradiation effect but to experimental error. The drop in area is of the order of 5% or less, and since the errors in measurement of intensities

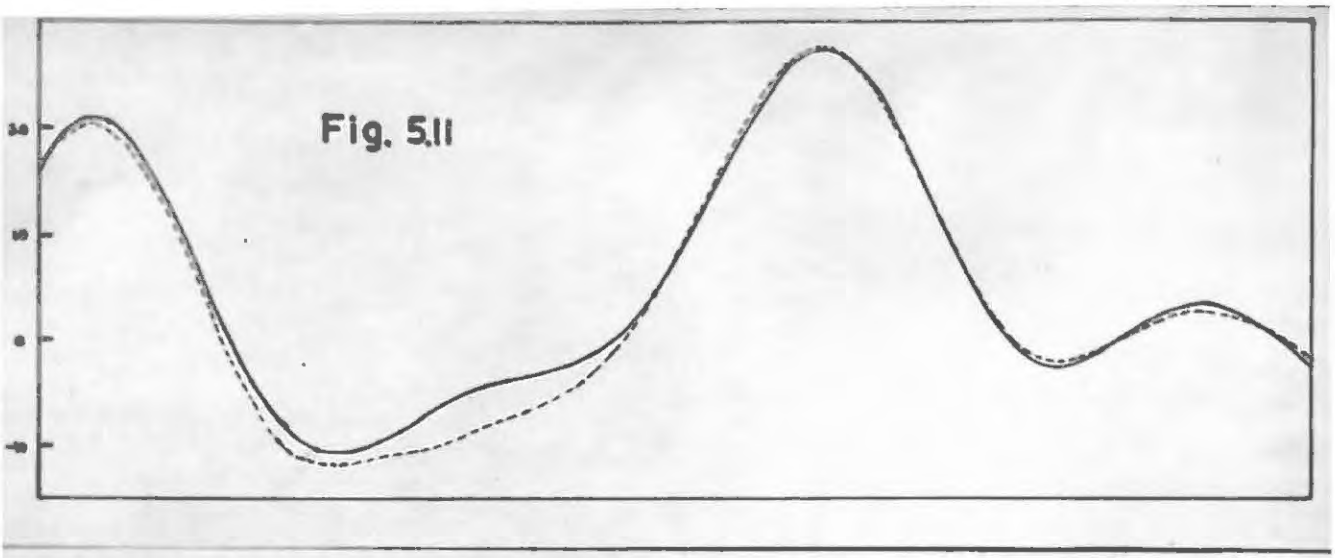

Fig. 5.11

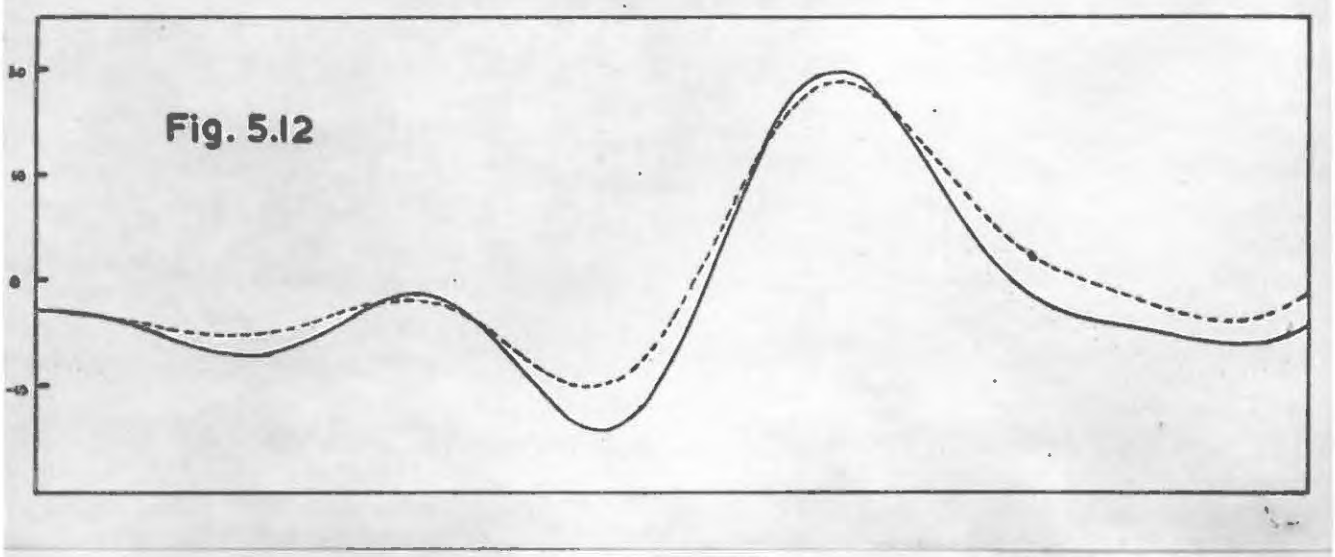

Fig. 5.12

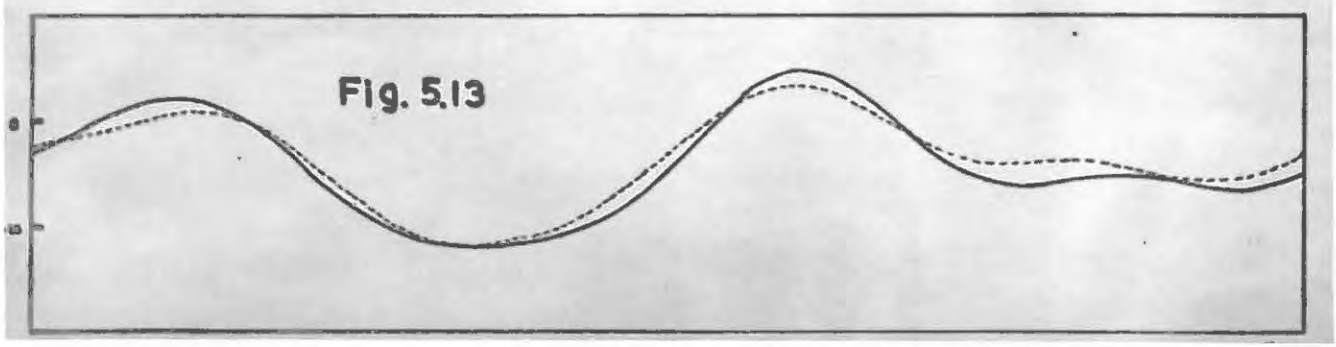

Fig. 5.13

are estimated as being of the order of 10%, a small difference must be expected. The magnitude of the drop in area under the boron peak in Tucker and Senio's[97] investigation of neutron irradiated boron carbide is 47%, which is well outside the limits of experimental error, and must thus definitely be real, and since it is unlikely that the small drop shown in silver permanganate would account for the enormous irradiation effect evidenced by the thermal decomposition the drop must be ascribed to experimental error. This conclusion is borne out by the fact that the profiles drawn through the silver and manganese peaks projected on 100, where the error in measurement of intensities, and hence in the structure factors used for computation was higher than in the projection on 001, actually show an increase in area after irradiation (see figures 5.9 - 5.12). The results obtained thus preclude the ejection of silver ions, or for that matter manganese ions, into interstitial positions, as a process of irradiation. The irradiation effect must be of a different character altogether.

Examination of the listed structure factors F(hk0) (table 5.3) for unirradiated and irradiated specimens is of interest. Comparison of $|F|$ for unirradiated and irradiated specimens shows that the value is smaller for most reflections in the irradiated specimen having $0 < \sin\theta/\lambda \times 10^{8} < 0.400$ whereas for $\sin\theta/\lambda > .400\ \text{Å}^{-1}$ the structure factors of the unirradiated and irradiated specimens are very nearly equal. An examination of the plot of the scattering factor, f, for oxygen, against

$\sin \theta/\lambda \times 10^{-8}$ shows that the value of f is negligibly small after $\sin \theta/\lambda \times 10^{-8} = 0.400$. Since the electron density profiles show no movement of silver or manganese ions, and since the structure factors for those reflections where oxygen plays no part in contributing to diffraction remain equal the drop in the values of $|F|$ for the high angle reflections might be due to the movement of oxygen atoms on irradiation; this would tend to lower the structure amplitudes of those reflections where oxygen plays a relatively major role in diffraction, while it would not affect those reflections where the oxygen contribution to the structure amplitude is negligible. Accordingly, since single oxygen peaks do not appear in the Fourier analysis, it was decided that a profile along y (120^{ths}) at y = 8/120 might show up a peak due to two oxygen atoms superimposed in projection parallel to [100], because Sasvari gives the parameters of O(3) and O(4) as both being y = 8/120, z = 30/120. A synthesis of the unirradiated $AgMnO_4$ shows no peak at this point, but a peak appears at z = 36/120 (see figure 5.13). It is dubious whether this peak is due to oxygen atoms in projection, however; it is more likely a series termination effect[112], very often found in Fourier syntheses when there is a very heavy atom in the structure and insufficient spots are recorded on the X-ray film. Moreover, once again the peak for the irradiated specimen (full line) is higher than that for the unirradiated (dotted line); thus it is felt that a hope of showing up oxygen movement in the analysis is rather optimistic.

- In addition to -

In addition to the fact that irradiation does not produce a drop in area under the peaks, it is seen from all the profile diagrams that there is no shift in the parameters of either the silver or manganese produced by irradiation. Both these results lead us to discard Prout's suggestion for the irradiation mechanism postulated for permanganates.

5.3 The Investigation of the Thermal Decomposition of Unirradiated Silver Permanganate.

The general form of the p/t curve for silver permangante is known from previous work[17]. Since it was decided initially to confine attention to the induction and acceleratory periods only, the characteristic curve for the particular batch of crystals under study was limited to that part of the curve up to the inflexion point.

Crystals were decomposed at 108°C in the electric furnace. For a single run 16 mg. of crystals were decomposed in a platinum bucket previously treated with concentrated nitric acid and washed with distilled water, and finally heated to redness.

Data for a typical run are shown in table 5.9. The time is in minutes and pressure is in cm. mercury x 10^3. The resulting graph is shown in figure 5.14.

A single crystal of good shape was then selected from the unirradiated crystals and mounted on a short, thin glass rod with "araldit" adhesive, the rod being fitted into a brass mount which in turn fitted into the goniometer head. The crystal and goniometer head were then

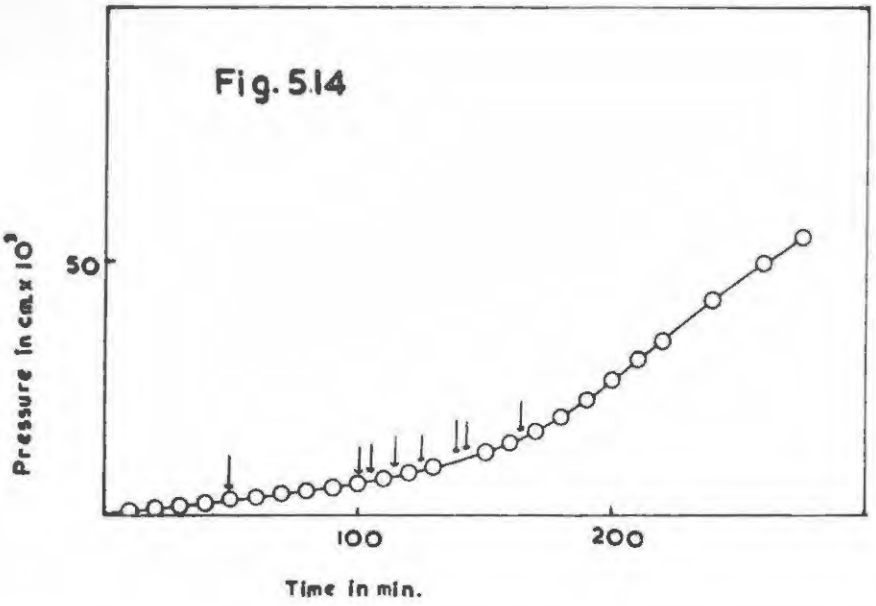
Fig. 5.14
Pressure in cm. x 10³
50
100
200
Time in min.

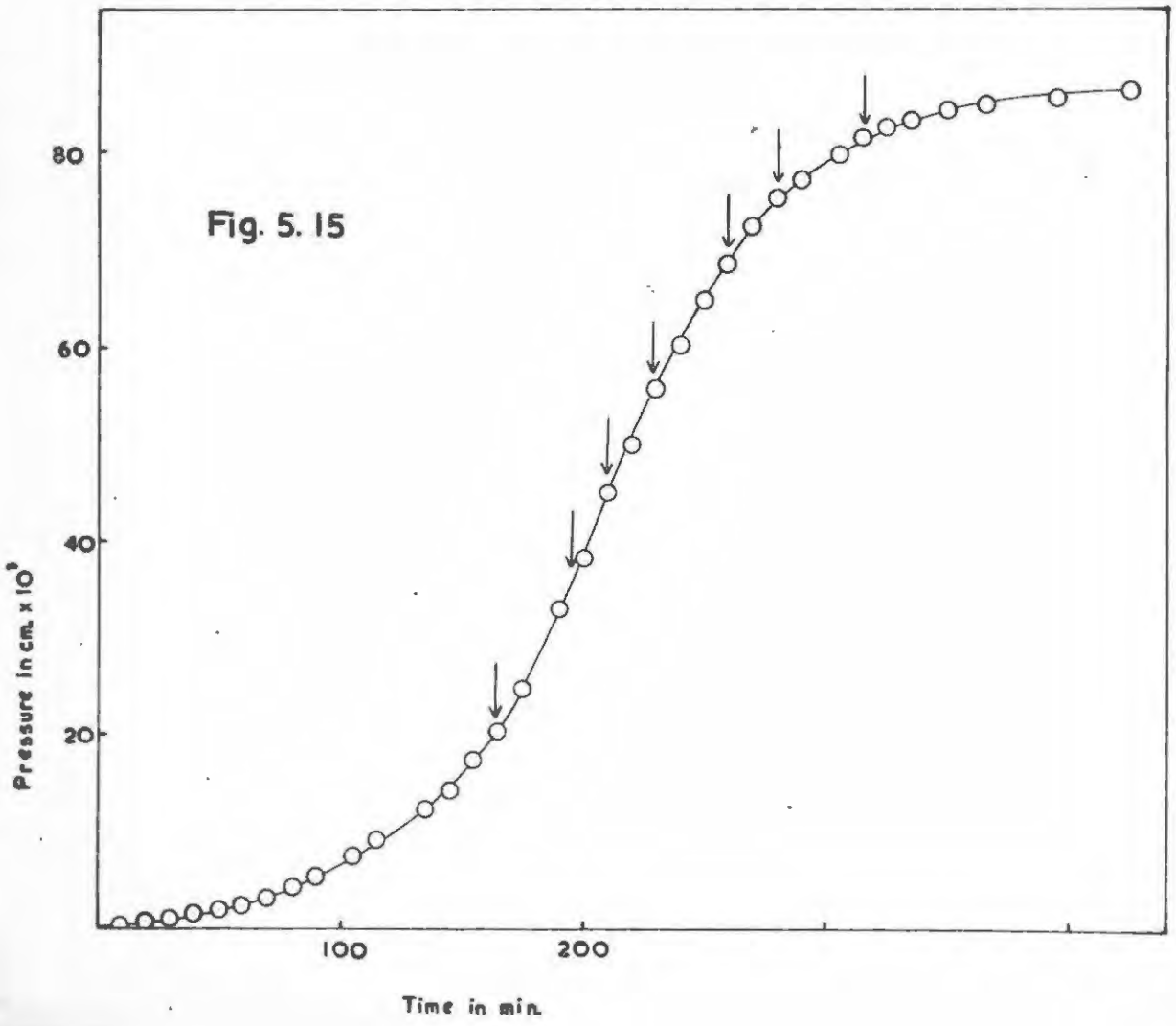
Fig. 5. 15
Pressure in cm. x 10³
80
60
40
20
100
200
Time in min.

TABLE 5.9

Time	Pressure	Time	Pressure	Time	Pressure	Time	Pressure
5	0.2×10^{-3}	75	4.5	145	11.6	215	32.5
10	0.9	80	4.9	150	12.4	220	34.4
15	1.0	85	5.2	155	13.2	225	36.4
20	1.4	90	5.5	160	14.3	230	-
25	1.4	95	6.0	165	15.2	235	40.3
30	1.9	100	6.4	170	16.5	240	42.2
35	2.1	105	6.9	175	18.0	245	44.5
40	2.5	110	7.2	180	19.4	250	45.8
45	3.0	115	7.9	185	21.0	255	48.0
50	3.1	120	8.6	190	22.8	260	49.4
55	3.3	125	9.1	195	24.9	265	50.9
60	3.6	130	9.5	200	26.8	270	-
65	3.9	135	10.9	205	28.2	275	54.1
70	4.3	140	-	210	30.7		

TABLE 5.10

10	0.5×10^{-3}	105	7.4	200	38.1	290	77.1
20	0.9	115	9.1	210	45.0	305	79.8
30	1.0	125	10.1	220	49.9	315	81.7
40	1.6	135	12.1	230	55.7	325	82.8
50	2.0	145	14.1	240	60.0	335	83.2
60	2.4	155	17.2	250	64.7	350	84.9
70	3.2	165	20.1	260	68.4	365	85.1
80	4.3	175	24.5	270	72.3	395	85.6
90	5.3	190	32.9	280	75.3	425	86.7

TABLE 5.11

10	0.1×10^{-3}	91	11.8	160	54.2	220	110.0
25	1.5	100	14.0	165	61.1	230	113.7
30	2.1	111	17.4	170	67.2	240	116.0
40	3.0	120	21.0	175	173.2	255	118.2
50	4.3	135	29.6	180	78.8	270	120.0
60	5.8	140	33.6	190	89.4	285	120.5
71	7.5	150	43.4	200	97.8		
81	9.6	155	48.3	210	104.8		

placed in the electric furnace for 4 minutes, withdrawn, and the crystal was then photographed. The rotation photograph was made with the c-axis as rotation axis, and the Laue photograph was taken with the b-axis parallel to the X-ray beam, the c-axis being perpendicular to the beam

The crystal was heated for additional periods of 46 minutes, 54, 9 14, 14, 19, 5, 6 and 25 minutes, and withdrawn and photographed after each insertion into the furnace. Since 4 minutes was estimated as warm-up time, these heatings correspond to 50, 100, 105, 115, 125, 140, 143 and 165 minutes heating respectively. No change was detected in any of the photographs until after 140 minutes of heating at 108°C; the first definite signs of strain, namely asterism of some of the more prominent spots on the Laue photographs, becomes apparent. The rotation photograph, in contrast, shows no signs of strain. It was also noticed that the faces of the crystal after this point gave no reflections; reflections had, however, been obtained after all heatings prior to this point.

The complete decomposition curve was then obtained by heating 17 mg. of crystals in the platinum bucket at 108°C. Data for this curve are given in table 5.10, and the accompanying graph is given in figure 5.15.

Once again, a crystal was selected and mounted on the goniometer head. It was decomposed for 165 minutes and then photographed; after after each subsequent heating of 30, 15, 30, 20, 35 and 110 minutes and finally 12 hours (corresponding to the points shown in figure 5.10) it was again photographed. These must be regarded as only very

- approximate -

aproximate positions owing to the arbitrariness of the time interval which must be allowed for the goniometer head and accompanying crystal to heat up. These preliminary runs nevertheless served to indicate what to expect in a more exact run to be done subsequently.

None of the photographs taken in conjunction with figures 5.14 and 5.15 are shown, owing to the indeterminateness of position along the time axis. It was realised at this stage that both the large heat capacity of the goniometer head, and the insensitivity of the large electric furnace were causing inaccuracies in the positions of the points of interruption. It was decided to conduct all further work in the double-boiler, and to use different crystals for each photograph, thus eliminating successive warm-ups of crystal and container.

Accordingly, 10 mg of unirradiated $AgMnO_4$ crystals were decomposed in the double boiler in a platinum bucket, at 110°C to obtain the characteristic p/t plot, shown in figure 5.16. Data for this curve are given in table 5.11. Figure 5.17 shows the fit of a plot of $\log(p/p_f-p)$ against t for these figures, with the origin taken at 70 minutes.

Since the platinum bucket caused a drop of 2° in temperature on insertion, in this run the bucket was lowered into the boiler at a temperature 2° higher than the decomposition temperature, and immediately afterwards maintained at 110°C by adjusting the temperature of the inner boiling liquid. Equilibrium at 110°C was attained within two minutes after

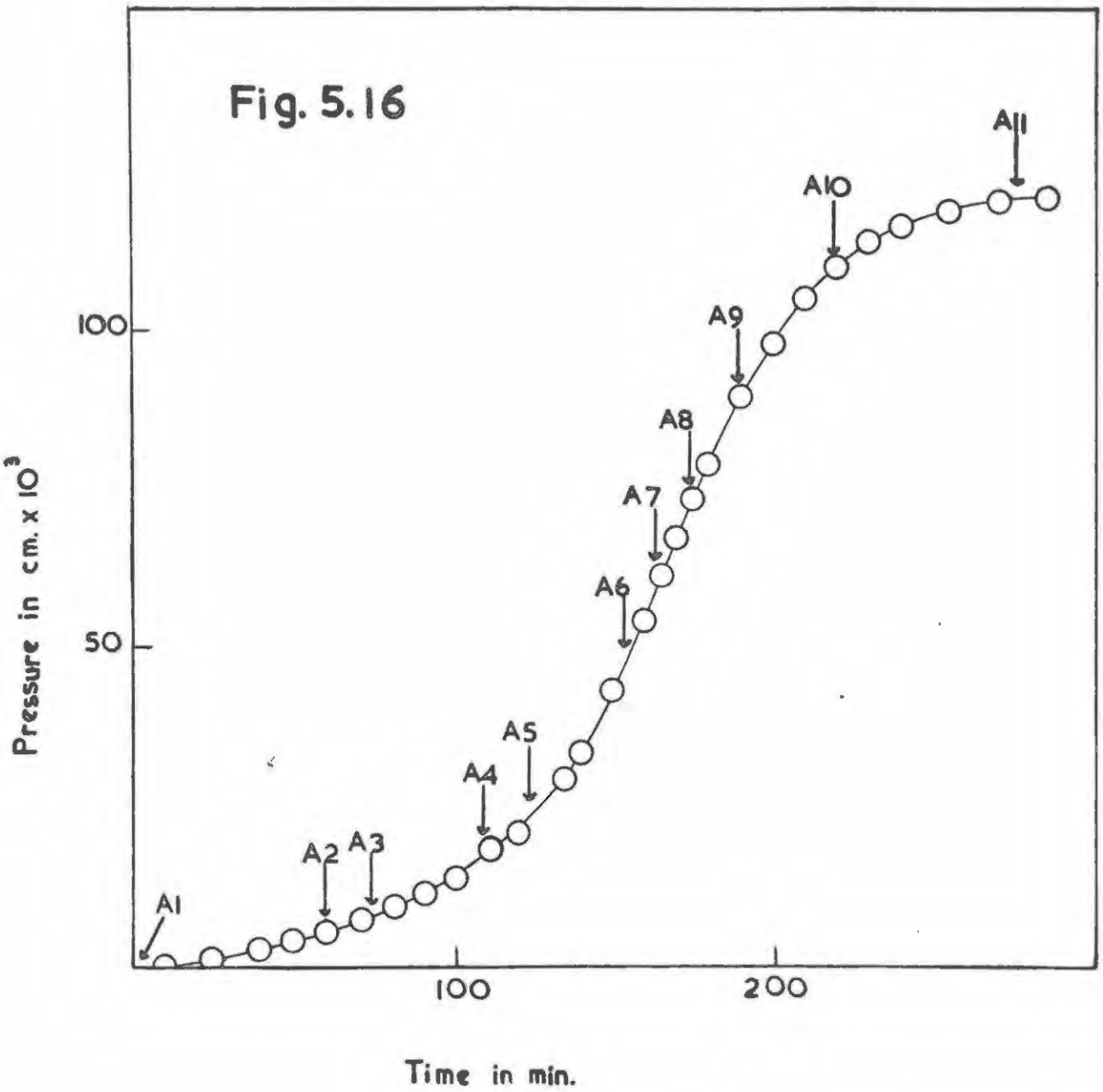
Fig. 5.16
A1
A2
A3
A4
A5
A6
A7
A8
A9
A10
A11
100
50
Pressure in cm. x 10³
100
200
Time in min.

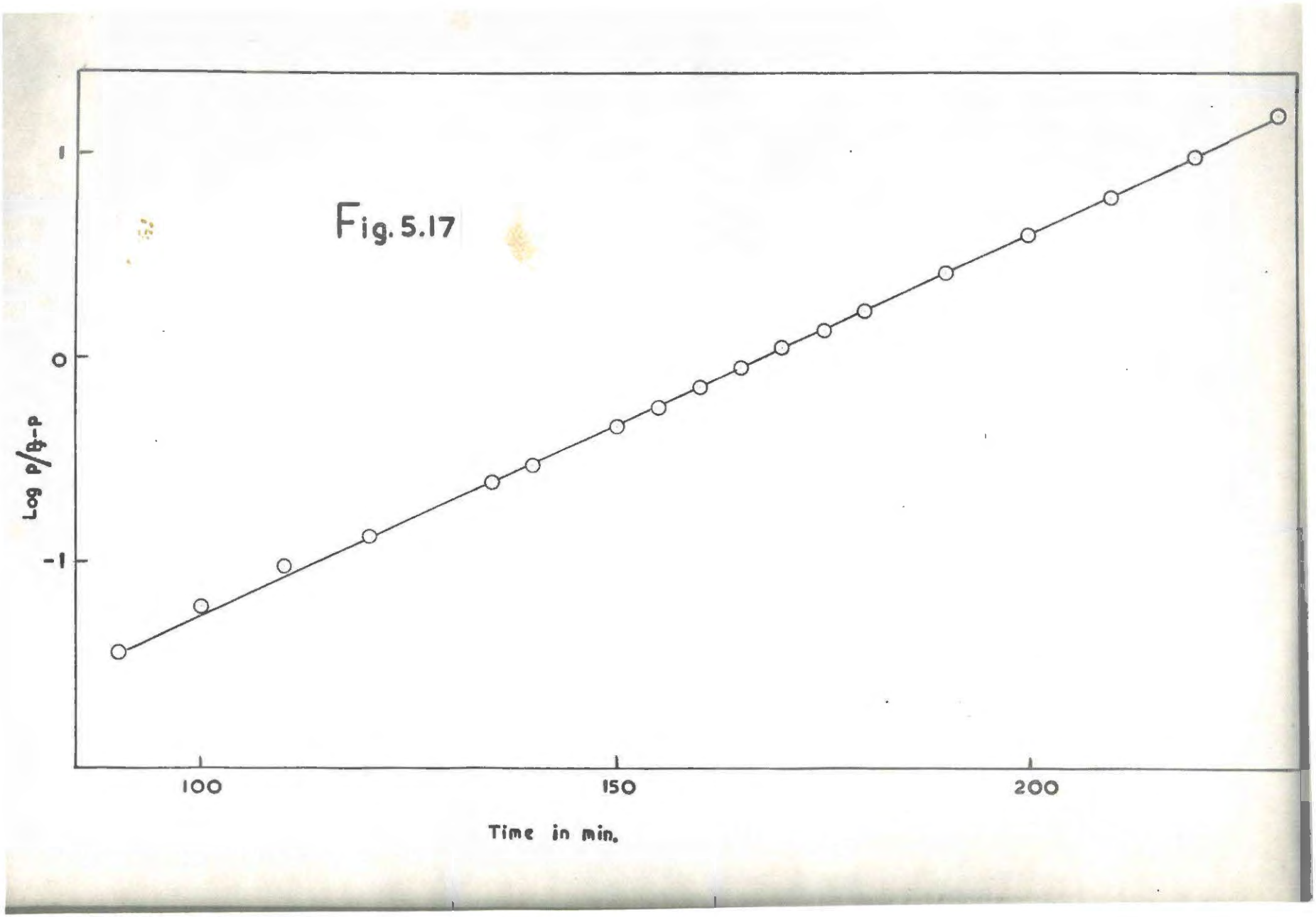
Fig. 5.17
1
0
-1
Log P/S-P
100
150
200
Time in min.

insertion of the bucket.

Single crystals of good shape were then selected under a microscope and mounted in brass mounts as described before. The crystal under examination was then placed in a light-weight copper wire cage constructed so as to prevent the mount from touching the walls of the decomposition chamber, and inserted into the chamber. Since the cage also caused a drop of 2° the procedure described above was followed; once again equilibrium at the decomposition temperature, $110^{\circ}C$, was attained within two minutes. It was considered valid to use the curve for bulk crystals in the bucket as being representative of single crystals because of the precautions described above. In any event, the position along the time axis is not inaccurate by more than 2 minutes.

Laue and rotation photographs marked A1 - A12 represent the points marked on figure 5.3 and correspond to periods of heating 0, 60, 75, 110, 125, 155, 165, 175, 190, 220 and 275 minutes and finally 12 hours respectively. Photographs in this series were taken also after 4, 10, 20 and 40 minutes but are not shown, as there is no marked difference between the photographs of an unheated and a heated crystal until at least 60 minutes decomposition.

All the photographs in this series were taken on the Philips PW 1009 Generator using a collimator of 0.5 mm diameter. "Kodirex" film was used for all photographs.

The Laue Photographs.

All Laue photographs were taken with the unique axis, b, in the

- plane of the -

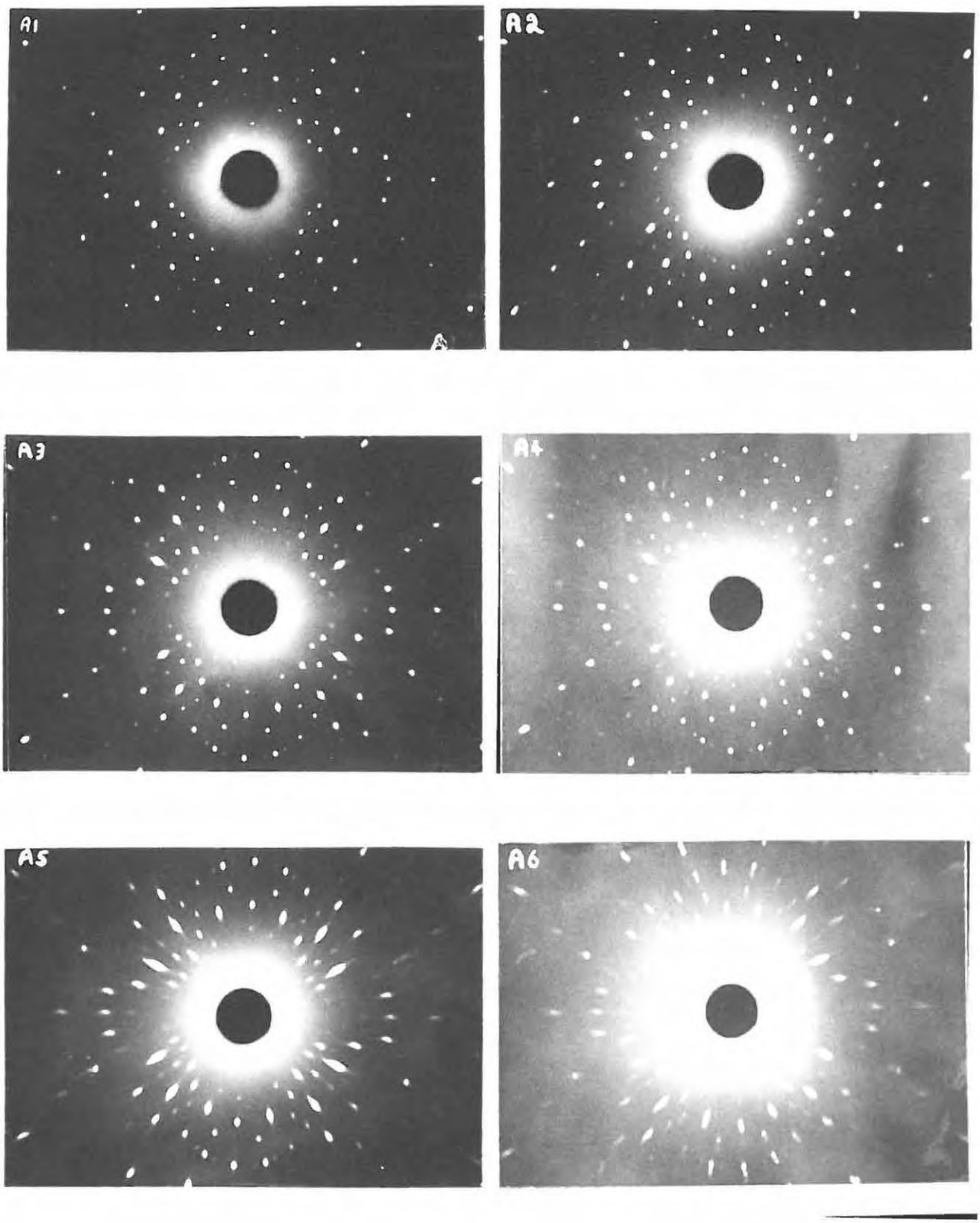
A1
A2
A3
A4
A5
A6


A7

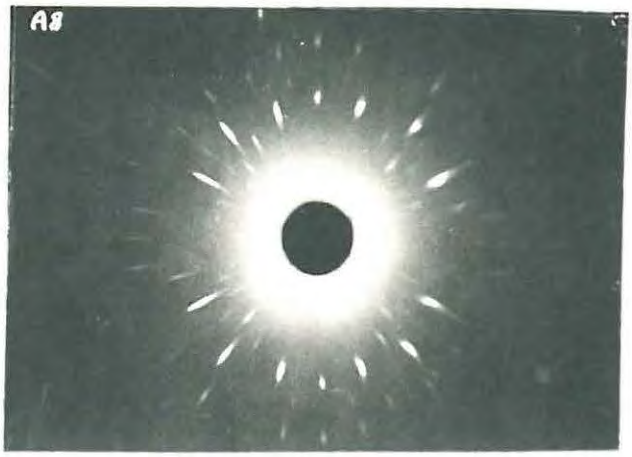
A8

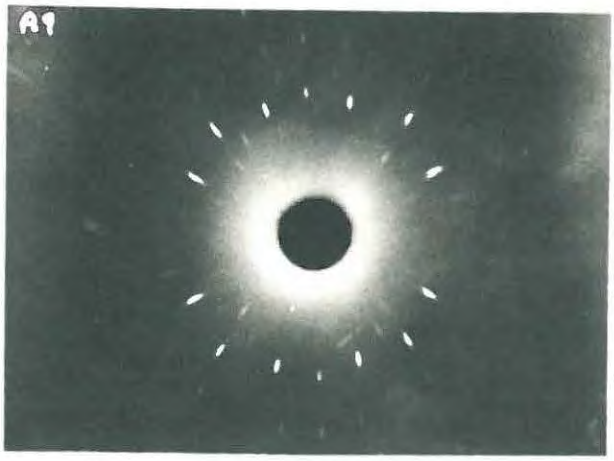
A9

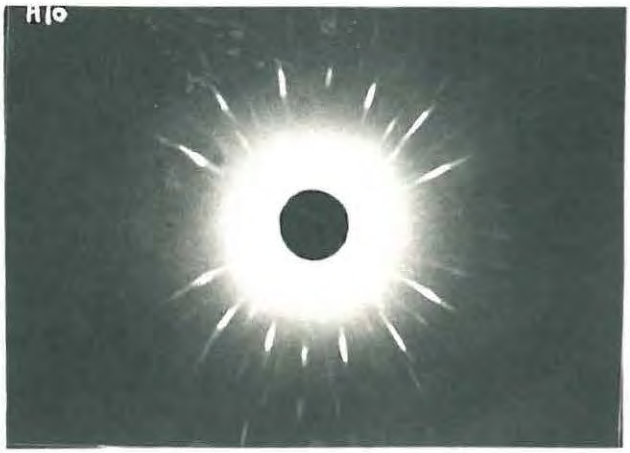
A10

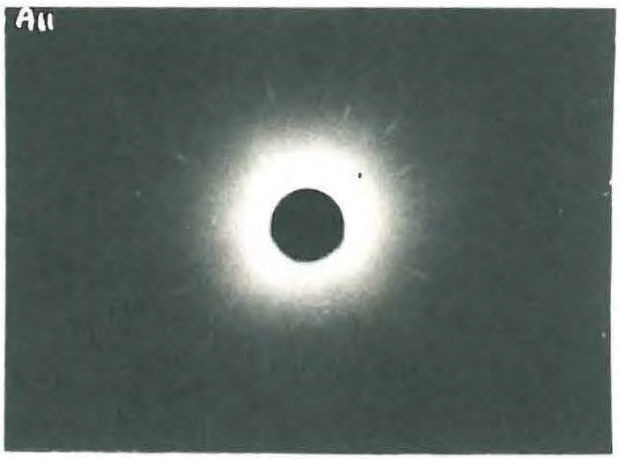
A11

plane of the incident beam, the c-axis being normal to the beam. The flat-plate Laue camera was placed 5 cm from the crystal, and exposures of 1 3/4 hours using iron-filtered copper radiation, generated at 40 kV and 20 mA, were used. A 0.5 mm diameter collimator was employed.

A1: this shows the unheated crystal.

A1a: inserted for four minutes at 110°C.

A1b,c,d: decomposed for 10, 20 and 40 minutes respectively. These photographs are not shown, as there is no detectable difference from A1.

A2: 60 minutes at 110°C. The spots have increased in size and intensity, and in addition, a very slight smearing is discernable on the more intense Laue spots, indicating the presence of very slight strain.

A3: 75 minutes at 110°C. The smearing has now become more pronounced, and the increase in size of the spots is considerable. Smearing is most pronounced near the centre of the film, particularly on the four most intense spots shown by a gnomonic projection to be 312, 314, 213 and 114.

A4: This photograph appears to be a misfit in the series since the effects here are not as pronounced as in A3 despite heating for a longer time, namely 110 minutes. This is attributed to differences in size and perfection of the various single crystals used.

A5-A7: heating for 125, 155 and 165 minutes respectively. The very slight smearing present in A3 and A4 develops into

pronounced asterism, accompanied by splitting up of especially the four most intense spots near the centre.

A8-A11: heating for 175, 190, 220 and 275 minutes. The streaked spots decrease progressively in intensity, and background scatter due to amorphous material becomes pronounced.

The Rotation Photographs.

Nickel-filtered copper radiation was used. The camera was a cylindrical one of radius 3 cm. Crystals were orientated, using the optical collimator on the Unicam rotation goniometer, so that the c-axis was the rotation axis. All exposures were of 1 hour 20 minutes duration and the generator was run under the same conditions as for the Laue photographs.

A1: the unheated crystal.

A1a,b,c,d: these photographs are not shown, but represent 4, 10, 20 and 40 minutes heating respectively, at 110°C. There is no apparent difference between A1d and A1.

A2: 60 minutes at 110°C. Comparison of this picture and A1 shows a small increase in size and intensity, particularly of the darkest spots.

A3: 75 minutes at 110°C. No apparent difference between A3 and A2.

A4: 110 minutes at 110°C. The most pronounced effect here is the relatively large decrease in intensity of the high-angle spots compared with those at lower angles.

- A5 and A6 -

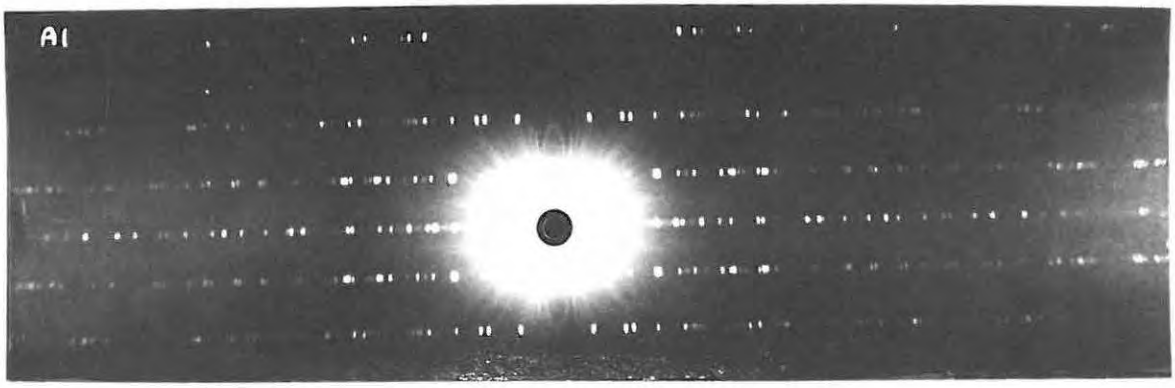
A1

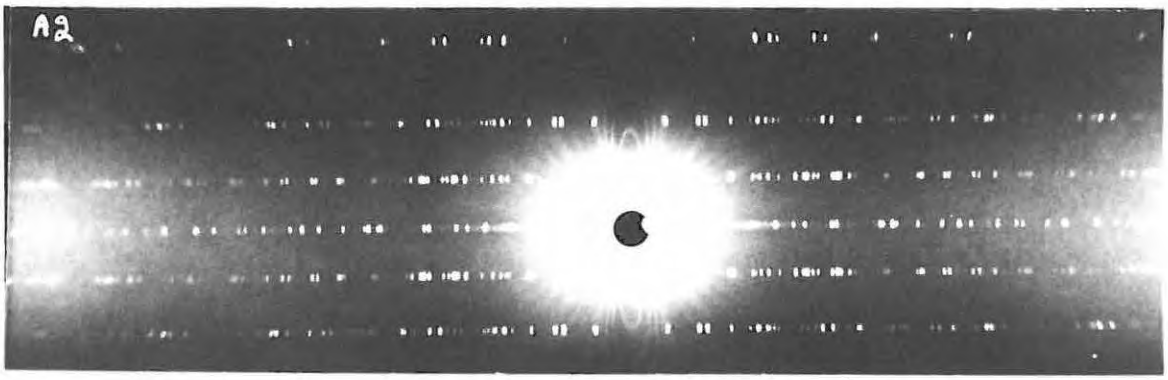
A2

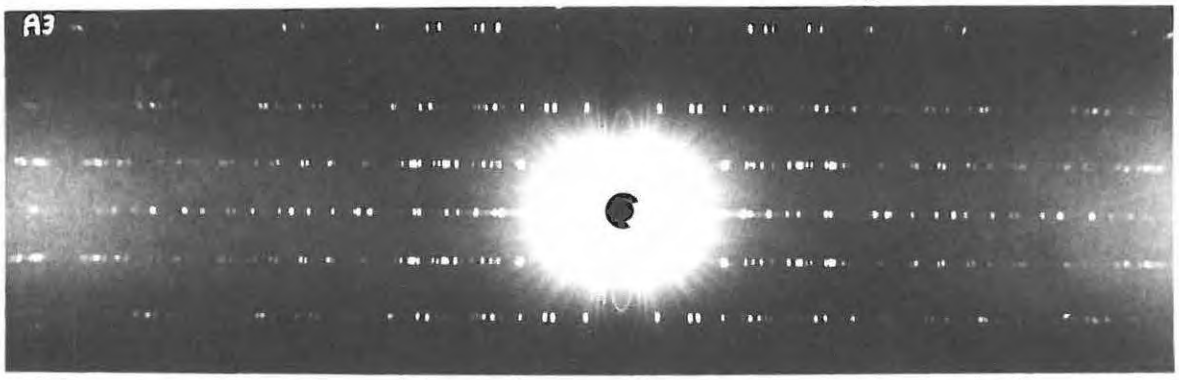
A3

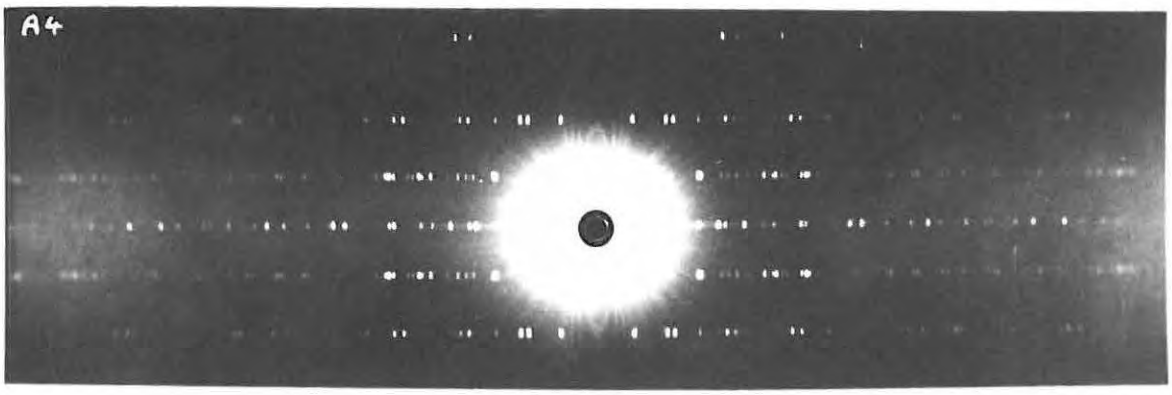
A4

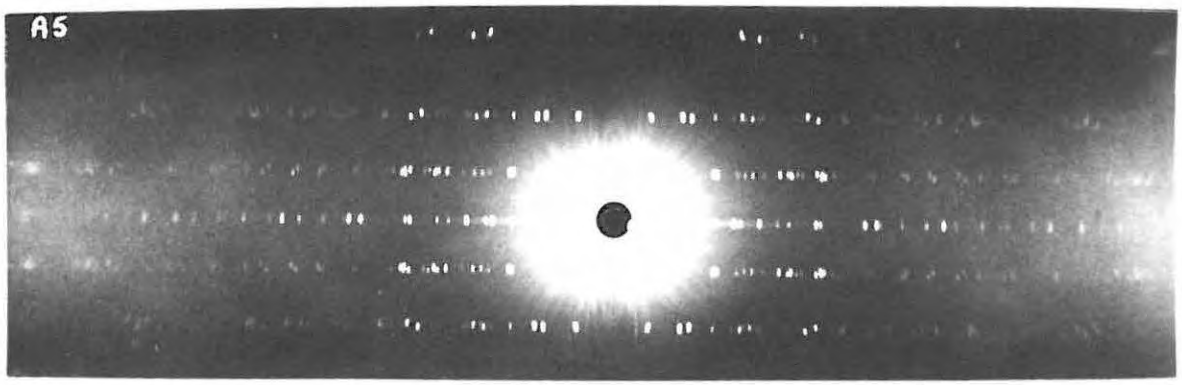
A5

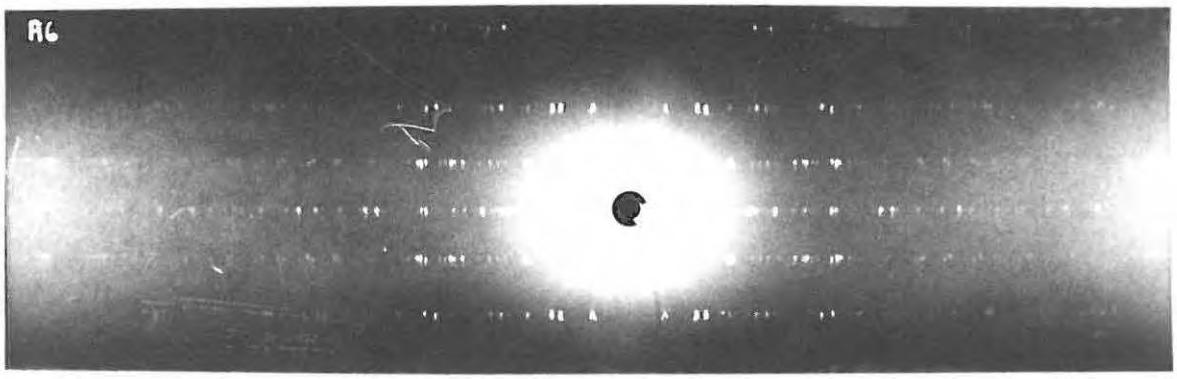
A6

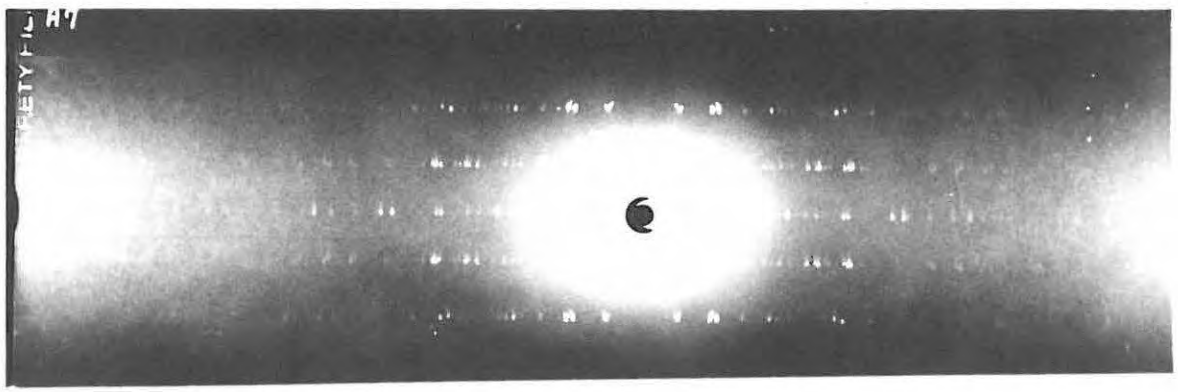
A7

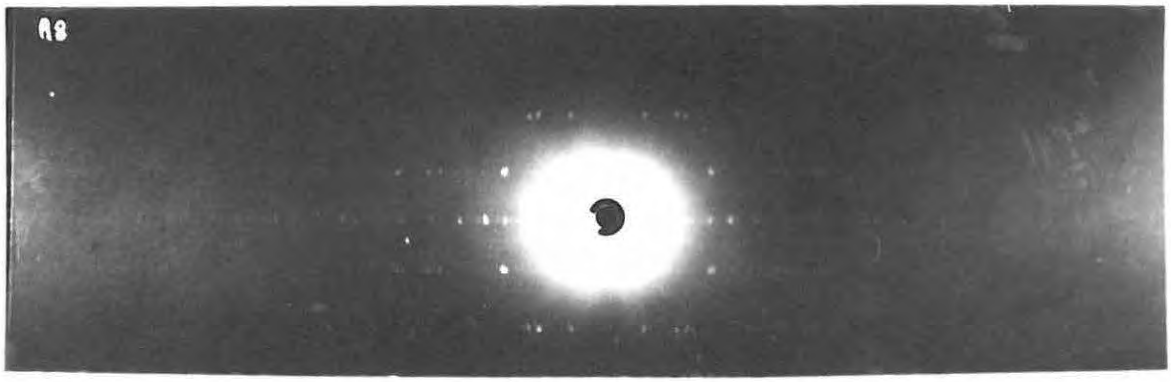
A8

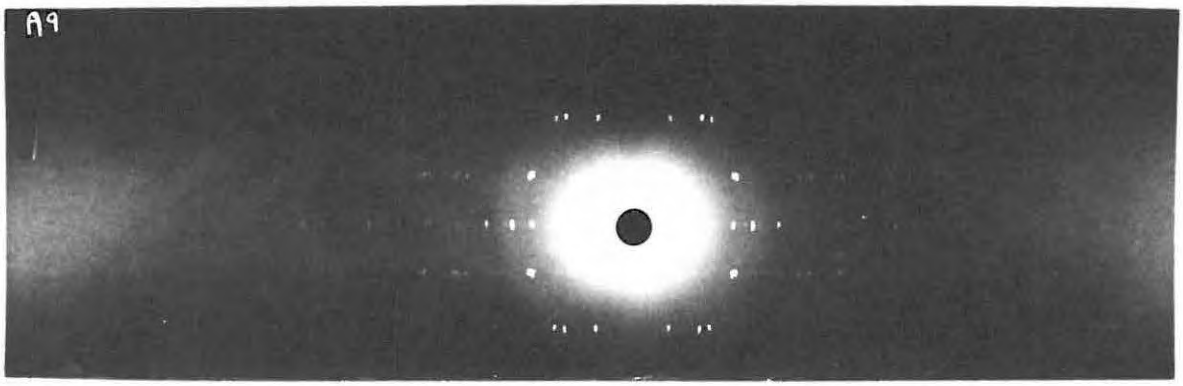
A9

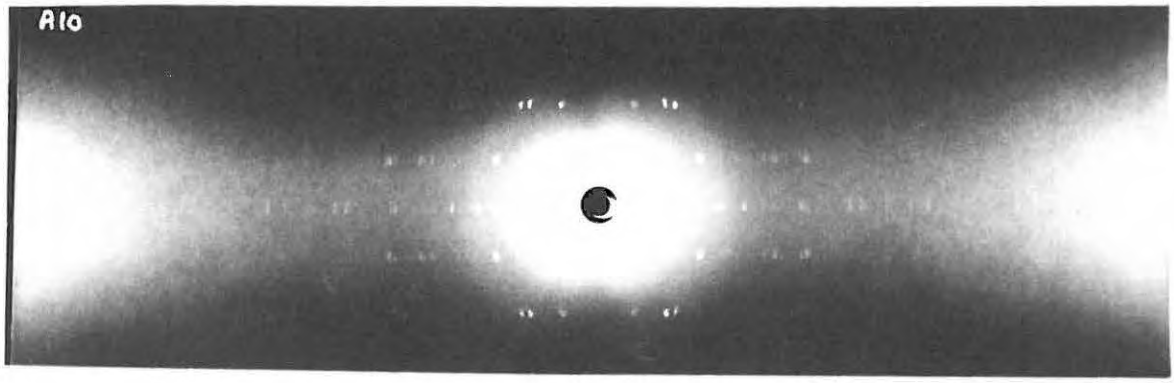
A10

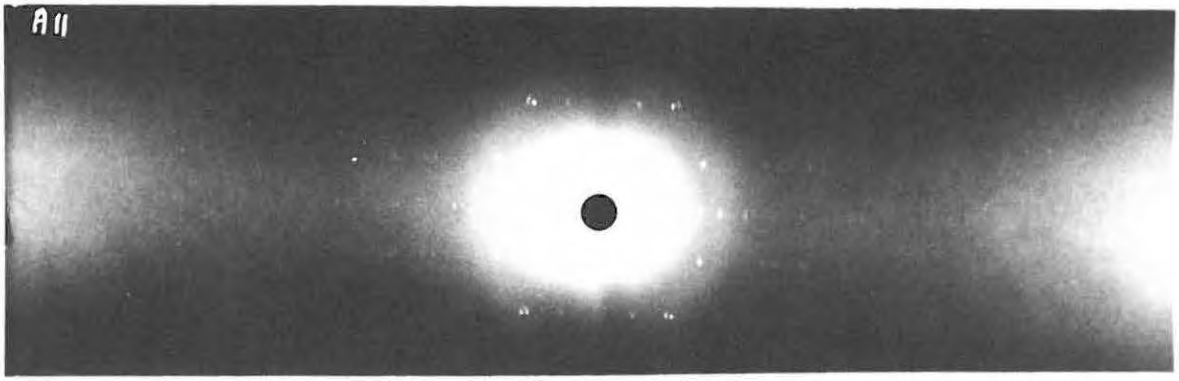
A11

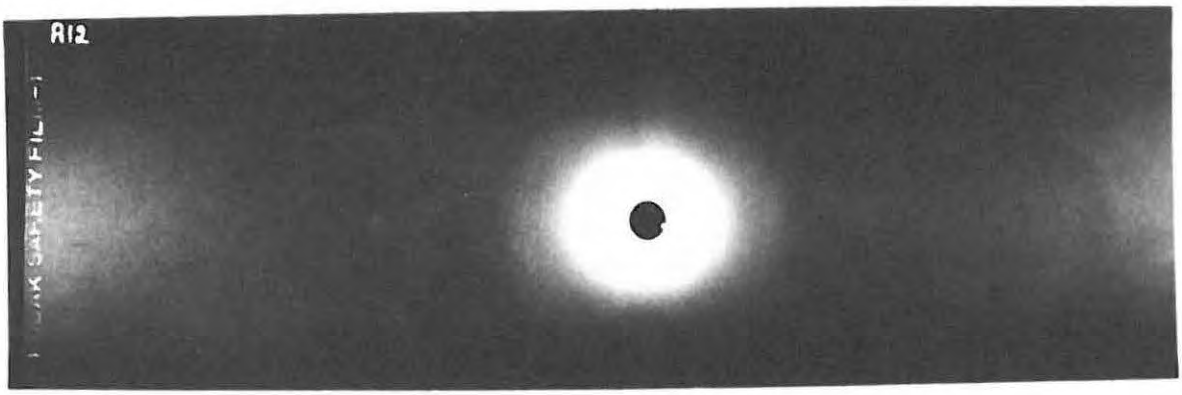
A12

A5 and A6: 125 and 155 minutes at 110°C respectively. The decrease in intensity of the high-angle spots is even more pronounced and all spots are seen to have a broken up appearance. At this stage it became increasingly difficult to orientate the crystal exactly, as reflections previously obtained from the crystal faces had disappeared, rendering the optical collimator useless.

A7-A11: 165, 175, 190, 220 and 275 minutes at 110°C, respectively. A7 shows the first faint traces of a broad diffuse ring due to amorphous product material. This becomes steadily more intense as the reaction proceeds, while both the Bragg spots and lines of constant ρ diminish in intensity. Even after 275 minutes, however, representing almost 100% decomposition, there is still crystalline material left.

A12: All permanganate structure has now disappeared leaving only a diffuse ring in the region of $\sin\theta/\lambda \approx .185$ Å^{-1} due to product material. The external morphology of the crystal, however, remains unchanged right to the end of the reaction.

Examination of the Diffuse Reflections from Silver Permanganate.

Huang[94] has shown that randomly scattered centres of distortion in a monatomic lattice produce, amongst other effects detectable on X-ray photographs, the development of diffuse scattering around the reciprocal

lattice points. His concern was with the distortion caused by the substitutional metal atoms in dilute alloys; Tucker and Senio have however based their analysis of neutron-irradiated boron carbide on Huang's theory, despite its relatively more complicated structure. The centres of distortion in this case were interstitials and vacancies caused by irradiation; in accordance with Huang's theory, heavy diffuse scattering was found around reciprocal lattice points after large integrated neutron fluxes of up to 10^{20} nvt. This diffuse scattering exists over and above that produced by normal thermol movements of atoms in the crystal.

It was thus decided to examine partly decomposed $AgMnO_4$ for the presence of distortion centres in the form of random and isolated nuclei of decomposed material in the body of the crystal. It was reasoned that if such "decomposition spikes" did in fact form over the induction period, they might give rise to diffuse scattering around the Bragg directions.

It was decided to examine firstly the 220 reflection from crystals heated for 110 minutes at $108^{\circ}C$ (see figure 5.16). A crystal was mounted so that it would reflect the characteristic CuKα radiation present in the continuous radiation (i.e. unfiltered) from the 220 plane, in the following manner.

It was first necessary to orientate the crystal so that the b-axis lay in the plane of the incident beam. On clockwise rotation of the crystal, two faces are encountered, $73^{\circ}12'$ apart. The first in succession was located exactly by means of the optical collimator; subsequent anticlockwise rotation of $8^{\circ}\ 24'$ (for geometry see figure 5.18a) ensured that the b-axis lay in the plane of the incident beam of X-rays.

Now, for a monoclinic lattice,[111]

$$\frac{1}{d(hkl)^2} = \frac{1}{\sin^2\beta}\left(\frac{h^2}{a^2} + \frac{k^2\sin^2\beta}{b^2} + \frac{l^2}{c^2} - \frac{2hl\cos\beta}{ac}\right)$$

$$d(hkl) = 1/(h^2a^{*2} + k^2b^{*2} + l^2c^{*2} + 2hl\ c^*a^* \cos\beta^*)^{\frac{1}{2}} \quad \ldots \quad 5.27$$

and hence:

$$d(hko) = 1/(h^2a^* + k^2b^{*2})^{\frac{1}{2}} \quad \ldots\ldots \quad \ldots\ldots \quad 5.28$$

where $a^* = (a \sin\beta)^{-1}$, $b^* = b^{-1}$, $c^* = (c \sin\beta)^{-1}$ and $\beta^* = 180^\circ - \beta$. a, b and c are the lattice translations and β is the non-orthogonal angle of the lattice.

Now:

$$\sin\Theta(hko) = \lambda/2d(hko) \quad \ldots\ldots \quad \ldots\ldots \quad 5.29$$

$$= 1.54/2\ (h^2/a^2\sin^2\beta + k^2/b^2)^{\frac{1}{2}}$$

$$= 0.77(4/5.67^2 \times 0.9996^2 + 4/8.27^2)^{\frac{1}{2}}$$

$$\therefore\ \Theta(220) = \sin^{-1} 0.3296 = 19^\circ\ 15'$$

Hence for the 220 plane to reflect CuKα ($\lambda = 1.54$ Å) it must be inclined at $\Theta = 19^\circ\ 15'$ to the incident beam. A check on this angular setting is provided by measurement of the distance from the centre of a rotation photograph to the 220 reflection (indexed after Bernal[95]). If this distance is d, and the radius of the camera is r, then the angular setting in degrees is given by

$$\Theta = (d/2r)(180/\pi) \quad \ldots\ldots \quad \ldots\ldots \quad 5.30$$

$$= (2.02/6)(180/\pi) \text{ in this instance}$$

$$= 19^\circ\ 18'$$

This is in good agreement with the calculated value for Θ. Now, to locate the 220 plane, it was necessary to know the angle between it and the b-axis, which latter direction is already located. This angle, ϕ, is calculated as follows (see figure 5.18b):

$$\phi = \tan^{-1} \frac{a}{2} / \frac{b}{2} = \tan^{-1} a/b = 34^\circ\ 26' \quad \ldots\ldots \quad 5.31$$

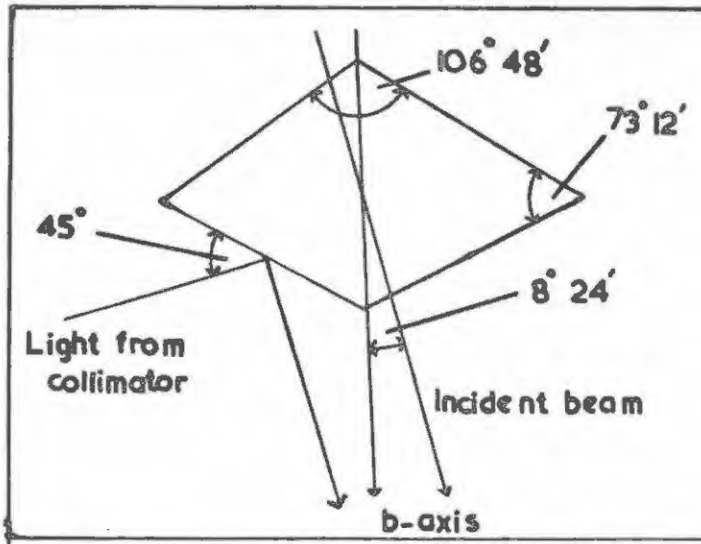

FIG. 5.18a

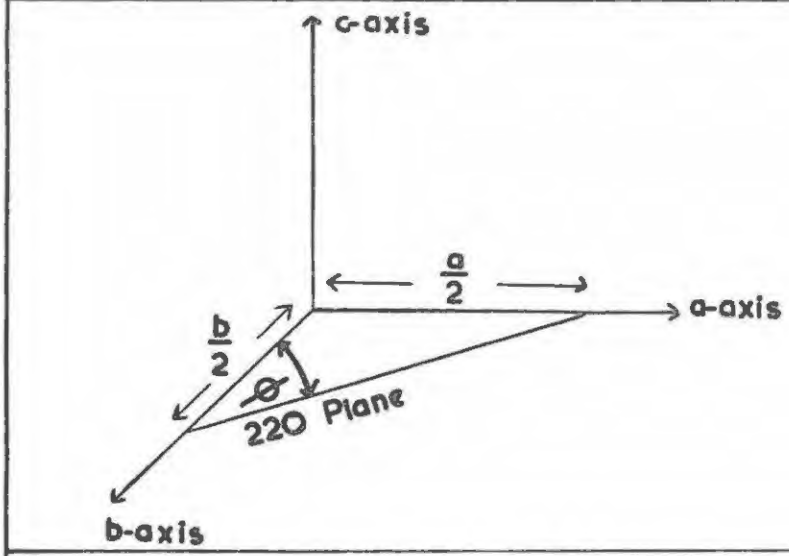

FIG. 5.18b

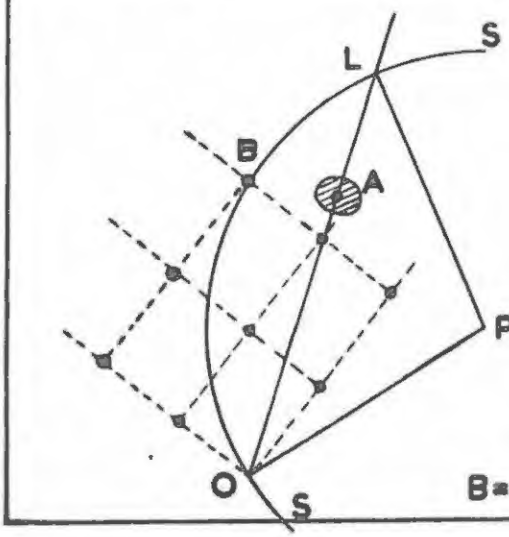

B= 220 Reflection

FIG. 5.18c

Thus, to locate the 220 plane to reflect CuKα radiation, the b-axis was first placed in the plane of the incident beam; the crystal was then moved 34° 26' to bring the 220 plane into this direction, and a final movement of 19° 15' brought the 220 plane into the position for reflection.

Calculation showed that the 220 spot should fall on a flat-plate camera set 3 cm from the crystal at a distance of 2.4 cm from the centre of the film on the equatorial line, and this is verified by experiment.

The diffuse reflections arising from Huang-type distortion centres must not be confused with those associated with thermal vibration of the atoms in the crystal. Thermal motion has the effect of "smearing" out the atoms, and this in turn causes the otherwise sharp reciprocal lattice points to be surrounded by regions of diffuse scattering. This has been found in many organic crystals such as sorbic acid, urea nitrate and benzil[114]; it is however, found in inorganic substances, such as sylvine[114] and rock-salt[115], as well.

The existence of diffuse reflections may be shown as follows. Consider figure 5.18c, showing a layer of the reciprocal lattice of say, silver permanganate.

The initial position of the reciprocal lattice point (220) corresponding to the wavelength CuKα is shown by point A. P is the centre of the sphere of reflection, and L, the intersection of the 2ko direction, OA, with the sphere of reflection, defines the direction of the Laue reflection 220. Suppose that the lattice rotates in a counter-clockwise direction about an axis through O perpendicular to the plane of the paper. The point L moves along the circle SS and the Laue spot approaches the position of the characteristic (CuKα) spot, coinciding with it when A

- reaches the -

reaches the position B on the sphere of reflection. Before this condition is fulfilled however, the diffuse domain about A intersects the sphere of reflection in a region lying between B and L. A faint diffuse reflection then appears, and as A approaches B, so it gets stronger, and finally Laue spot, characteristic spot and diffuse reflection coalesce when A reaches B.

Consider now the photographs of series C taken in connection with the diffuse reflection surrounding the 220 reciprocal-lattice point in the heated silver permanganate. All these photographs were taken with a flat-plate camera set 3 cm from the crystal using unfiltered copper radiation. Exposures were for $3\frac{1}{2}$ hours and "Industrex D" film was used.

C1: This shows the coincidence of diffuse, Laue and Bragg spots; i.e. the crystal is set so that the 220 plane reflects characteristic CuKα radiation. This corresponds with the situation in the diagram of the coalescence of A and B.

C2: This shows the diffuse reflection and accompanying Laue spot after moving the crystal 1° 58' off the above setting. The diffuse reflection is very faint, but still is discernable.

C3: The setting is 48' off that for C1. The Laue spot is seen to approach the diffuse reflection which is itself more intense than in C2.

C4: Once again the Laue and characteristic reflection coalesce.

An unheated crystal was then mounted and orientated so that the Laue spot was just off the position for reflection of characteristic radiation (miss-set by 35'.) Photograph C5 resulted; once again a diffuse reflection was observed.

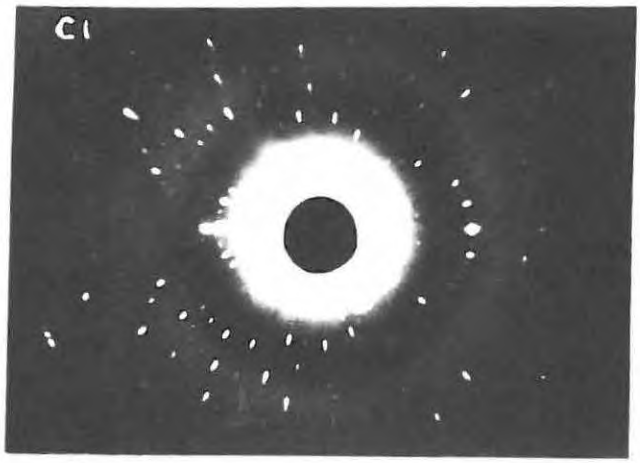
C1

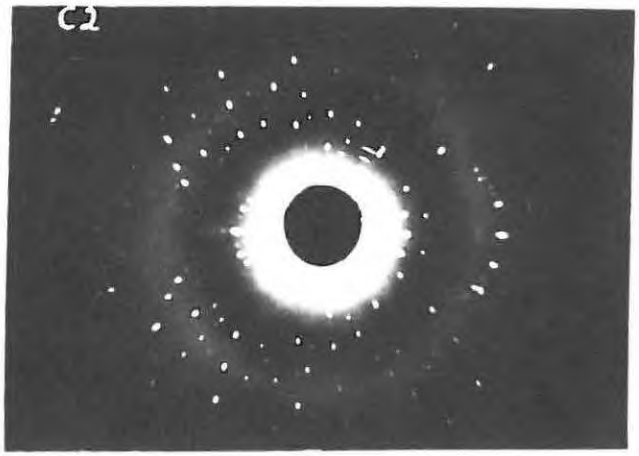
C2

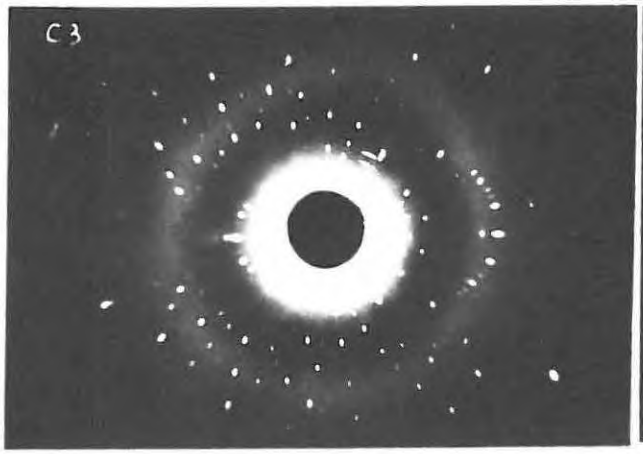
C3

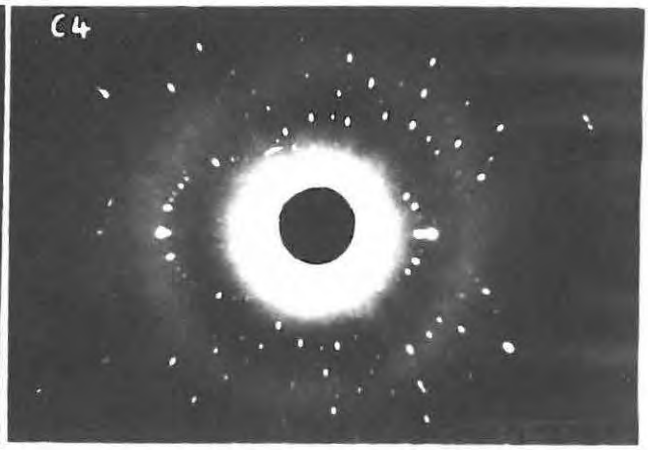
C4

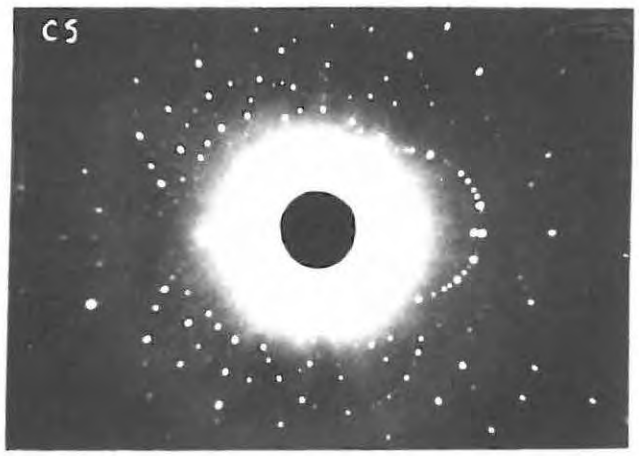
C5

with that shown by Laue photographs of cold worked metals[116].

During the acceleratory period we envisage the progression of

The diffuse reflections of the heated permanganate are thus very likely due to thermal movements of the atoms only, and very probably not due to any decomposition nuclei causing distortion in the body of the crystal. This is confirmed by the fact that photographs of the same crystal used for photographs C1 - C4, taken after a further heating of 25 minutes at 108°C, showed no increase in the size of the diffuse reflections. Neither was there any apparent increase in the intensity of the diffuse reflections; however, it must be stated that if there was in fact any small increase in intensity, it would be extremely difficult to see, and hence might be missed.

Discussion of the Photographs.

The photographs taken during decomposition bear out in a remarkable way the mechanisms advanced by Prout and Tompkins (see pp. 7 - 12), for the initiation and propagation of reaction in permanganates.

During the induction period, 0 - 70 minutes on figure 5.16, the most pronounced effect in the Laue photographs is the small increase in size of the Laue spots and the smearing of the more intense ones. This indicates a very small strain in the crystal, this strain being associated with the product/reactant interface on the surface of the crystal, where reaction is initiated. Only after the end of the induction period does strain of any large magnitude become apparent in the slight elongation of the Laue spots.

During the acceleratory period, represented by Laue photographs A4 - A7, the slight elongation develops into pronounced radial asterism of all the diffraction spots on the photograph. This asterism is comparable

with that shown by Laue photographs of cold worked metals[116].

During the acceleratory period we envisage the progression of reaction into the body of the crystal by way of cracks which develop perpendicular to the crystal surface. In this way it would be expected that small blocks of unreacted permanganate would form in a net-work matrix of the product. These permanganate blocks would not be expected to be parallel, but to be disorientated by the intervening product planes, and this explains the radial streaking of the Laue spots. Bragg[117] has shown that radial asterism of Laue spots is expected if there is a random deviation of the normal to crystal plane all round its mean direction owing to distortion.

Suppose that a plane is reflecting a narrow beam at a small glancing angle whose mean value is θ, and that it is rocked so that its normal describes a cone of semi-vertical angle E. The rocking of the normal in the plane of incidence makes a difference of 4E in the direction of the reflected beam, and if the image is distant D from the point of reflection, this makes the spot more horizontally a distance 4DE. The rocking at right angles to the plane of incidence gives a lateral movement of $4D\theta E$ (approximately) to the spot, and the spot thus describes an ellipse. The ratio of the major to the minor axis of the ellipse in $1/\theta$, and Bragg shows that for $\theta = 3^{\circ}$ the major axis is twenty times as long as the minor axis, and lies in a radial direction. This accounts for the radial streaks on the Laue photographs: the small blocks of unreacted permanganate are disorientated by intervening product material so that the normals to a particular crystallographic direction lie on a cone about this direction.

Macroscopic cracks must also develop in the crystal as well; this is shown by the fine structure or streakiness of the individual spots, and by the broken up appearance of the rotation reflections.

During the decay period these isolated blocks of permanganate decompose slowly. The reaction proceeds inwards from the parent-product interface, and as this interface falls in total area, so the rate of reaction and hence rate of oxygen evolution drop. The thickening planes of product should now begin to be observable; in fact rotation photograph A7 shows the first signs of amorphous product as evidenced by the diffuse ring. This ring increases in intensity as the reaction proceeds, and the corresponding disappearance of crystalline permanganate is shown by the gradual diminution in intensity, and finally disappearance of both Laue and rotation spots. It is remarkable that crystallinity should be detectable even at such an advanced stage of the reaction as obtains after 275 minutes of heating at $110^{o}C$.

The results obtained by studying the diffuse reflections do not preclude absolutely the formation of decomposition nuclei in the body of the crystal during the induction period, but the evidence tends rather to support strongly the Prout-Tompkins mechanism, where product first covers the crystal surface (during the induction period) and the progresses into the crystal by way of cracks which develop normal to the crystal surface (during the acceleratory period).

Thus it is seen that the X-ray photographs following the thermal decomposition of silver permanganate may be interpreted extremely well on the basis of the Prout-Tompkins theory.

5.4 The Investigation of the Thermal Decomposition of Irradiated Silver Permanganate.

Crystals of silver permanganate were irradiated in a sealed evacuated ampoule with a dose of 100 Mrad in the spent fuel facility at Harwell. Irradiations were carried over at 25°C; the γ-ray energy is 1.1 MeV, and the dose rate 4.0 Mrad $hour^{-1}$.

Decompositions were carried out in the double-boiler in order to obtain the p/t curve for the irradiated $AgMnO_4$. A typical curve, obtained by heating 7 mg crystals in a platinum bucket at 95°C, is shown in figure 5.19. The data for this curve is given in table 5.12; time is in minutes and pressure in cm mercury x 10^3. A run carried out in a glass bucket at the same temperature so as to allow visual observation of the crystals showed that fracture commenced between 75 and 77 minutes after insertion of the bucket into the decomposition chamber.

A series of Laue and rotation photographs (series B) were taken after various times of heating, shown in figure 5. These photographs are described and discussed below. The time of heating was unbroken up to the time of withdrawal of the crystals; thus for each time of interruption a fresh batch of 1-2 mg of crystals was used. The crystals used for X-ray study were then selected from the particular batch.

The Laue Photographs.

The photographs in series B were taken under the same conditions as for the unirradiated crystals (series A), with the exception of photographs B1 and B2, were a 1/4 mm diameter collimator was used, and the exposures were accordingly higher (viz. 7 hours) than usual.

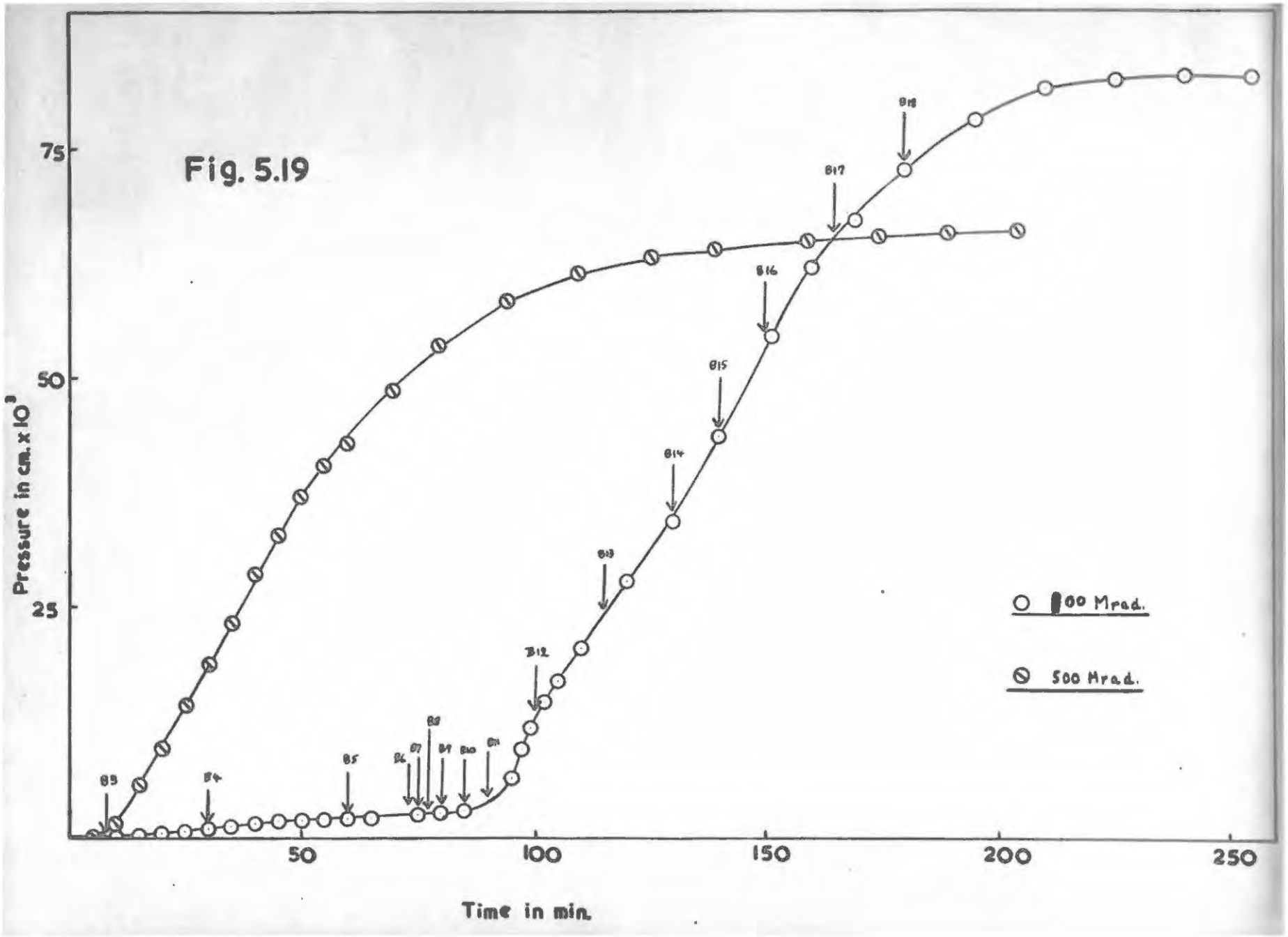
Fig. 5.19
75
50
25
Pressure in cm. x 10³
50
100
150
200
250
Time in min.
B5
B6
B12
B16
B17
B18
500 Mrad.

T A B L E 5.12

t	p	t	p
5	0×10^{-3}	95	6.5
10	0.2	97	9.6
15	0.3	99	11.9
20	0.5	102	14.9
25	0.7	105	17.1
30	1.0	110	20.6
35	1.3	120	27.8
40	1.5	130	34.3
45	1.8	140	43.6
50	1.8	160	62.2
55	1.9	170	67.2
60	2.0	180	72.8
65	2.1	195	78.2
75	2.4	210	81.6
80	2.6	225	82.1
85	3.0	240	83.0
		255	83.0

T A B L E 5.13

t	p	t	p
0	0×10^{-3}	55	40.3
5	0.2	60	42.8
10	1.6	70	48.6
15	5.7	80	53.5
20	9.7	95	58.6
25	14.3	110	61.6
30	18.8	126	63.4
35	23.3	140	64.2
40	28.6	160	65.4
45	32.9	175	66.0
50	37.0	190	66.6
		200	66.8

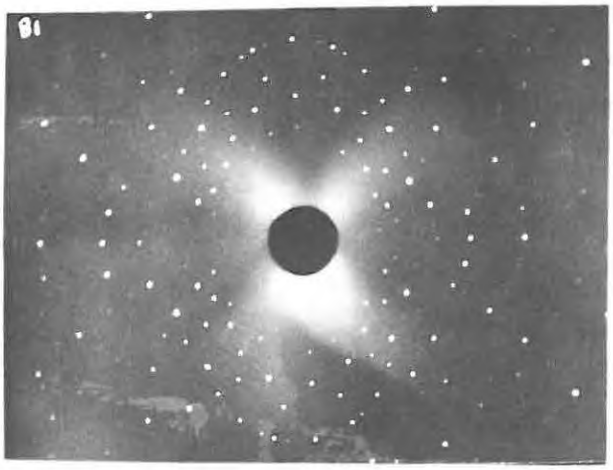
B1

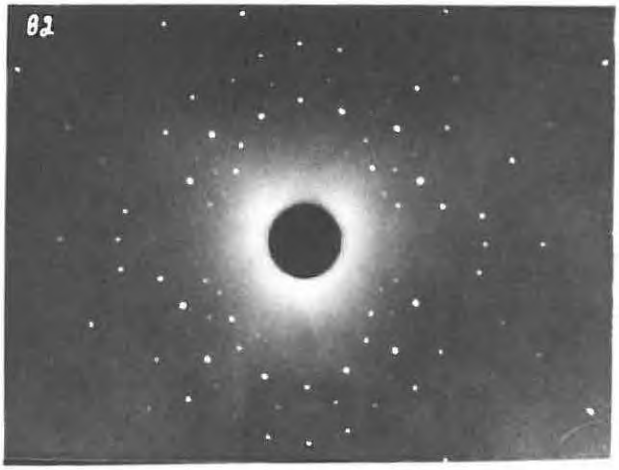
B2

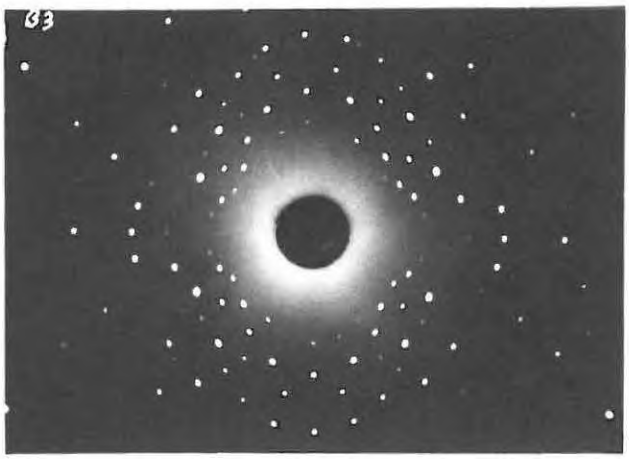
B3

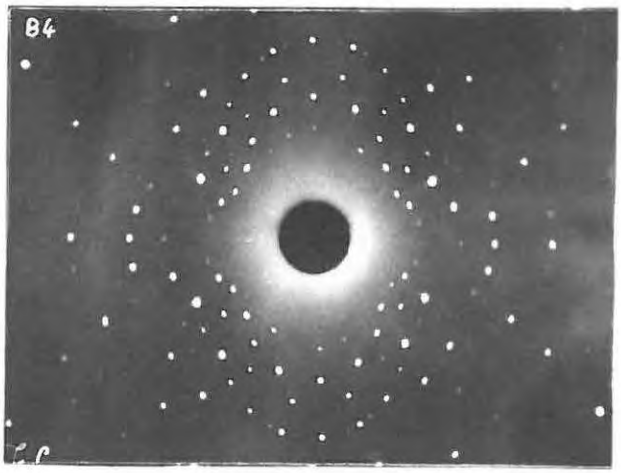
B4

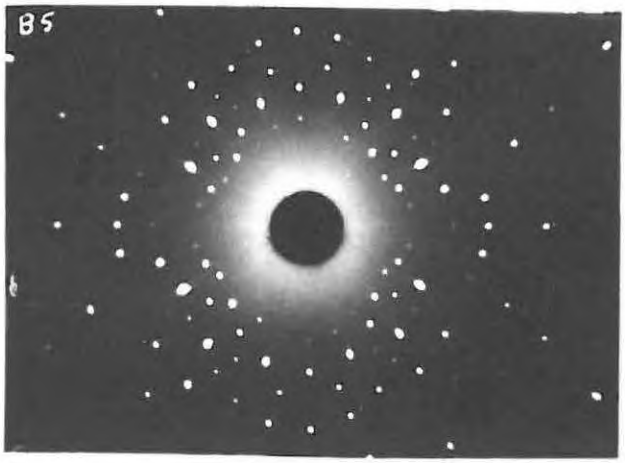
B5

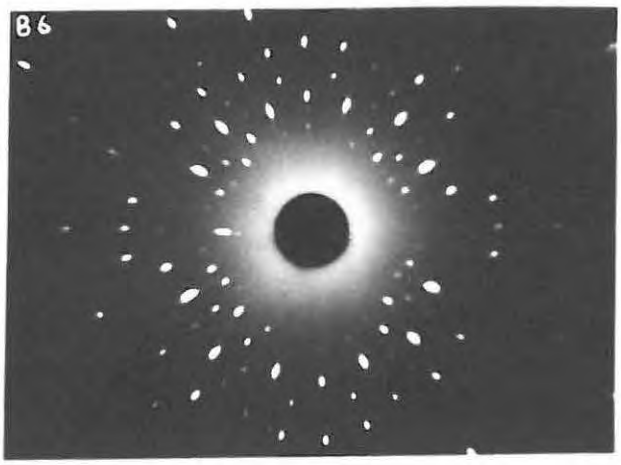
B6

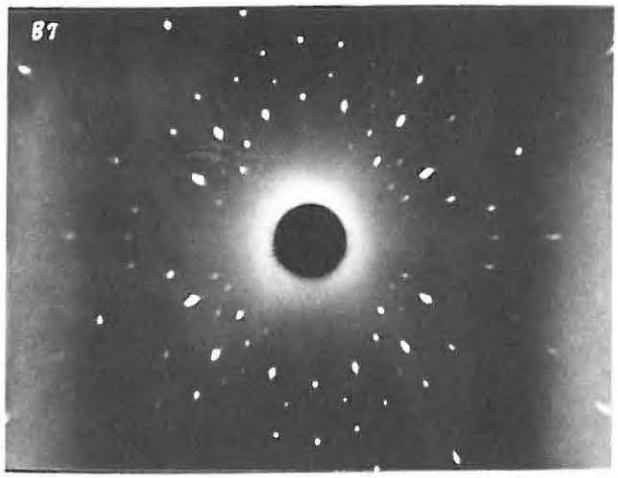
B7

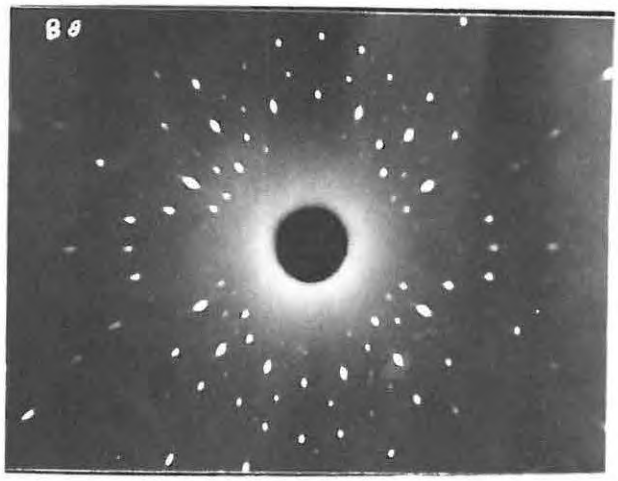
B8

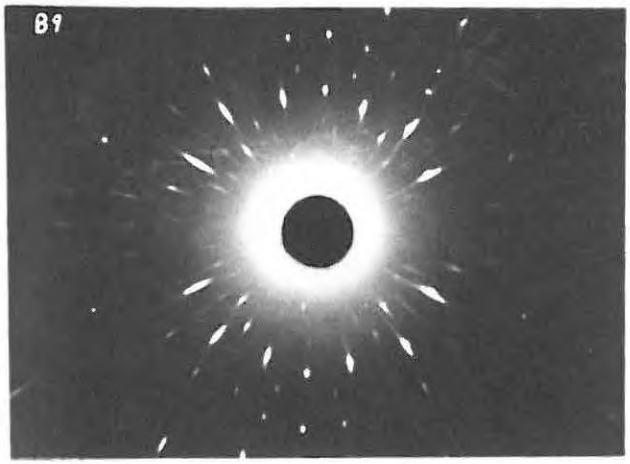
B9

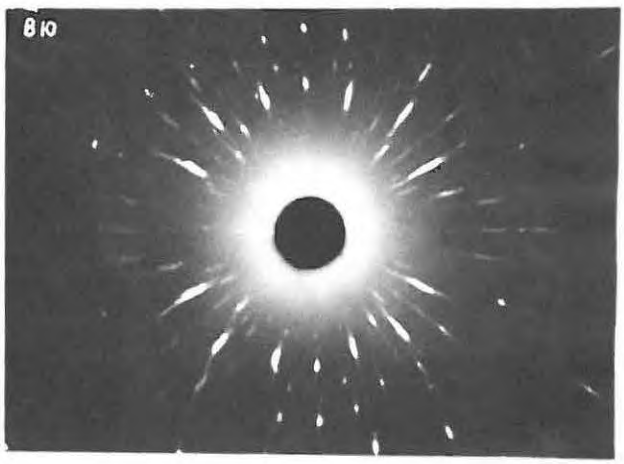
B10

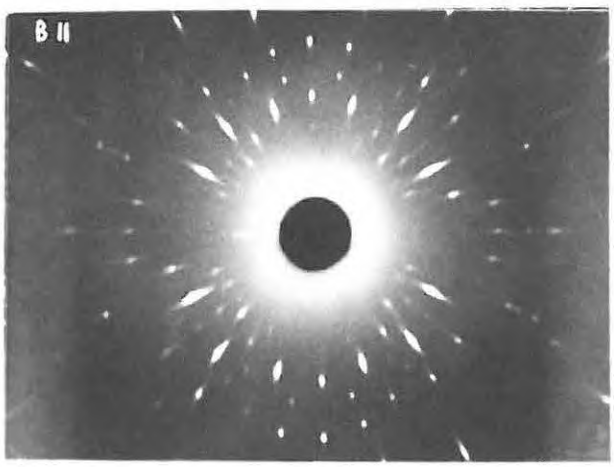
B11

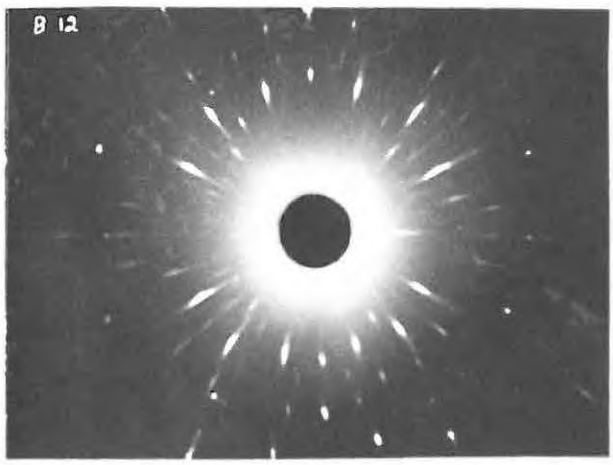
B12

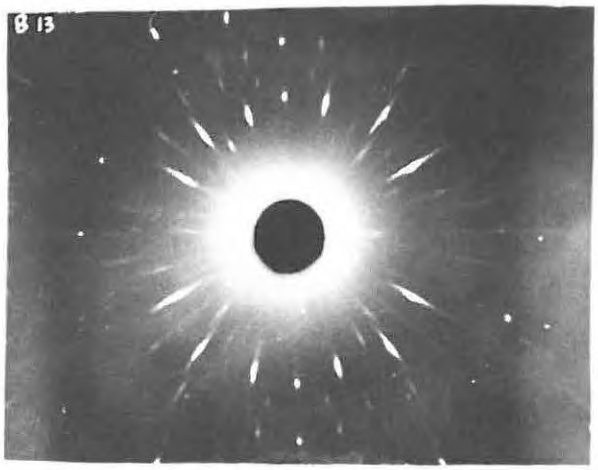
B 13

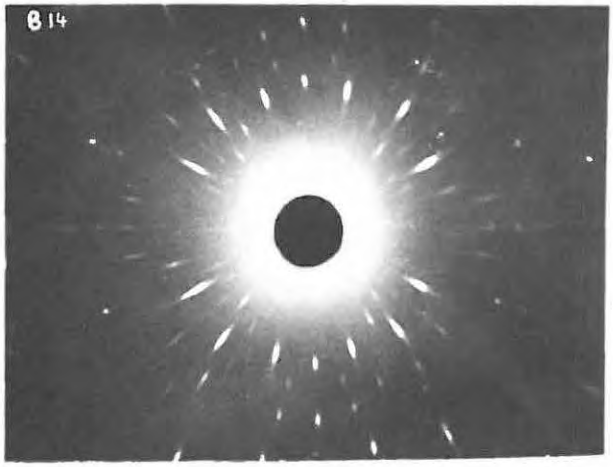
B 14

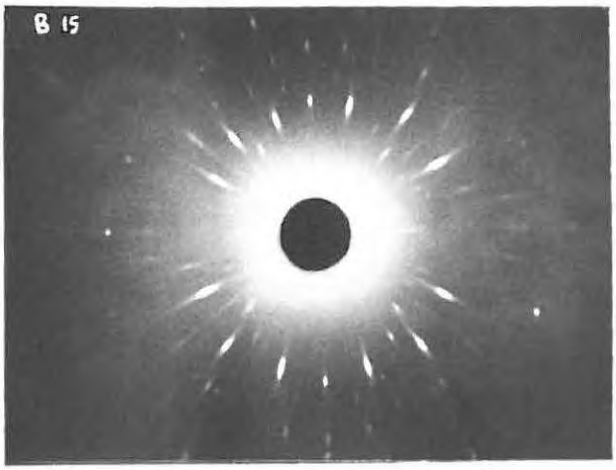
B 15

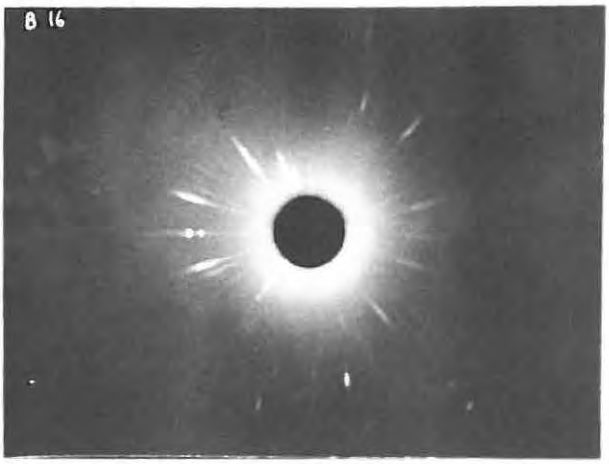
B 16

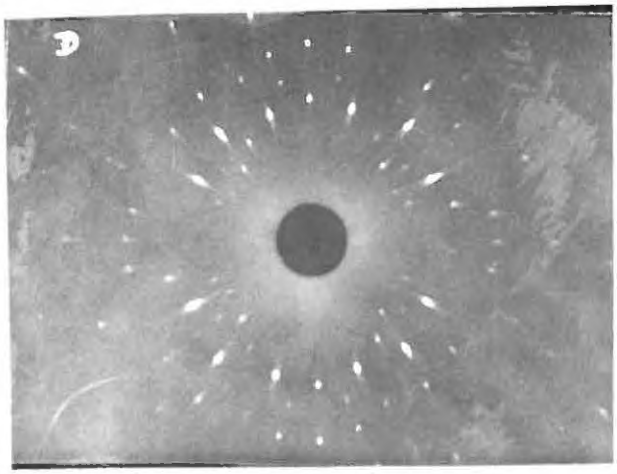
D

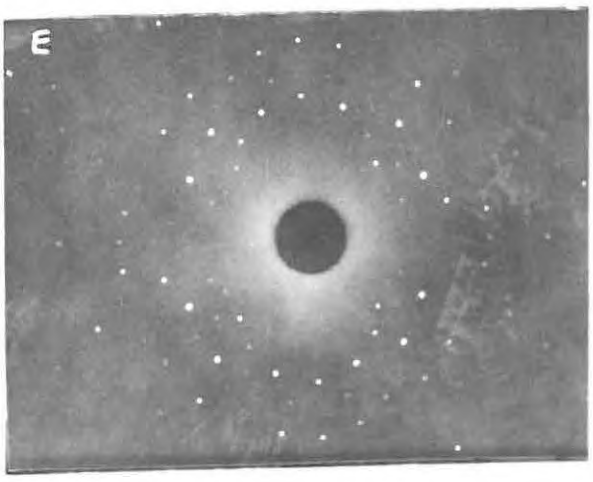
E

B1: Unirradiated, unheated crystal; seven hour exposure with the small 1/4 mm diameter collimator.

B2: Irradiated, unheated crystal. Care was taken to choose a crystal of the same size as used for B1, in order that comparisons might be drawn. Once again the exposure was of seven hours duration, and the 1/4 mm collimator was employed. The fine collimator was used in the hope that if any small changes were brought about by irradiation, they would show up more clearly than if the $\frac{1}{2}$ mm collimator were used. Comparison of B1 and B2 shows, however, no detectable diffenence

B3: Heated for 8 minutes at 95°C. (This photograph and all subsequent ones were taken with exposures of 1 3/4 hours using the $\frac{1}{2}$ mm diameter collimator). The most intense spots show a very slight smearing, hardly noticeable even on the negative.

B4: 30 minutes at 95°C; the slight smearing of the more intense Laue spots becomes definitely noticeable.

B5: 60 minutes at 95°C. The less intense spots now also tend to smear slightly.

B6: 73 minutes at 95°C. This represents the end of the induction period, just prior to fracture. Strain begins to build up enormously, as evidenced by the elongation of the Laue reflection.

B7, B8: 75 1/4 and 77 minutes respectively at 95°C. These times represent the commencement of fracture and splintering of the majority of the crystals.

B9-B16: These photographs are for periods of heating of 80, 85, 90, 100,

115, 130, 140 and 150 minutes respectively. Fracture of the crystals is evident from the streaky appearance of the elongated Laue spots. The gradual diminution in the intensity of the streaks in B13-B16 shows the consumption of permanganate as the reaction proceeds.

The Rotation Photographs.

The rotation photographs in series were taken under the same conditions as those in series A, of the unirradiated $AgMnO_4$.

B1: Unirradiated unheated crystal.

B2: Irradiated, unheated crystal. No apparent difference between B2 and B1.

B3, B4: 8 minutes and 30 minutes respectively at 95°C. Once again there is no apparent difference between B3 and B2.

B5: 60 minutes at 95°C. No observable difference from B4.

B6: 73 minutes at 95°C. This is just prior to the onset of the acceleration of the reaction. The high angle spots have a streaky appearance.

B7, B8: 75 1/4 and 77 minutes respectively at 95°C. This represents the onset of fracture and the commencement of the acceleratory process. The streakiness of the spots becomes very pronounced and is due to the fracture of the crystals.

B9, B10. 80 and 85 minutes respectively at 95°C. Very definite signs of fracture are now apparent in the photographs. It became increasingly difficult, after 80 minutes, to select a crystal from the heated batch for photographing, as microscopic

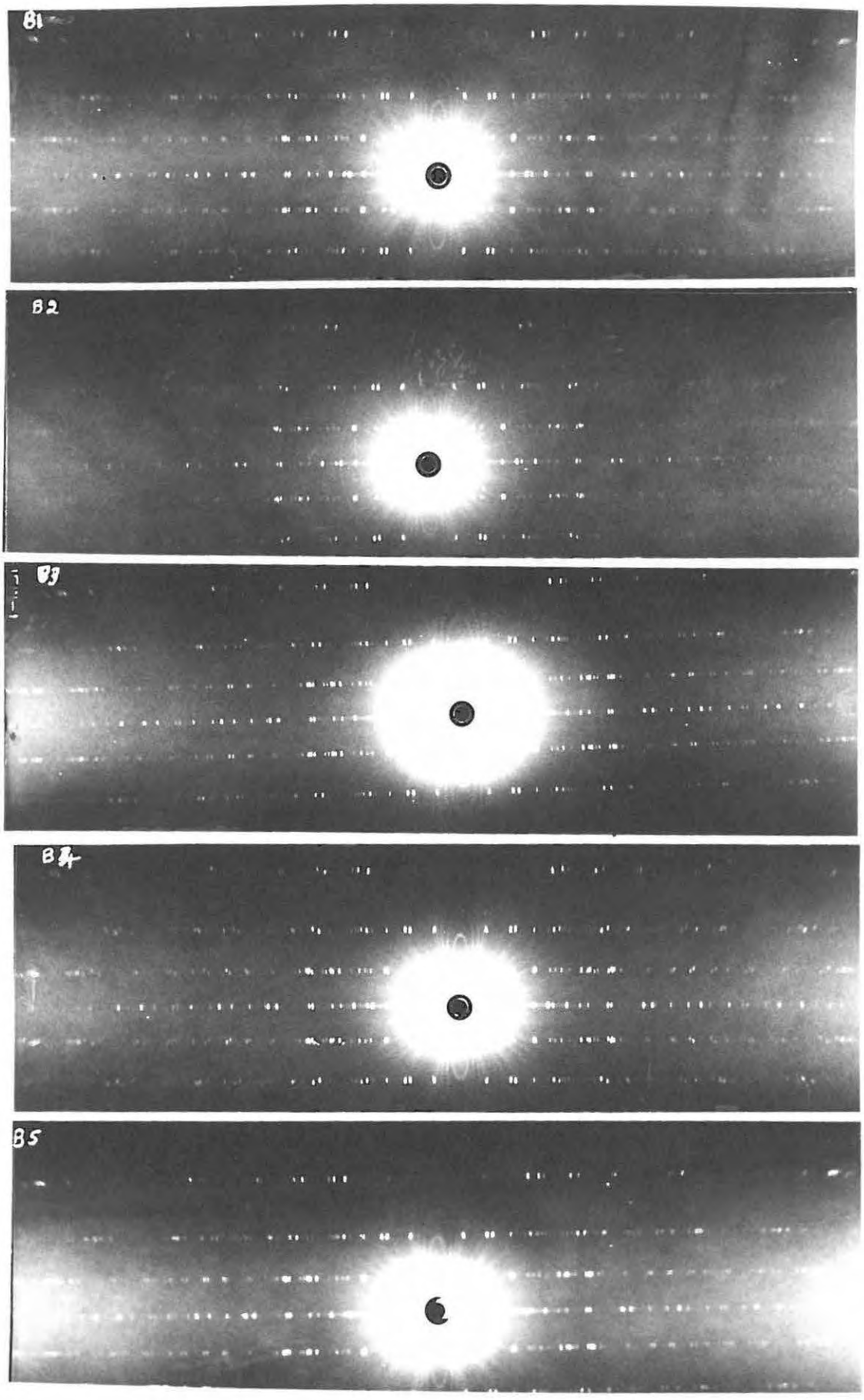
B1
B2
B3
B4
B5

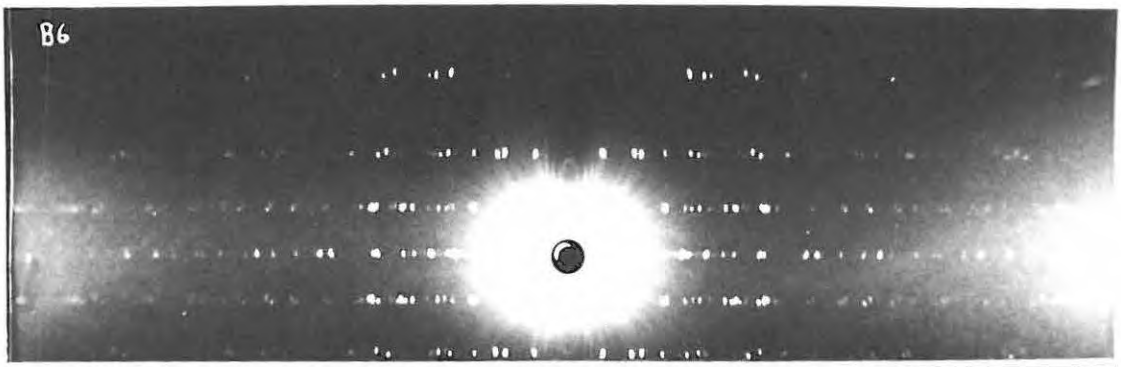
B6

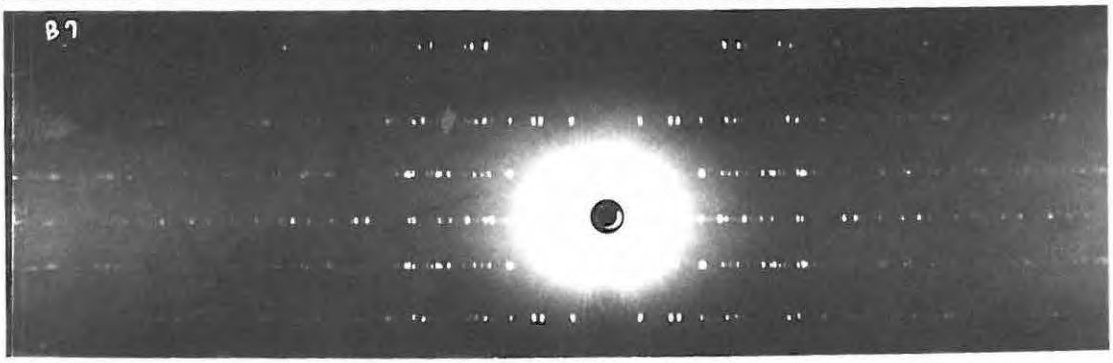
B7

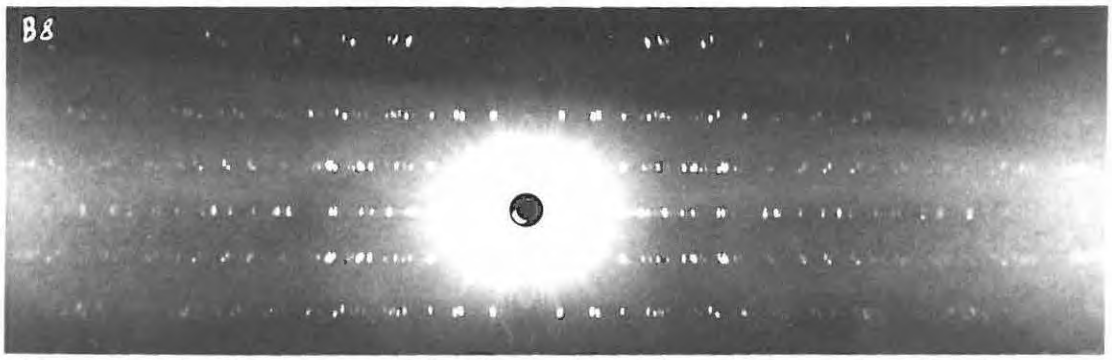
B8

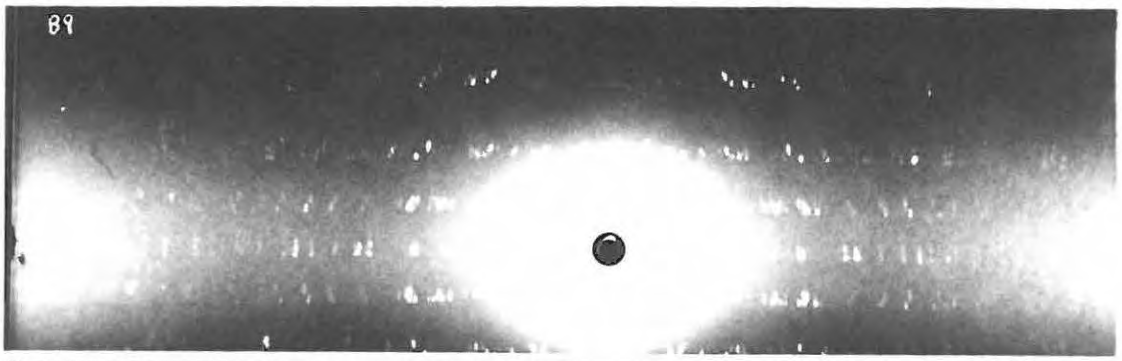
B9

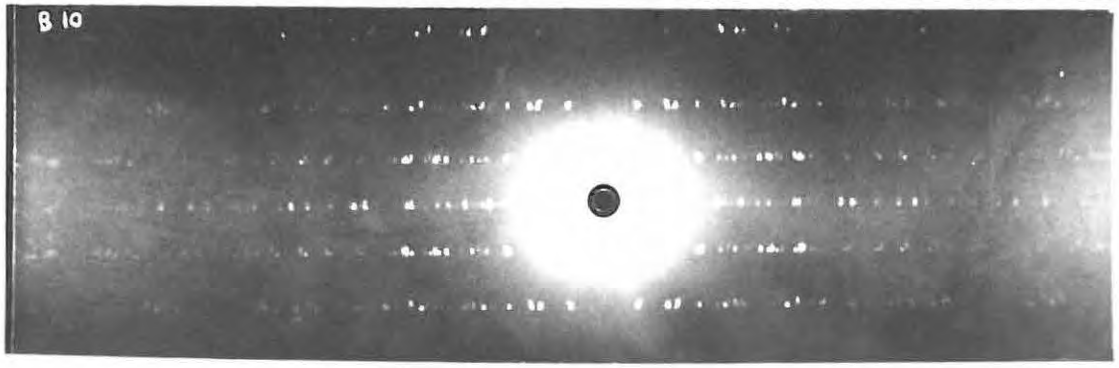
B 10

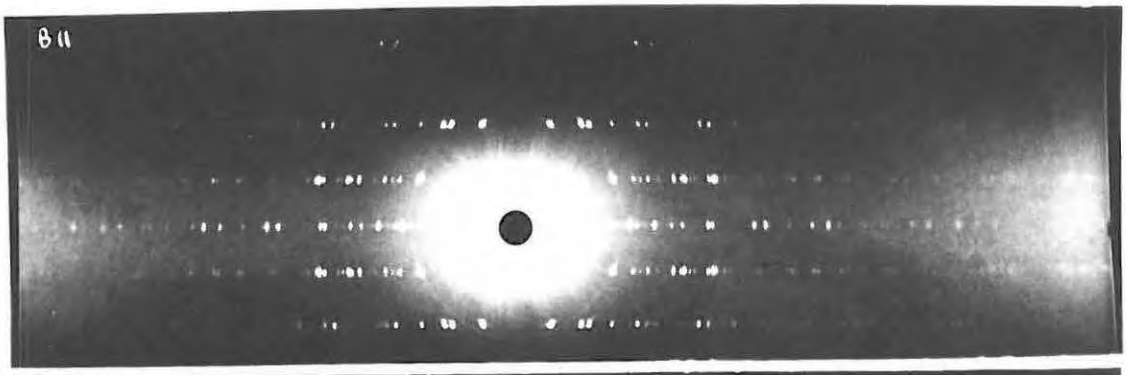
B11

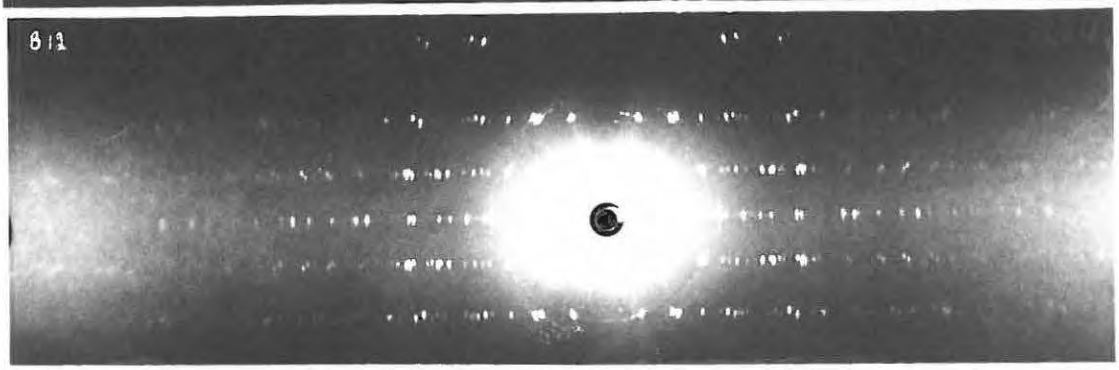
B12

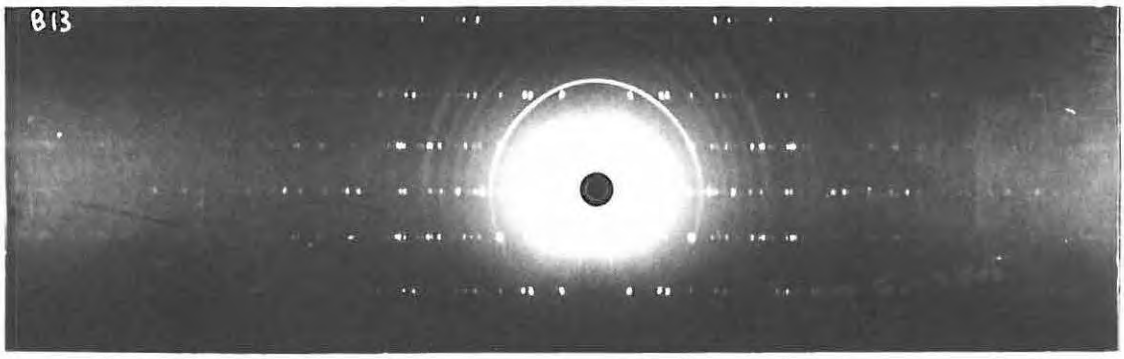
B13

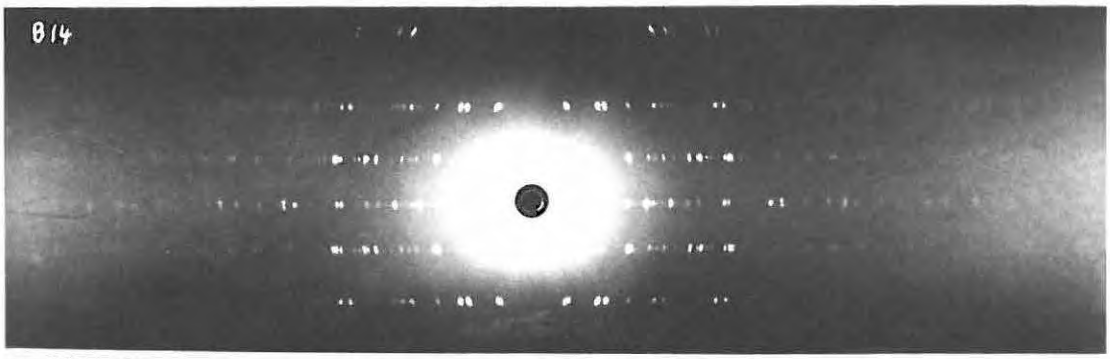
B14

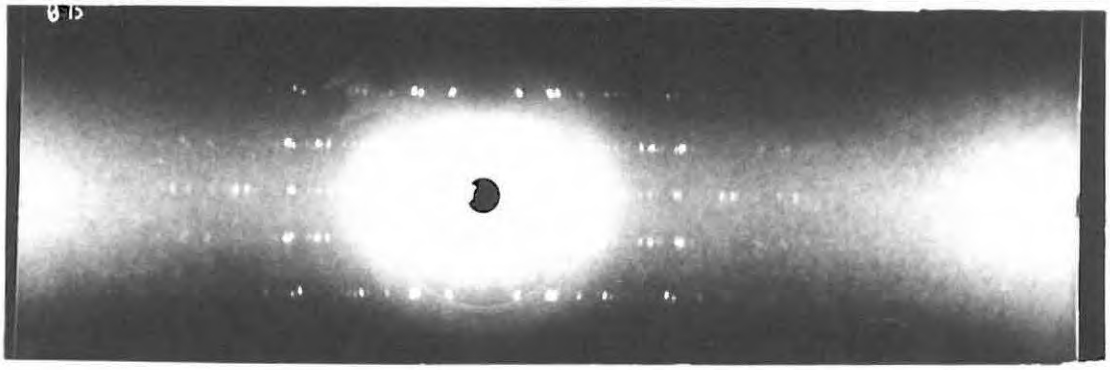
B15

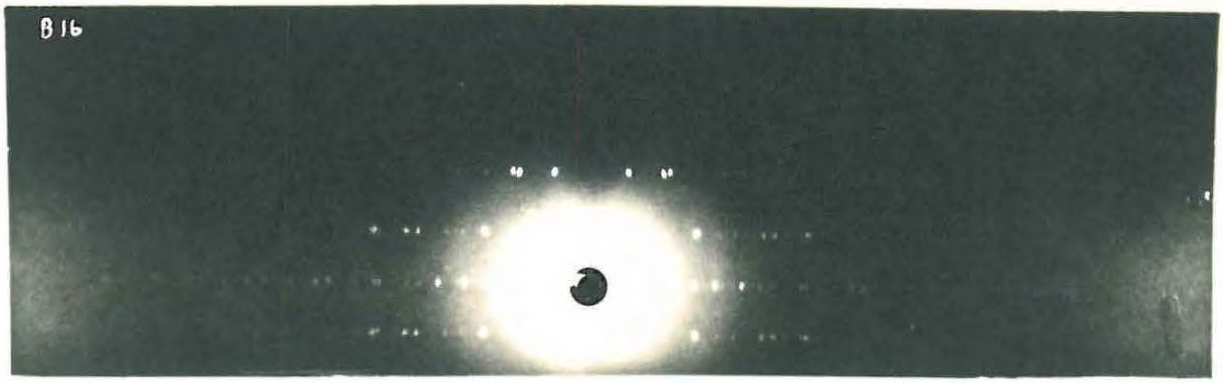
B 16

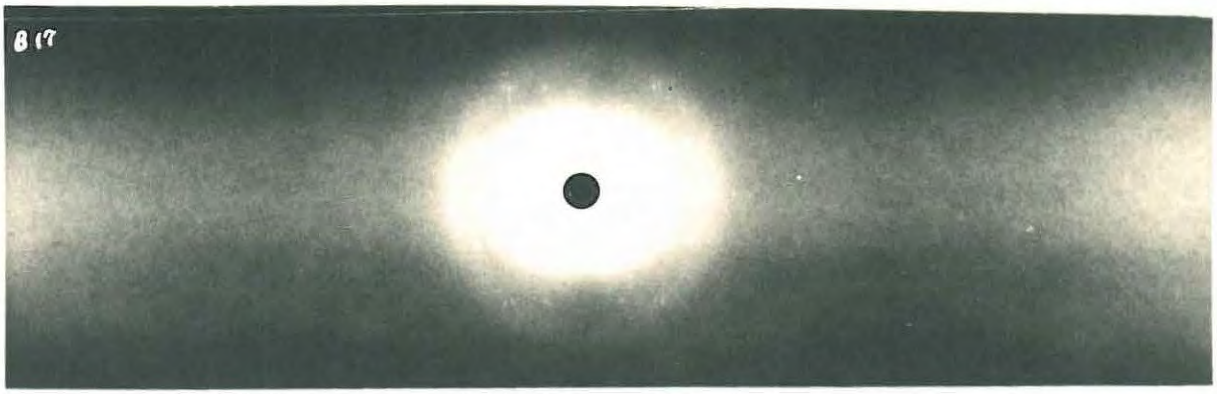
B 17

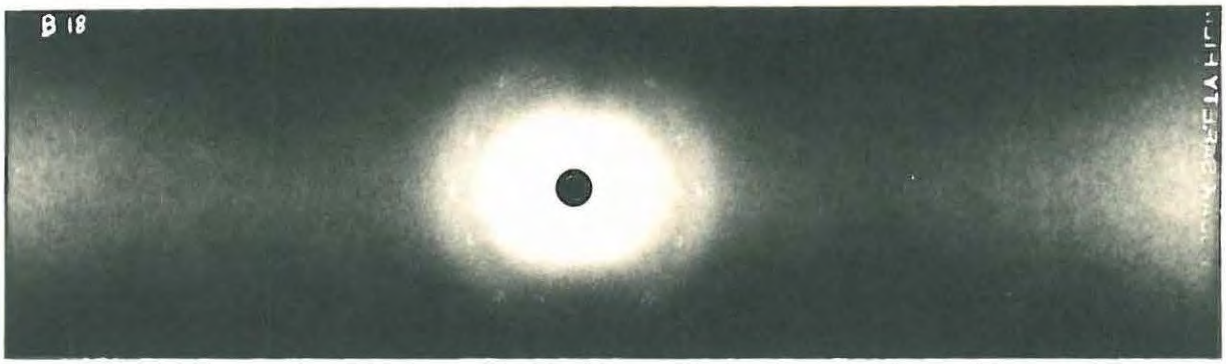
B 18

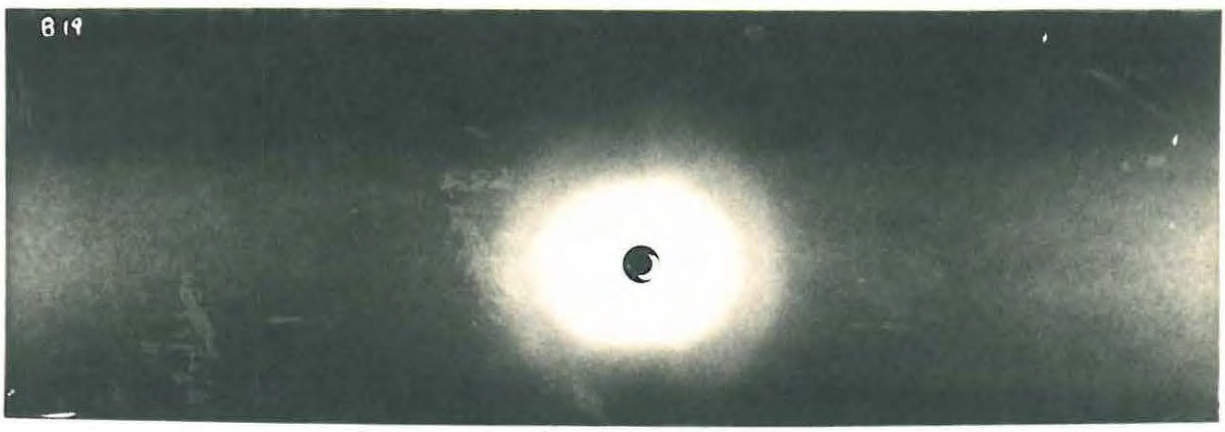
B 19

examination showed that after this length of heating, all crystals had fractured to a greater or lesser extent. The difficulty experienced in orientating fractured crystals, owing to the absence of light reflections which enable the optical collimator to be used, is shown by the imperfect layer lines of B9.

B11: 90 minutes at 95°C. Faint rings appear on the photograph; these are due to the adherence of powdered permanganate, produced by fracture, to the faces of the crystal. Apart from this, it is seen that the spots have become more streaky.

B12-B19: These photographs represent periods of heating of 100, 115, 130, 140, 150, 165 and 180 minutes and finally 12 hours respectively at 95°C. The high angle spots firstly, and then also the low angle spots decrease in intensity and finally disappear. The disappearance of spots and gradual appearance of a broad, ill-defined diffuse ring show the gradual consumption of permanganate and formation of amorphous product. The sequence of events in the irradiated $AgMnO_4$ over the decay period is thus seen to be identical to that in the unirradiated substance.

Discussion of the Photographs.

Huang, as mentioned previously, has shown that elastic singularities randomly distributed in a face centred cubic lattice give rise to effects on X-ray diffraction photographs. The theory predicts that such

singularities will cause the X-ray scattering to divide into two terms, the first of which gives the Laue-Bragg scattering with the following features: (i) The intensities are altered as if by an artificial (isotropic) temperature factor; (ii) there is a change in the positions of the Laue-Bragg maxima corresponding to an isotropic lattice expansion. The second term predicts the appearance of diffuse maxima surrounding the reciprocal lattice points.

According to Prout's theory regarding the process involved in the irradiation of permanganates, interstitial ions and vacancies are produced by the expulsion of cations from their lattice positions following the multiple ionisation of permanganate ions and/or the cations themselves. Such singularities may conceivably act as centres of strain giving rise to the effects predicted by Huang.

Effects Predicted by Huang.

(i) There was no noticeable artificial temperature factor in the irradiated samples, either before heating or during the induction period.

(ii) The lattice parameters a, b and c of the irradiated $AgMnO_4$ were examined in order to see if there were any changes as a result of irradiation. Rotation photographs were taken about each of the three axes in turn, using a semi-cylindrical camera of radius 5.73 cm. If the distance of any layer line from the equatorial line is y, and the camera radius is r , the lattice parameter in question is given by $n\lambda/\cos\phi$, where $r/y = \tan\phi$ and n is the number of the layer line selected. Industrex D film was used ,

and since film shrinkage was negligible, and photographs of irradiated and unirradiated crystals superposed exactly, no detectable change in any of the lattice parameters was found. This result was supported by readings taken from Weissenberg photographs which were taken of irradiated and unirradiated crystals.

(iii) The diffuse reflection associated with the 220 reflection was examined in an irradiated unheated crystal as described previously. Comparison of the diffuse reflection of the irradiated $AgMnO_4$ with that of an unirradiated crystal showed that no apparent increase either in size or in intensity had occurred as a result of irradiation.

Thus, none of the effects predicted by Huang was found. (In contrast, all three effects were found in neutron-irradiated boron carbide[97].) This result, when taken in conjunction with the inferences drawn from the study of the electron-density profiles of irradiated $AgMnO_4$ seems to invalidate the theory advanced by Prout for the irradiation process in permanganates. However, it is possible by means of conclusions drawn from the photographs of decomposed irradiated $AgMnO_4$ to advance a mechanism which will explain the process involved in irradiation.

Examination of the Laue photographs taken during the induction period shows that there is a much greater build-up of strain during this period in the irradiated than in the unirradiated crystals. Even after only 8 minutes at 95°C, there are signs of strain as evidenced by the smearing of the most prominent Laue spots, and after 60 minutes smearing is pronounced in all spots. After 73 minutes, strain builds up enormously,

and at the end of the induction period (75 - 77 minutes) violent physical disintegration of the crystal takes place. The fact that there is no evidence for a random distribution of distortion centres in the crystal brought about by irradiation, and the violent fracture at the end of the induction period, lead us to conclude that the damage done by irradiation is associated with imperfections in the crystal structure, such as dislocations and grain boundaries. If nucleation of some sort is initiated by irradiation along such discontinuities, then subsequent heat treatment will cause product to form primarily at these sites. At the end of the induction period the "decomposition spikes" formed will cause disintegration of the crystal to take place, if the specific volumes of product and reactant are different.

After the fracture at the end of the induction period, the rapid acceleration of reaction is attributed to the exposure of fresh surfaces of permanganate and their decomposition. Comparison of series A and series P (both Laue and rotation photographs) shows that after the induction and acceleratory periods, all further reaction is exactly similar for irradiated and unirradiated $AgMnO_4$. Thus the difference between reaction in irradiated and unirradiated samples is limited to the process occurring during the induction period. In the latter case, reaction is initiated at the crystal surface, while in the former, discontinuities within the crystal play a role of comparable importance.

Prout and Sole[1] originally suggested that decomposition spikes would form preferentially along dislocation lines. However, formation of product at such sites was assumed to be preceded by migration of

of the interstitial ions, the release of energy of recombination causing decomposition to occur. It seems certain now, however, that damage is produced in situ along dislocation lines. The possible nature of this damage will be considered in the next section.

6. GENERAL DISCUSSION.

On the grounds of the foregoing evidence, it seems certain now that displacement of ions either by collision with Compton electrons or as a result of multiple ionisation does not occur in permanganates on irradiation. No evidence of displacement has been found on examination of electron-density profiles of irradiated $AgMnO_4$, and the thermal decomposition of irradiated $AgMnO_4$ tends to inidcate that some other mechanism operates. The following theory is thus proposed.

During irradiation those permanganate ions adjacent to dislocations or grain boundaries are subjected either to ionisation or to complete dissociation, possibly into MnO_3^- ions and free oxygen atoms. It is considered likely that electronic deformation of permanganate ions due to the adjacent discontinuities will render them much more prone to the action of ionising radiation than those ions on normal lattice sites. Examination of the structure factors F(hkO) of the irradiated $AgMnO_4$ tends to point to the removal of oxygen as a result of irradiation; and further, a thermal decomposition of 7 mg of $AgMnO_4$ subjected to a massive of dose of 500 Mrad (see figure 5.19, data in table 5.13) showed that the final pressure was indeed less than that obtained with the decomposition of the same mass of crystalsirradiated with a dose of 100 Mrad. Evolution of oxygen by $KMnO_4$ subjected to very heavy γ-ray doses from a Co^{60} source has also been detected[118]. Therefore it seems highly probable that complete dissociation occurs on irradiation.

It has been estimated that there are approximately 10^{12} dislocation

lines cutting every square centimetre cross-section in a normal crystal; the formation of "decomposition spikes" in such a number would account for the violent physical disintegration of the irradiated crystals at the end of the induction period. The altered permanganate ions along the dislocation lines or grain boundaries act as nuclei for the reaction; during the induction period reaction takes place preferentially at these sites, and the difference in molecular volume of the product and parent compound causes strain which fractures the crystal.

This theory and the evidence on which it is grounded are in accordance with the suggestion[101] that the process involved in irradiation is of a purely electronic nature, and affects only the permanganate ions. On the other hand, no trace of the "new phase" arising in the solid as a result of radiolysis[101] has been detected. A second phase usually refers to a macroscopic amount of substance; if however, it is meant to indicate an array of altered permanganate ions along a discontinuity, then perhaps a new phase is introduced by radiolysis.

It should be noted here that the Laue photograph of a 500 Mrad crystal showed that strain was present in the crystal, since all the spots showed considerable asterism (see Laue photograph marked D). This is however due to the fact that this very heavy dose actually caused oxygen to be evolved (in a quantity sufficient to create pressure in the crystal) and consequent fracture. The photograph E of 300 Mrad $AgMnO_4$ however, shows no sign of strain. In this case the crystals returned intact after irradiation. Thus it may be supposed that an extremely heavy dose has the same effect as heat treatment.

The failure to detect any of the effects predicted by Huang in the 100 Mrad irradiated crystal supports the idea that random formation of interstitials and vacancies does not occur. It may not be argued that a continuous "chain" of altered permanganate ions should give rise to the same effect as isolated singularities in the structure.

The results with the unirradiated salt strongly support the theory advanced by Prout and Tompkins[16]. The absence of any large strain in the crystal until after the onset of acceleration, which is postulated to occur when the reaction starts progressing into the body of the crystal, supports the idea that, during the induction period, reaction is limited to the crystal surface. We may stress again here, then, that the reaction in the unirradiated salt differs from that in the irradiated salt, only in that, in the latter case, reaction occurs during the induction period also along grain boundaries and dislocations.

At this point some tentative suggestions may be made with regard to future research into the subject of the irradiation process in permanganates. It would be instructive firstly to investigate the permanganate of potassium for the movement of oxygen atomsin the crystal lattice during irradiation. The crystal structure of $KMnO_4$ is known, and moreover, the series-termination effect due to a heavy atom would not be as noticeable as in the case o of the silver salt. Because of this it may be possible to resolve the oxygen atoms in the structure, by means of a Fourier analysis, expecially if a molybdenum target were used in the taking of the X-ray photograph, when many more reflections would be recorded than if a copper anticathode were used. Secondly, an investigation of the structure after various increasing doses may allow a more precise mechanism for the reaction to be formulated.

7. SUMMARY.

The effect of irradiation by γ-rays on $AgMnO_4$ has been investigated by X-ray methods. On the grounds of the results obtained, the ion displacement theory put forward to account for the increased reactivity during subsequent thermal treatment has been rejected, and a new theory, based on the formation of nuclei by ionisation along crystal discontinuities has been proposed. This latter theory is in accordance with the results obtained by other investigators[101].

The X-ray investigation of the thermal decomposition of irradiated $AgMnO_4$ has lent support to the above theory. The mechanism proposed by Prout and Tompkins for the thermal decomposition of the unirradiated salt has been substantiated by an X-ray investigation of the decomposition.

BIBLIOGRAPHY.

1. Prout and Sole: J. Inorg. Nucl. Chem., 9, (1959).
2. Garner and Tanner: J. Chem. Soc., 47, (1930).
3. Garner: Chemistry of the Solid State p.185: Butterworth Scientific Publications, London (1955).
4. Wischin: Proc. Roy. Soc., A172, 314 (1939).
5. Bright and Garner: J. Chem. Soc., 1872 (1934).
6. Cooper and Garner: Trans. Farad. Soc., 32, 1739 (1936).
7. Garner and Southam: J. Chem. Soc. 1705 (1935).
8. Bagdassarian: Acta. phys. chim., U.R.R.S, 20, 441 (1945).
9. Thomas and Tompkins: Proc. Roy. Soc.,
10. Tompkins and Young: unpublished work.
11. Garner and Reeves: Trans. Farad. Soc., 50, 254 (1954).
12. Bartlett and Tompkins: unpublished work.
13. Finch, Jacobs and Tompkins: J. Chem. Soc., 2053 (1954).
14. Garner and Hailes: Proc. Roy. Soc., A139, 576 (1933).
15. Hailes: Trans. Farad. Soc., 29, 544 (1933).
16. Prout and Tompkins: Trans. Farad. Soc., 40, 488 (1944).
17. Prout and Tompkins: ibid, 42, 468 (1946).
18. Tompkins: Symposium, South African Chemical Institute, (1962).
19. Bircumshaw and Edwards: J. Chem. Soc., 1800 (1950).
20. Bircumshaw and Harris: ibid 1898 (1948).
21. Herley and Prout: J. Inorg. Nucl. Chem., 16, 16 (1960).
22. Prout and Herley: J. Phys. Chem., 65, 208 (1961).
23. Herley and Prout: J. Phys. Chem., 64, 675 (1960).
24. Prout and Herley: J. Phys. Chem., 66, 961, (1962).
25. Simpson, Taylor and Anderson: J. Chem. Soc., 2378 (1958).
26. Garner: Chemistry of the Solid State: p.198 et seq. Butterworth Scientific Publications, London (1955).
27. Avrami: J. Chem. Phys., 7, 1103 (1939); 8, 212 (1940); 9, 177 (1941).
28. Erofeyev: C.R. Acad. Sci. U.R.S.S., 52, 511 (1946).
29. Seitz: Rev. Mod. Phys., 18, 384 (1946).
30. Seitz: Rev. Mod. Phys., 26, 7 (1954).

31. Frenkel and Anastasivich: J. Exp. and Ther. Phys., U.S.S.R., 11, 127 (1941).
32. Garner and Maggs: Proc. Roy. Soc., A172, 299 (1939).
33. Gurney and Mott: ibid, A164, 151 (1938).
34 Mott: ibid, A172, 325 (1939).
35. Jacobs and Tompkins: ibid, A215, 254 (1952), A215, 265 (1952).
36. Jacobs, Tompkins and Young: Disc. Farad. Soc., No.28, 234 (1959).
37. Jacobs, Tompkins and
38. Deb: J. Chem. Phys., in press.
39. Maggs: Trans. Farad. Soc., 35, 433 (1939).
40. Garner and Moon: J. Chem. Soc., 1398 (1938).
41. Garner,
42. McDonald: ibid, 832 (1936).
43. Prout and Tompkins: Trans. Farad. Soc., 43, 148 (1947).
44. Benton and Cunningham: J. Amer. Chem. Soc., 57, 2227 (1935).
45. Tompkins: Trans. Farad. Soc., 44, 206 (1948).
46. Meiler and Noyes: J. Amer. Chem. Soc., 52, 527 (1930).
47. Noyes and Vaughn: Chem. Rev., 7, 239 (1930).
48. Muller and Brous: J. Chem. Phys., 1, 482 (1933).
49. Groocock and Tompkins: Proc. Roy. Soc., A223, 267 (1954).
50. Bowden and Singh: ibid, A227, 22 (1954).
51. Heal: Canad. J. Chem: 31, 1153 (1953).
52. Heal: ibid, 31, 91 (1953).
53. Seitz and Koehler: Int. Conf. Peaceful Uses of Atomic Energy, 7, 615 (1956).
54. Kinchin and Pease: Rep. Prog. Phys., 18, 1, (1955).
55. Brinkman: J. Appl. Phys., 25, 961 (1954).
56. Seitz: Solid State Physics (Academic Press), 2, 305 (1955).
57. Flanagan: Trans. Farad. Soc., 57, 797 (1961).
58. Flanagan: J. Phys. Chem: 66, 416, (1962).
59. Haynes and Young: Disc. Farad. Soc., No.31, 229 (1961).
60. Dugdale: Proc. Bristol. Conf. Phys. Soc., London, 246 (1955).
61. Cleland, Crawford and Holmes: Phys. Rev., 102, 722 (1956).
63. Anderson, Freeman and Campisi: J. Phys. Chem., 64, 1727 (1960).
64. Prout: J. Inorg. Nucl. Chem: 7, 368 (1958).

65. Kinchin: Int. Conf. Peaceful Uses of Atomic Energy, 7, 472 (1955).
66. Bowen, Eggleston and Kropschot: J. Appl. Phys., 23, 630 (1952).
67. Evans: "The Atomic Nucleus": McGraw Hill, N.Y. (1955).
68. Dienes and Vineyard: Radiation Effects in Solids, Interscience Publishers, (1957).
69. Varley: J. Nuclear Energy, 1, 130 (1954).
70. Durup and Platzman: Disc. Farad. Soc., No.31, 156 (1961).
71. Prout: Symposium, South African Chemical Institute, (1962).
72. Prout and Herley: Nature: 184, 445 (1959).
73. Prout: ibid, 183, 884 (1959).
74. Simpson, Taylor and Anderson: J. Chem. Soc., 2378 (1958).
75. Griffith: J. Chem. Phys., 14, 408 (1946).
76. Burgers, Rootsaert, Bogers and Cornet: Proc. Konink. Nederl. Akad. v. Wetensch., B63, 113 (1960).
77. Sawkill: Proc. Roy. Soc., A229 , 135 (1955).
78. Goodman: ibid, A247, 346 (1958).
79. Johnson and Forten: Disc. Farad. Soc., No.31, 238 (1961).
80. Cunningham and Heal: Trans. Farad. Soc., 54, 1355 (1958).
81. Tucker and Senio: Phys. Rev., 99, 1777 (1955).
82. Simmons and Balluffi: Bull. Amer. Phys. Soc., II2, 151 (1957)A.
83. Crawford and Wittels: Int. Conf. Peaceful Uses of Atomic Energy, 7, 654 (1955).
84. Woods, Bupp and Fletcher: ibid, 7, 455 (1955).
85. Levy and Kammerer: Phys. Rev., 100, 1787 (1955).
86. Bragg: The Crystalline State; A General Survey, p. 191. G. Bell and Sons Ltd., London (1955).
87. Keating: unpublished work.
88. Pabst: Am. Mineralogist, 37, 137 (1952).
89. Chipman, Warren and Dienes: J. Appl. Phys., 24, 1251 (1953).
90. Fleeman and Dienes: ibid, 26, 652 (1955).
91. Wittels and Sherrill: ibid, 27, 643 (1956).
92. Dienes and Vineyard: Radiation Effects in Solids, p.108, Interscience Publishers, New York, (1957).
93. Bunn: Chemical Crystallography, p.204 (Oxford Univ. Press).
94. Huang: roc. Roy. Soc., A190, 102 (1947).

95. Bernal: Proc. Roy. Soc., A113, 117 (1926).

96. Keating: Phys. Rev., 97, 832 (1955).

97. Tucker and Senio: Acta Cryst., 8, 371 (1953).

98. Büssem and Herrmann: Zeitschr. für Krist., 74, 458 (1930).

99. Sasvari: . Krist., 99, 9 (1938).

100. Sasvari: Math. Naturwiss. An . ungar. Akad. Wiss., 57, 988 (1938).

101 Boldyrev, Pinaevskaya, Boldyreva, Zakharov and Konshev: Kinetika i Kataliz: 2, 184 (1961).

102. Herley and Prout: Nature, 188, 717 (1960).

103. Herley: M.Sc., Thesis, Rhodes University, 1959.

104. Brandt: M.Sc., Thesis, Rhodes University, 1962.

105. Buerger: X-Ray Crystallography, p.179 (John Wiley and Sons, 1942).

106. Henry, Lipson and Wooster: The Interpretation of X-Ray Diffraction Photograph, Table 3, (MacMillan, 1960).

107. Dawton: Proc. Phys. Soc., 50, 419 (1938).

108. Buerger: Crystal Structure Analysis, p.95 (John Wiley and Sons, Inc.) (1960).

109. Buerger: ibid p.98.

110. Buerger: ibid p.99.

111. Bradley: Proc. Phys. Soc., 47, 879 (1935).

112. Buerger: Crystal Structure Analysis, p.596 (John Wiley and Sons, Inc.), (1960).

113. Int. Tables for X-Ray Crystallorgraphy, 2, 107 (1959).

114. Lonsdale and Smith: Proc. Roy. Soc., A179, 8 (1942).

115. Jauncey and Baltzer: Phys. Rev., 59, 699 (194).

116. Bragg: The Crystalline State: A General Survey: Plate XVI (Bell, 1955).

117. Bragg: ibid p.202.

118. J.M. Blaunshtein and S.V. Starodubstev: Tr. Tashkensk. Kong. po Mirnomu Ispol'z. at. Energii, Akad. Nauk. Ux. SSR 1, 163 (1961).